THE PETROLOGY, GEOCHEMISTRY AND PETROGENESIS OF THE RIWAKA COMPLEX, SOUTH ISLAND, NEW ZEALAND

JEFFREY KEITH SAUNDERS

INFORMATION TO USERS

This manuscript has been reproduced from the microfilm master. UMI films the text directly from the original or copy submitted. Thus, some thesis and dissertation copies are in typewriter face, while others may be from any type of computer printer.

The quality of this reproduction is dependent upon the quality of the copy submitted. Broken or indistinct print, colored or poor quality illustrations and photographs, print bleedthrough, substandard margins, and improper alignment can adversely affect reproduction.

In the unlikely event that the author did not send UMI a complete manuscript and there are missing pages, these will be noted. Also, if unauthorized copyright material had to be removed, a note will indicate the deletion.

Oversize materials (e.g., maps, drawings, charts) are reproduced by sectioning the original, beginning at the upper left-hand corner and continuing from left to right in equal sections with small overlaps. Each original is also photographed in one exposure and is included in reduced form at the back of the book.

Photographs included in the original manuscript have been reproduced xerographically in this copy. Higher quality 6" x 9" black and white photographic prints are available for any photographs or illustrations appearing in this copy for an additional charge. Contact UMI directly to order.

UMI

A Bell & Howell Information Company
300 North Zeeb Road, Ann Arbor MI 48106-1346 USA
313/761-4700 800/521-0600

THE PETROLOGY, GEOCHEMISTRY AND PETROGENESIS OF THE RIWAKA COMPLEX, SOUTH ISLAND, NEW ZEALAND.

By
Jeffrey Keith Saunders, B.Sc. (Hons.)

A Thesis Submitted to the School of Graduate Studies in Partial Fulfilment of the Requirements for the degree of Master of Science

Department of Earth Sciences,
Memorial University of Newfoundland

August, 1997

St. John's *Newfoundland*

National Library of Canada
Acquisitions and Bibliographic Services
395 Wellington Street
Ottawa ON K1A 0N4
Canada

Bibliothèque nationale du Canada
Acquisitions et services bibliographiques
395, rue Wellington
Ottawa ON K1A 0N4
Canada

Your file Votre référence

Our file Notre référence

0-612-34224-7

Canada

Frontispiece: The Graham Valley from the Motueka River valley.

ABSTRACT

The Riwaka Complex is a tholeiitic igneous intrusion (40km long, up to several km wide) located in the northwestern part of the South Island of New Zealand. It intrudes the Takaka Terrane which represents an assemblage of sedimentary rocks that are part of New Zealand's geologic Western Province. The Takaka Terrane is thought to have formed in a fore - arc environment associated with either one or two westward dipping Benioff zones.

In this subduction zone environment the tholeiitic magma crystallized in a manner similar to that, that form Alaskan - type ultramafic complexes. Its distinctive petrological features include: cumulate olivine and clinopyroxene and interstitial amphibole; absence of orthopyroxene and plagioclase; and little or no Fe - enrichment, but a Ca - enrichment in the clinopyroxenes. The Riwaka Complex's geochemical evolution was dominated by olivine and clinopyroxene fractionation from as many as five pulses of magma, which gave rise to an intrusion made up almost entirely of ultramafic rocks ranging from clinopyroxene - bearing dunites to olivine - hornblende clinopyroxenites. Some minor gabbros and diorites are also present.

The small amount of gabbro present represents an important part of the Riwaka Complex as these rocks contain significant amounts of primary sulphides which are rich in nickel, copper and platinum group elements. The nickel and copper ratios indicate that the composition of the parental magma was similar to that of a komatiite. This magma evolved to a basaltic type composition which gave rise to the gabbroic rocks. The high

temperature platinum group elements (Os, Ir and Ru) are not found in the same abundances within the gabbroic rocks as their lower temperature counterparts (Rh, Pt and Pd) indicating that they have undergone an earlier fractionation, possibly within the early crystallized ultramafic rocks. These rocks may therefore represent an important exploration target.

ACKNOWLEDGEMENTS

There are numerous individuals who require acknowledgement for their contribution to this study. Firstly, I would like to thank Dr. John Malpas who initiated and supervised this project. His financial support, friendship and patience throughout the course of this study are greatly appreciated. Also, Dr. Derek Wilton who served on my supervisory committee and made time in his busy schedule to proof read this thesis.

In New Zealand, I would like to thank Dr. Ian Smith for arranging use of the facilities at the University of Auckland and Mr. Mike Johnston of the Department of Scientific and Industrial Research (DSIR) whose discovery of Cu - Ni sulphides in the Riwaka Complex eventually led to this study. He also provided me with maps and shared some of his in - depth knowledge of my field area with me. Nick Mortimer of DSIR in Wellington provided me with copies of all the publications concerning my field area and access to the drillcore samples located in DSIR's drillcore storage facility in Christchurch.

Staff from Memorial's Department of Earth Sciences are thanked for their help, especially noting; Darryl Clarke (XRF), Bev Chapman (ICP - MS), Pam King (ICP - MS, XRF, probe and other trouble shooting), Mervin Goodyear (computer support) and Maggy Piranian (probe).

Students R. Churchill, G. Thompson, D. Johnstone, C. Lee, P. Ivany, V. Bennett, K. Deveau, A. and N. Aydin and D. Ritcey made this study take a lot longer than it should have, but made all of the time much more enjoyable.

Finally, I would like to thank my field assistant and wife Brenda for her patience, support and understanding during the course of this study.

TABLE OF CONTENTS

Chapter 3: Field Relationships and Petrography

Chapter 4: Mineral and Whole Rock Geochemistry

Chapter 5: Economic Mineralization and Potential

Appendix B: Analytical Methods

Appendix C:Drill Core Samples

LIST OF TABLES

LIST OF FIGURES

LIST OF PLATES

LIST OF ABBREVIATIONS AND SYMBOLS USED

Weights and measures

km	kilometre
m	metre
cm	centimetre
ppb	parts per billion
ppm	parts per million
μ	microns (10^{-6}m)
g	grams
ml	millilitres
wt%	weight percent

Mineral abbreviations

cpx	clinopyroxene
ol	olivine
amp	amphibole
po	pyrrhotite
pe	pentlandite
cp	chalcopyrite

Miscellaneous

PPL	plane polarized light
XP	crossed polars
X	times magnification
et al.	and others
S.D.	standard deviation
Det.	lab determination
Pub.	published value
na	not analysed
-	not detected
ddh	diamond drill hole

Lithological names

AM	Arthur Marble
OS	Onekaka Schist
FS	Fractionation Suite
CG	Cumulus Gabbro
LSD	Late Stage Diorite
SPG	Separation Point Granite

Geochemical expressions

REE	rare earth element
LREE	light rare earth element
HREE	Heavy rare earth element
LOI	lost on ignition
FeO	total Fe
Fo	forsteritic composition
En	enstatite composition
CNPGE	chondrite normalized platinum group element diagram
MNPGE	mantle normalized platinum group element diagram
MORB	mid - ocean ridge basalt

Analytical procedures

ICP - MS	inductively coupled plasma mass spectroscopy
XRF	X - Ray florescence

Chapter 1

Introduction

1.1 Introductory Statement

New Zealand is located in the southwest corner of the Pacific Ocean. It comprises three main islands, the North, South and Stewart Islands. Its land mass occupies approximately 260,000 km^2 and its population is close to 3 million. Much of this population is located in the northern part of the North Island in and around the city of Auckland. Most peoples are of European descent, but the native Maori people are very visible in today's society. They are descendants of Polynesian tribes that migrated southward from the Hawaiian Islands about one thousand years ago.

The largest industries in New Zealand are farming and tourism. It has one of the largest sheep populations per km^2 of any place in the world (approximately 70 million in total). Cattle and deer farming also make up a large portion of the livestock industry.

New Zealand constitutes a landmass more remote from a neighbour (Australia, 1600km) than any other landmass on the globe.

"Its long - term isolation from continental influence has been reflected not only in the rocks but also in the fossil record and the present biota. Long term mobility at the Pacific margin has resulted in a complexity in geological development perhaps unsurpassed elsewhere

in so small a region." R. P. Suggate et al. (1978)

The geological complexity of New Zealand is brought about because of its location at the boundary of two major lithospheric plates, the Indian - Australian and Pacific Plates (Figure 1.1). It is an area of active destructive and transform plate motions. These factors make New Zealand one of the most geologically interesting countries in the world.

1.2 Location and Access

The Riwaka Complex is located in the northern part of the South Island of New Zealand. It lies approximately 50 km west of Nelson in the foothills of the Mount Arthur Range (Figure 1.2). It is linear, approximately 40 km long and up to several kilometres wide. The field area for this study is in the central portion of the Riwaka Complex. It lies between the north and south branches of the Graham River (Figure 1.3), and can be accessed via a public road from the Motueka Valley (Route 61). The Graham Valley road winds through the Graham Valley and several private dirt tracks lead off the main road into the field area.

1.3 Field Work

The field work for this study was carried out from November 2 to December 20, 1991. Field mapping was undertaken in the area of the Graham Valley between the North and

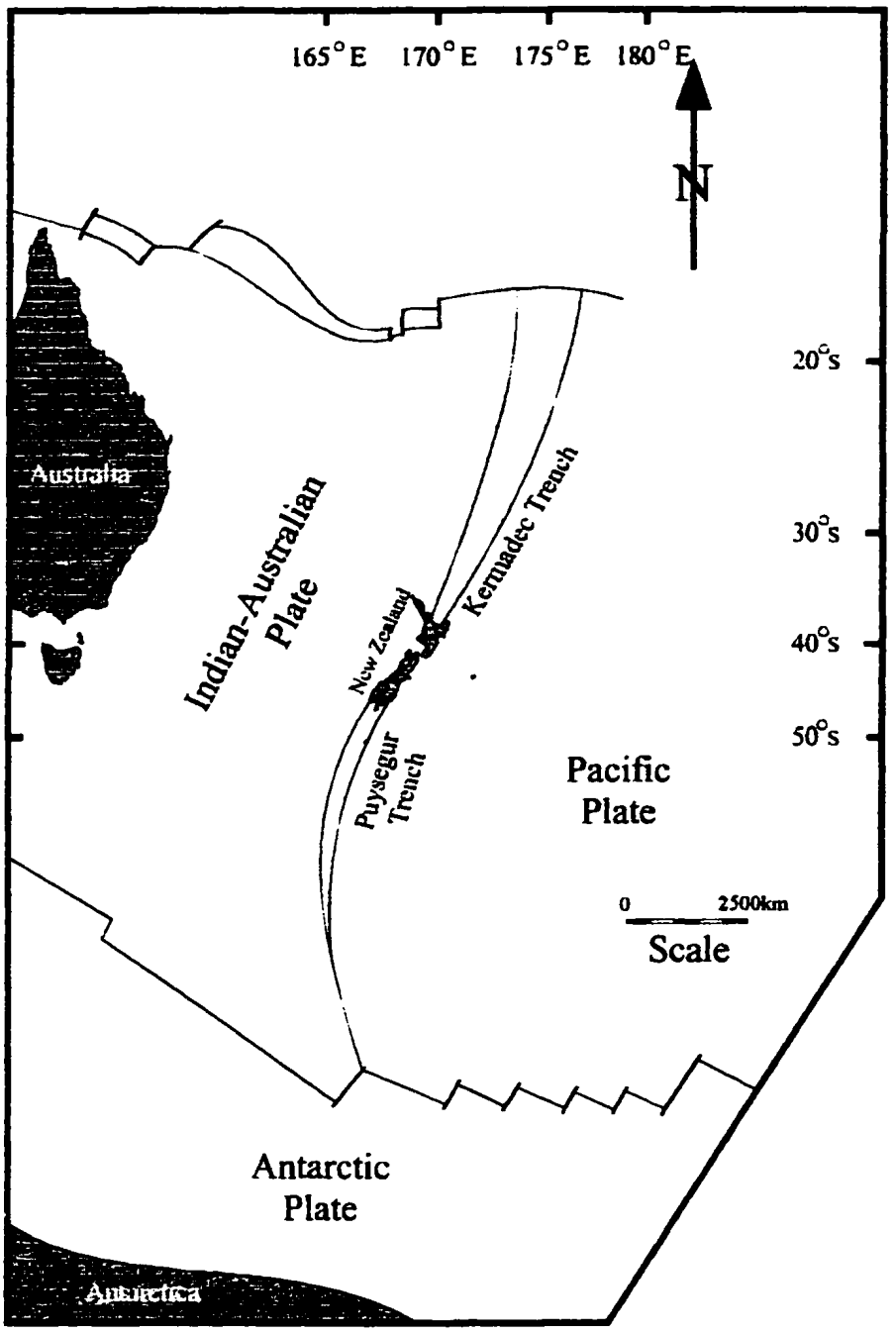

Figure 1.1 Relative position of New Zealand with respect to the Indian-Australian, Pacific and Antarctic plates (Korsch and Wellman, 1988).

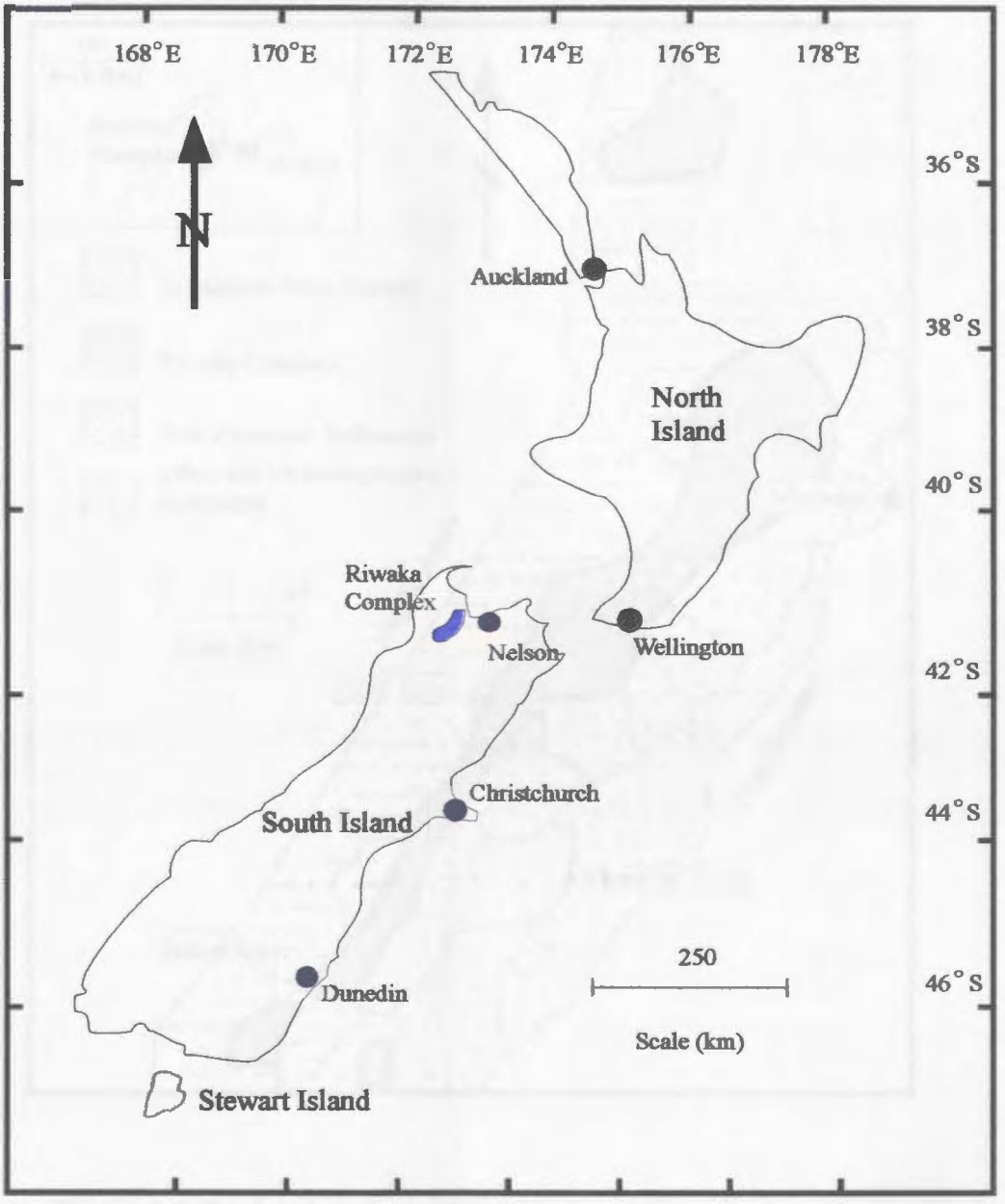

Figure 1.2 Location map of field area.

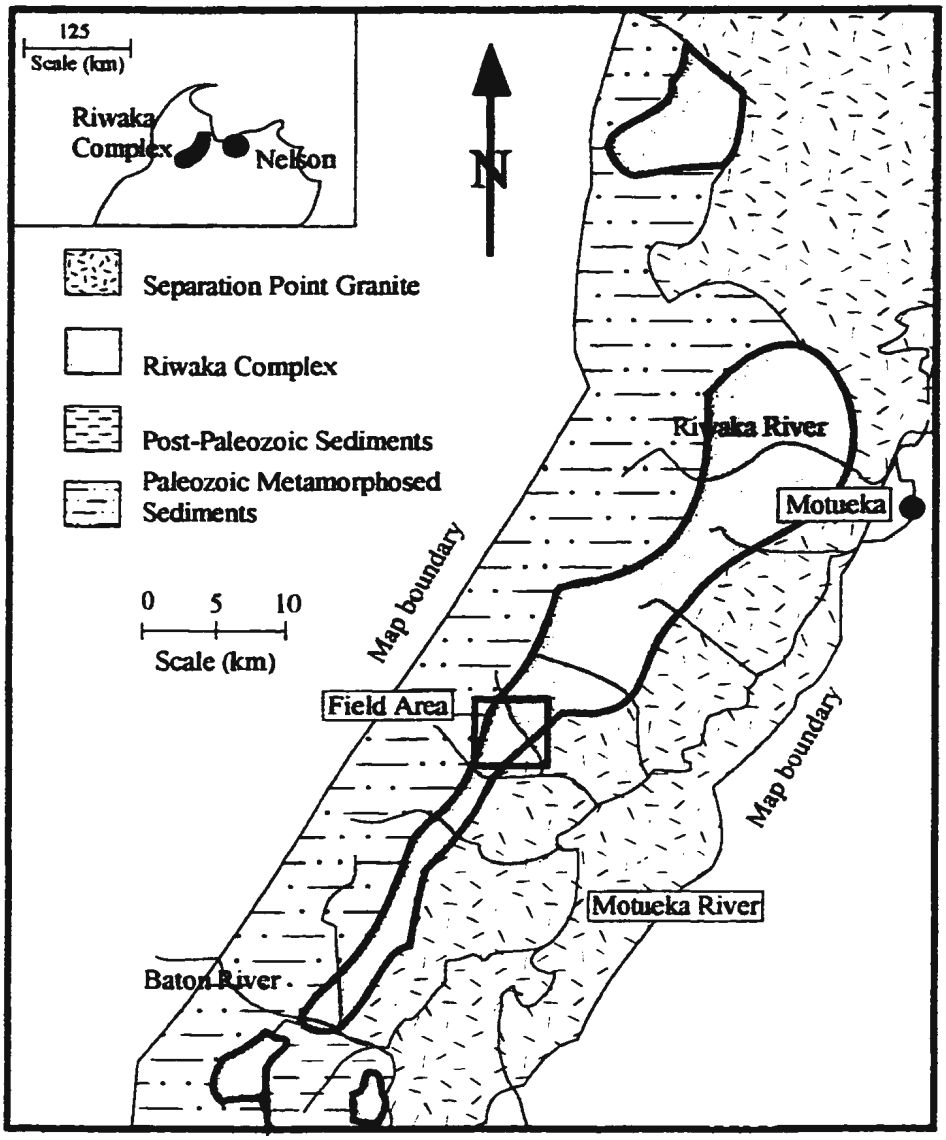

Figure 1.3 Regional geology of the northwestern part of the South Island of New Zealand.

South Graham Rivers using topographic maps at a scale of 1:6000. Approximately 175 samples were collected in the field. Another 35 samples of drillcore were also made available by the government (then DSIR, Department of Scientific and Industrial Research) drillcore storage facility in Christchurch. Additional references, information about previous work and 1:6000 topographic base maps were obtained from the DSIR offices in Nelson and Lower Hutt.

1.4 Physiography

The majority of the Riwaka Complex lies in the relatively high and steep terrain (up to 700 m above sea level) of the Mount Arthur foothills. The area is a mixture of pasture, scrub land, native forest and exotic pine forest plantations. The field area consists of steep hills covered mainly in gorse and rotting stumps with some small areas of native forest (Plate 1.1). Much of this forest had been burned-over a number of years before it was visited for this project. Outcrop is limited to road cuts and small streams, making accurate correlation and field mapping difficult (Plate 1.2).

1.5 Previous Work

Previous work on the Riwaka Complex and more specifically the Graham Valley area is considered in two parts. The first provides a detailed account of the previous geological

Plate 1.1 Mount Arthur foothills covered in native shrubs and forests.

Plate 1.2 Typical outcrop in the Graham Valley area of the Riwaka Complex.

work. The second is a brief account of the mineral exploration history of the Graham Valley area.

1.5.1 Earlier geological work

The first geological work undertaken in this area was by McKay (1879). He mapped the area between the Baton and Graham Rivers (Figure 1.3), and recognized that the basic rocks in the area were of an igneous origin and that they intruded metasedimentary rocks, then considered to be of Silurian age, at Baton River. He thus assigned a Devonian age to the Riwaka Complex.

In their detailed mapping Henderson et al. (1959) showed these basic rocks as a discontinuous, linear intrusive belt. Two years later Grindley (1961) described the basic rocks as metavolcanics, mapping them as the Riwaka Metavolcanics of Devonian age. Work carried out by Willis (1965) confirmed the earlier work of Henderson et al. and McKay, but suggested that the rocks were post-Devonian intrusives. In the same year, Cooper (1965) mapped the rocks as the Riwaka Group consisting of a lower gneissic metasedimentary unit and an upper metavolcanic unit of Devonian age.

Gill and Johnston (1970) showed that the basic rocks continue without interruption from the Baton River northward to the Riwaka River Valley. They noted that all the contacts, with the exception of fault contacts, were intrusive and cross-cut the metasediments. Their petrological and geochemical analyses revealed that all of the basic rocks were of an igneous

origin, although many had undergone extensive amphibolitization and serpentinization, and that some of the rocks were partially recrystallized.

Gill and Johnston (1970) separated the metasediments from the basic intrusive rocks. The metasediments were mapped as Onekaka Schist and the term Riwaka Complex was confined to the intrusive rocks. These include peridotites, pyroxenites, gabbros and pyroxene - mica and hornblende - quartz diorites.

During field work in the Graham Valley area of the Riwaka Complex by M. R. Johnston in 1967, a large gossan outcrop was discovered. This outcrop contained abundant sulphides; mainly pyrrhotite, pyrite and chalcopyrite. Further work revealed that the pyrrhotite was accompanied by pentlandite. This discovery led to further exploration work in the area in the hopes of finding a Cu-Ni deposit of economic importance.

The next detailed study was by Bates (1977); it concentrated on the Graham Valley. He divided the Riwaka Complex into sixteen units ranging from dunites to diorites, and gave detailed descriptions of mineralized horizons, suggesting that the sulphides were primary and were present in the magma as immiscible droplets at the time of emplacement. He suggested that the initial magma was not sulphur saturated but that saturation occurred at an advanced stage of crystallization. In addition, he considered that emplacement of the intrusion was controlled by tensional fracturing in mid - Paleozoic marginal basin sediments as a result of subduction of oceanic crust to the east. Bates concluded that the intrusion occurred at several centres along a major fracture, that it occurred in several phases and that magmatic differentiation took place prior to emplacement. Continuing subduction after emplacement

resulted in basin closure, the deformation of host sediments and the intrusion of the Separation Point Granite.

Bates (1977) classified the Riwaka Complex as tholeiitic and a member of the Picritic subgroup of Naldrett and Cabri (1976). He suggested that the intrusion was Permian in age and that similar rocks which outcrop in Fiordland, on the east side of the Alpine Fault, may be part of the same complex.

Maxwell (1977) divided the sulphides into three major types: early cumulate sulphides, late cumulate sulphides and interstitial sulphides. His detailed petrographic work led Bates (1980a) to subdivide the Riwaka Complex into three main suites: the Fractionation Suite, the Cumulus Gabbro and the Late Stage Diorite. Subsequently, Bates (1980b) published a summary of his work. Pirajno (1980), in an overview paper related to magmatic sulphide deposits in New Zealand, concurred with the work of Bates (1977, 1980a, 1980b) and Maxwell (1977).

1.5.2 Exploration history

After the initial discovery of sulphides by M. R. Johnston in 1967, McIntyre - Porcupine Mines obtained mineral rights to the majority of the Riwaka Complex. They drilled a total of 22 diamond drill holes (ddh) in three main target areas. When they withdrew in 1970, Western Compass N. L. obtained title and drilled an additional 4 ddh at Prospect Creek (original discovery by M. R. Johnston). They abandoned the properties in 1972.

From 1974 until 1978, the central part of the Riwaka Complex was explored in a joint venture between Otter Minerals and Gold Mines of New Zealand. They drilled one ddh but abandoned the property in 1979. No further work was done until Sigma Resources acquired the mineral rights in 1987. They carried out some sampling, mapping and trenching in 1987 and 1988. They still held the mineral rights in the Graham Valley at the time when this field work was completed (September 1991). For a detailed exploration history, readers are refered to Cowden et al. (1988).

1.6 Purpose and Scope

The purpose of this thesis is to develop an understanding of the geochemical evolution of the mafic and ultramafic rocks that make up a large portion of the Riwaka Complex in the Graham Valley area. This is done using field relationships, petrography, mineralogy and whole rock geochemistry. The data is used to: classify the igneous rocks; put some constraints on the parental magma composition; and test the economic viability of the Cu - Ni sulphides and platinum group elements.

Chapter 2

Regional Geology

2.1 Introduction

The complex geological evolution of New Zealand can be attributed to its position with respect to the Indian - Australian, Antarctic and Pacific plates (Figure 1.1). To understand the present day geology, one needs to consider a series of superimposed major tectonic events.

2.2 Regional Geology of New Zealand

New Zealand can be divided into two distinct geological provinces, an older Western Province, and a younger Eastern Province (Figure 2.1). These provinces are separated by the Median Tectonic Line (Landis and Coombs, 1967). The Western Province consists of a lower Paleozoic assemblage of sedimentary, volcanic, intrusive and metamorphic rocks. Because of dextral faulting along the Alpine Fault this Province now occurs in two major regions, northwest Nelson and Fiordland, separated by approximately 500 km. Uplift and erosion has exposed the higher grade metamorphic rocks in Fiordland making correlation of lithologic units in the two regions difficult (Korsch and Wellman, 1988). The crust of the Western

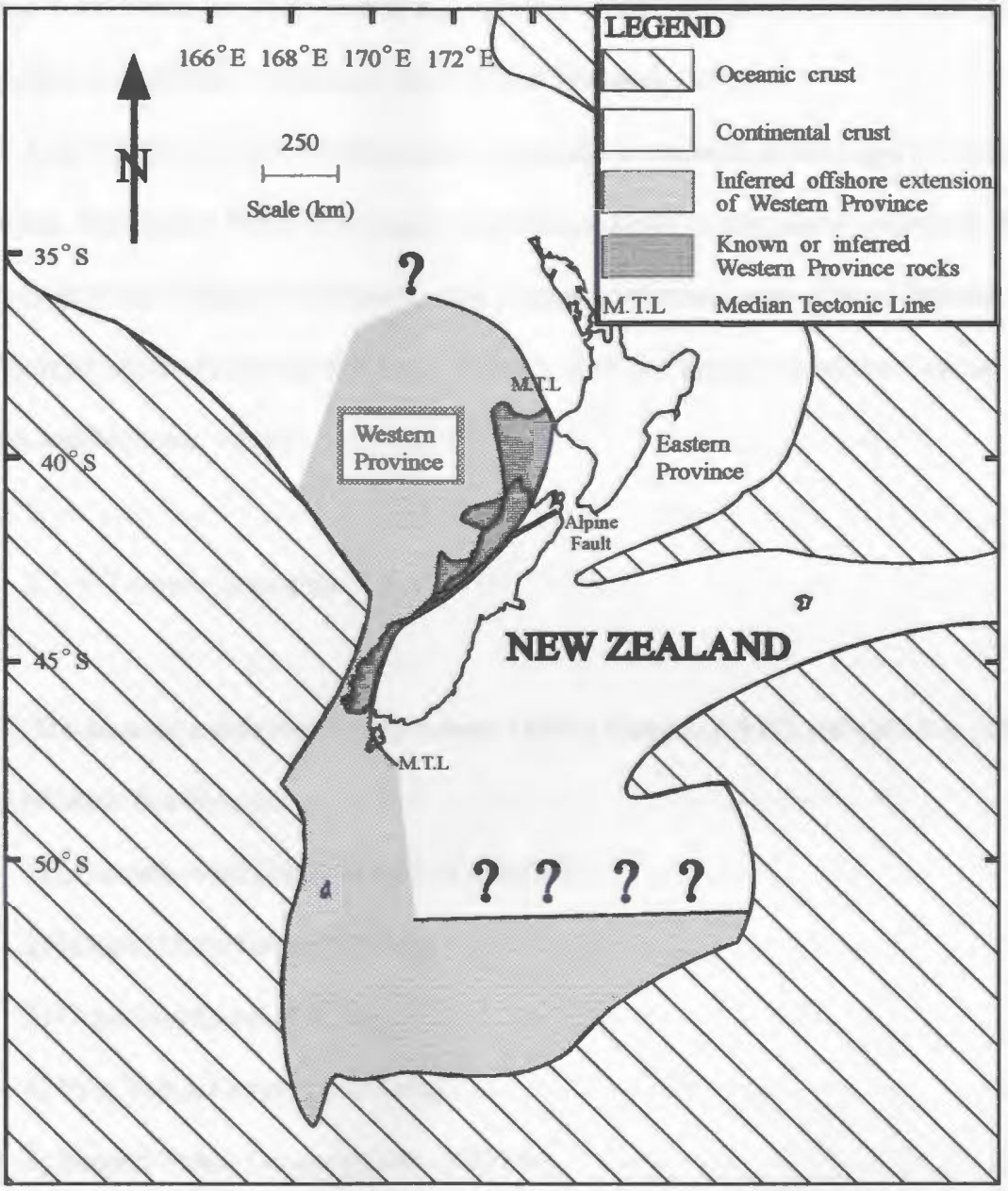

Figure 2.1 Map depicting the two main geological provinces of New Zealand, an older Western Province and the younger Eastern Province.

Province is Ordovician or older, while in the Eastern Province nowhere is it older than Upper Carboniferous to Middle Cretaceous (Korsch and Wellman, 1988).

The Western Province is believed to represent a remnant of the super - continent Gondwana. The Eastern Province represents material accreted to this microcontinental sliver or derived from the margin of Gondwana. The present continental core of New Zealand was isolated from Australia during the Early Tertiary with the formation of the Tasman Sea (Korsch and Wellman, 1988).

2.2.1 Tectonic evolution

The tectonic events reported by Adams (1975), Cooper (1979) and Grindley (1980) for the Western Province are:

1) unnamed event (Early to Mid - Cambrian)

2) Haupiri Disturbance (525 Ma)

3) Greenland Event (440 Ma)

4) First Tuhua Orogeny (400 Ma)

5) Second Tuhua Orogeny (380 - 360 Ma)

6) Rangitata Orogeny (120 - 100 Ma)

7) Kaikoura Orogeny (25 Ma - present day)

The Second Tuhua Orogeny was the first to affect all parts of the Western Province

simultaneously (Aronson, 1968; Hunter, 1977; Oliver, 1980; Harrison and McDougall, 1980). This orogeny represents the amalgamation of Western Province terranes, with associated metamorphism and tectonism, and with the ensuing emplacement of granitoid rocks, marks the consolidation of much of the Western Province basement rocks (Bradshaw et al., 1980).

The Tuhua Orogeny was followed by the Rangitata Orogeny, which resulted in the juxtaposition of the Eastern Province against the margin of Gondwana (Crook and Feary, 1982). Bradshaw (1989) suggested that there may have been several phases of the Rangitata Orogeny. During the first phase a convergent margin developed on the eastern margin of Gondwana and was active throughout most of the Mesozoic. At this time the six units of the Eastern Province were brought together. During the second phase, in the latter part of the Early Cretaceous, this convergent tectonic regime was replaced by extension and rifting. The final phase of the Rangitata Orogeny involved a period of major shortening, possibly due to the closure of a back - arc basin, which ceased approximately 105 + 5 Ma (Bradshaw, 1989). These phases of the Rangitata Orogeny resulted in the formation and consolidation of the present day continental crust in New Zealand.

Sporli (1987) proposed that Cretaceous - Early Tertiary rifting resulted in the New Zealand microcontinent becoming an independent entity. The microcontinent became separated from Australia by the formation of the Tasman Sea. However, it is not clear whether the Tasman Sea originated as a back - arc basin or was generated from a ridge - transform junction (Sporli, 1987).

The Kaikoura Orogeny began with increasing separation of Australia and Antarctica

at about 25 Ma. It established the presently active Pacific - Indian convergent transform plate boundary, including the Alpine Fault, together with the formation of the calc - alkaline Taupo Volcanic Zone (Figure 2.1). Increasingly stronger convergence across the plate boundary led to oroclinal bending of New Zealand and to uplift in excess of 10 mm per year along the Alpine Fault (Sporli, 1987).

2.3 Western Province

The nomenclature adopted here is that of Cooper (1989) which recognizes two main terranes in the Western Province, the Buller Terrane and the Takaka Terrane (Figure 2.2). The Buller Terrane is the same as the Western Sedimentary Belt of Cooper (1979) and the Greenland Terrane of Korsch and Wellman (1988). The Takaka Terrane is the same as the Central and Eastern Sedimentary Belts of Cooper (1979) and the Cobb and Arthur Terranes of Korsch and Wellman (1988).

2.3.1 Buller Terrane

The Buller Terrane consists of three main units; the Constant Gneiss of the Charleston Metamorphic Group (Shelley, 1970), the Greenland Group, and the Karamea Batholith.

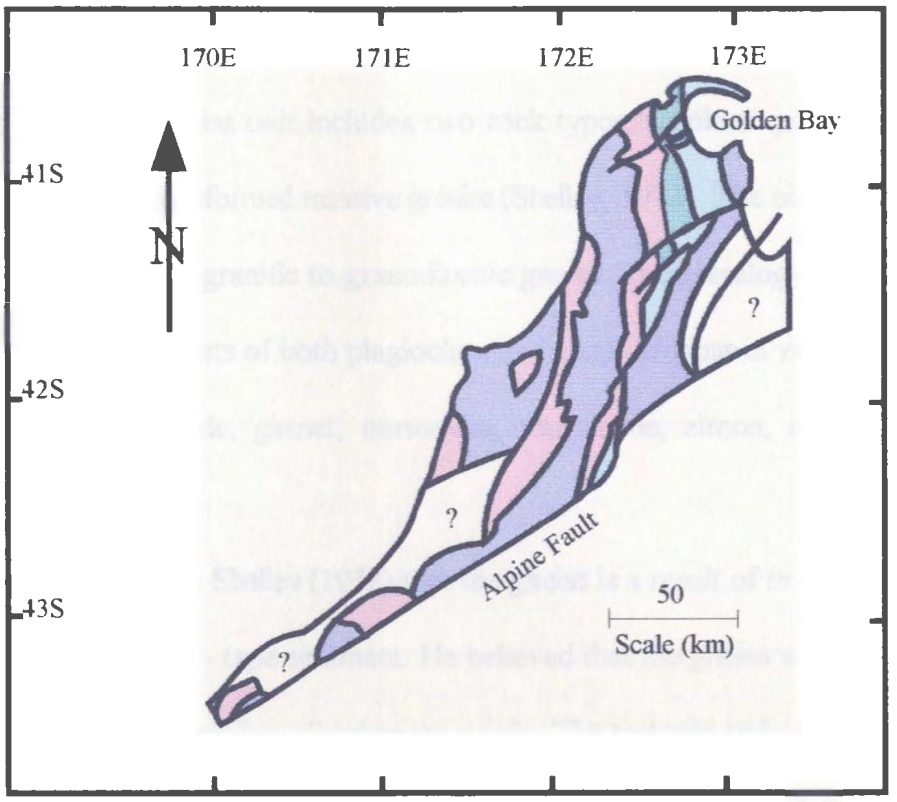

Figure 2.2 Distribution of Takaka Terrane (Central and Eastern Sedimentary Belts) and Buller Terrane (Western Sedimentary Belt) after Cooper (1979).

2.3.1.1 Constant Gneiss unit

The Constant Gneiss unit includes two rock types; an older polyphase deformed gneiss, and a relatively undeformed massive granite (Shelley, 1972). The older gneiss is a well foliated, phenocryst - rich granitic to granodioritic gneiss. Its mineralogy consists of quartz and biotite, with phenocrysts of both plagioclase and alkali feldspar in varying proportions. Accessory minerals include; garnet, muscovite, tourmaline, zircon, apatite and orthite (Shelley, 1972).

It was suggested by Shelley (1972) that the gneiss is a result of *in situ* partial melting of undeformed, greywacke - type sediment. He believed that the gneiss was formed in a thin zone between extensive granites of unknown origin. The tectonic style is one of flattening and arching over rising granite walls, with gravity sliding down the flanks.

The younger massive granite contains perthitic microcline, as both phenocrysts and a ground mass phase, oscillatory - zoned plagioclase, quartz, muscovite and biotite (Shelley, 1972).

2.3.1.2 Greenland Group

The Greenland Group is a sedimentary package that consists of a thick (minimum 1600m) sequence of mainly grey - green, highly indurated sandstones and mudstones (Laird, 1972). Some minor rock types in this group include: calc - schist, schistose marble, pink and

green tuff interbedded with sandstone, and biotite schist (Mutch, 1964). Conglomerate units are intercalated with the sandstone and mudstone belts. These rocks occupy an area west of the Alpine Fault and are exposed discontinuously from Milford Sound to Karamea.

Laird (1972) described the majority of sandstones as fine - to medium - grained sand, poorly sorted with angular grains floating in a fine - grained matrix. The sandstones are quartz - rich with minor albite and sodic oligoclase, the former, in some places, exhibiting myrmekitic texture. Quartz, plagioclase and rock fragments make up the majority of the rock, with some mica, pyrite and rare ferromagnesian minerals. The sandstones all lie in or near the subfelsarenite and sublitharenite fields of Folk et al. (1970) (Laird, 1972).

Laird (1972) suggested that the provenance of the detrital grains was an acidic terrane. He preferred a granitic or gneissic source because of the presence of detrital sodic oligoclase crystals, some with myrmekitic texture. Korsch and Wellman (1988) agreed with this theory and went further, suggesting that the source was likely either Australia or Greater (East) Antarctica.

The Greenland Group is a turbidite sequence, probably deposited as a submarine fan deposit (Laird, 1972). It is thought to have been deposited in the Ordovician. Fossils have provided ages of approximately 500ma (Cooper, 1974); this is in close agreement with Rb - Sr isochron argillite ages of 495 + 11ma (Adams, 1975).

2.3.1.3 Karamea Batholith

The term Karamea Batholith was used by Tulloch (1983) to refer to all granitic rocks in Westland, west and south of the Eastern Sedimentary Belt (Figure 2.3). The batholith consists of two main suites; the S - type Karamea Suite and the I - type Rahu Suite. Each of these in turn is made up of a number of separate plutons, which have two and possibly four distinct ages ranging from Silurian to Cretaceous (Tulloch, 1983). The following is a brief description of the most abundant rock types of each suite; for more detailed description readers are referred to Tulloch (1983).

2.3.1.3.1 Karamea Suite

Tulloch (1983) uses the term Karamea Suite to include the calc - alkaline to alkaline, mica and quartz - rich granitoids of mid - Paleozoic age. This suite contains relatively large plutons (> 150 km^2) and comprises the bulk of the Karamea Batholith.

The most widespread rock types are biotite granodiorites and tonalites. They are coarse - grained, inequigranular to porphyritic and commonly foliated (Tulloch, 1983). Within this suite the potassium feldspar is generally maximum microcline, with some minor twinning. Plagioclase compositions range from andesine to albite and the crystals generally lack complex zoning or twinning. The rocks also contain abundant quartz and biotite. Hornblende is a rare phase in the more mafic varieties, while almandine garnet is common in the

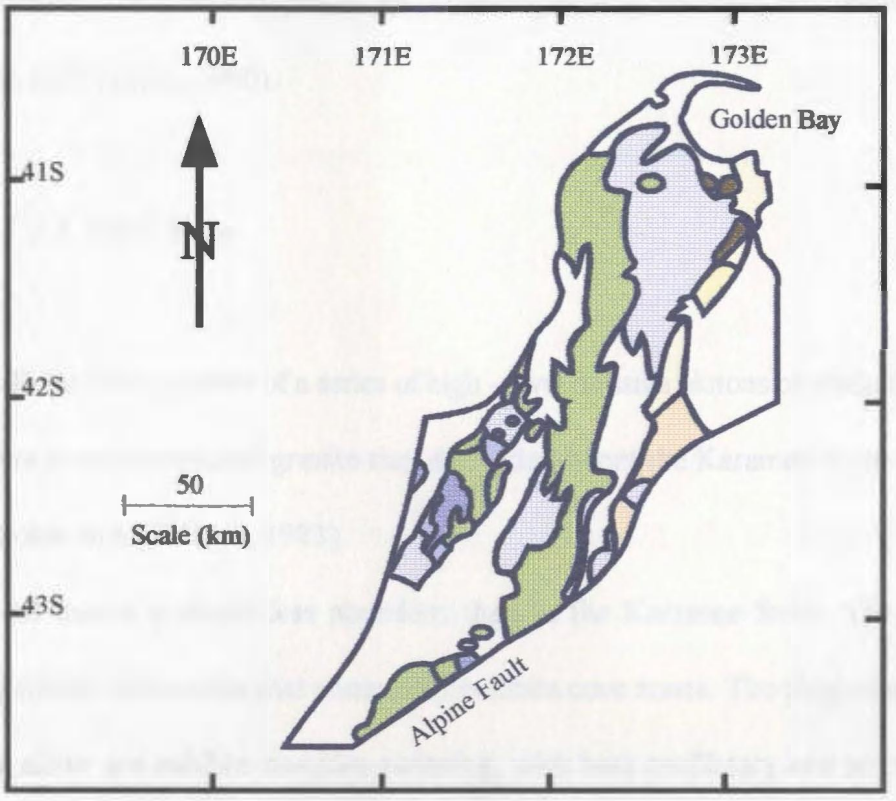

Legend

- Karamea Batholith (Karamea Suite, Rahu Suite)
- Separation Point Batholith
- Riwaka Igneous Complex
- Rotorua Igneous Complex
- Sedimentary rocks
- Nonmarine conglomerates
- Weakly metamorphosed sedimentary rocks
- Sillimanite-grade metasedimentary rocks

Figure 2.3 Distribution of intrusive rocks in the Western Province after Tulloch (1983).

leucocratic phases. The accessory phases are commonly apatite, ilmenite, and zircon (Tulloch, 1979; Smale and Nathan, 1980).

2.3.1.3.2 Rahu Suite

The Rahu Suite consists of a series of high - level massive plutons of medium - grained calc - alkaline granodiorite and granite that discordantly cut the Karamea Suite. They have a Late Mesozoic age (Tulloch, 1983).

Modal quartz is much less abundant than in the Karamea Suite. The potassium feldspar is perthitic microcline that commonly exhibits core zones. The plagioclase is calcic oligoclase to albite and exhibits complex twinning, with both oscillatory and normal zoning. Biotite is the only mafic phase with the exception of muscovite in the more evolved members of the suite. Accessory minerals include: magnetite, magnetiferous ilmenite, epidote, allanite, sphene, apatite, and zircon (Tulloch, 1983).

2.3.2 Takaka Terrane

The Takaka Terrane consists of complexly deformed Middle Cambrian to Early Devonian mafic and intermediate to felsic volcanics, volcanogenic and clastic sediments, ultramafic and mafic to granitic intrusive rocks. The oldest rocks are found to the west with a sequence of progressively younger rocks to the east.

The sedimentary and metamorphic units are summarized in Table 2.1. They have been intruded by four distinctive belts of igneous rocks; the Cobb Igneous Complex, the Rotorua Igneous Complex, the Riwaka Complex and the Separation Point Batholith.

2.3.2.1 The Cobb Igneous Complex

The Cobb Igneous Complex is interpreted as a stratiform ultramafic - mafic layered intrusion, approximately 2500 m thick (Grindley, 1971; Hunter, 1977). Hunter (1977) divided the intrusion into three parts, a lower zone of serpentinized layered peridotite and dunite, an intermediate transitional zone of partly serpentinized pyroxenites and an upper zone of gabbro.

The lower zone contains a base of dunite and well developed layered orthopyroxenite and harzburgite. The transitional zone, approximately 700m thick, has a base of orthopyroxenite that grades upward into websterite with increasing abundance of clinopyroxene. The overlying gabbros of the upper zone contain lenses of cumulate orthopyroxenite and websterite towards the base of the zone, ranging upwards to amphibolites, fine - grained epidiorites and quartz - albite dolerites (Grindley, 1980).

2.3.2.2 Riwaka Complex

The Riwaka Complex is the focus of this thesis and will be described in considerably

Table 2.1 Sedimentary and metamorphic formations of the Takaka Terrane.

TERRANE AND AGE	LITHOLGY	THICKNESS
Upper Ordovician		
Mount Patriarch Group		
Baldy Formation	Unfossilifeous sheared phyllitic siltstone and sandstone	100m
Summit Limestone	Fossiliferous, oolitic, micritic to sandy limestone	300m
Mount Patriarch Formation	Calcareous sandstone, siltstone and limestone	200m
Upper Cambrian		
Haupiri Group		
Anatoki Formation	Well bedded quartz sandstone of various colors	600m
Lockett Conglomerate	Non - marine conglomerate	
Tasman Formation	Finely laminated, green siltstone and mudstone	
Devil River Volcanics	Spilitised basic to intermediate volcanics	
Waingaro Schist	Volcanic derived, weakly foliated schist	200-600m
Balloon Formation	Dark siliceous sandstone and siltstone	2000m

Table 2.1 (continued) Sedimentary and metamorphic formations of the Takaka Terrane.

TERRANE AND AGE **Lower Devonian**	LITHOLGY	THICKNESS
Baton Formation	Massive, thick bedded, grey to blue, calcareous mudstones and siltstones, with thin shale and limestone beds.	2600m
Onekaka Schist	Quartz-albite-biotite-clinozoisite-muscovite-garnet schist and quartzite.	1300m
Hailes Quartzite	Grey to black quartzite, sandy shale, and quartzose sandstone.	1200m
Wangapeka Formation	Graphitic to silicious argillite, with quartz greywacke units.	1200m
Arthur Marble	Cream to grey calcite marble, with minor interbedded schist and quartzite.	1000m
Pikikiruna Schist	Biotite-garnet schist with lenses of quartzite.	

more detail in later chapters. The descriptions given here summarize the results of previous work. Bates (1980a) suggested the Riwaka Complex is a complex multiphase intrusion emplaced at a number of centres along a major fracture zone (Figure 2.4). He suggested that a tholeiitic magma was emplaced in primary magma chambers and was then intruded to higher levels as lopolithic bodies which form the main mass of the Riwaka Complex.

The rocks of the Riwaka Complex have been divided into three main groups; the Fractionation Suite, the Cumulus Gabbro, and the Late Stage Diorite (Bates, 1977). The Fractionation Suite makes up the bulk of the Complex and contains rocks that range in composition from dunite to feldspathic pyroxenites.

The Cumulus Gabbro is a hypersthene gabbro. It is somewhat restricted and is mostly seen in drill core, but is of importance because it contains significant sulphides (Bates, 1980a).

The Late Stage Diorite is described as a late stage, high level intrusive suite that is widespread throughout the Complex and in adjacent country rocks on the western side of the intrusion (Bates, 1980a). The lithologies in this suite range from leucocratic gabbro to granodiorite.

2.3.2.3 Separation Point Batholith

The Separation Point Batholith is an I - type granite and is approximately 114 my old (Cretaceous) (Tulloch, 1983; Harrison and McDougall, 1980).

It is composed of three elongate segments which average 10 km wide and have a

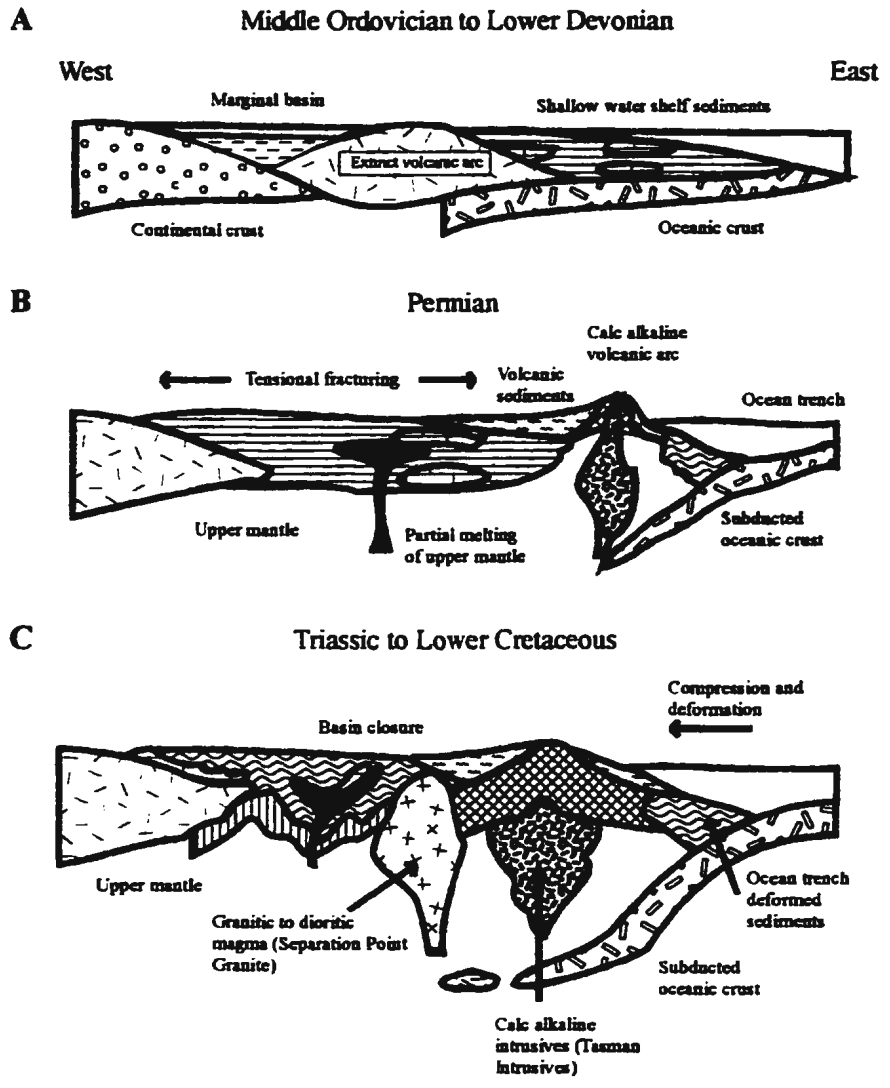

Figure 2.4 Schematic model for the intrusion of the Riwaka Complex after Bates (1980b).

length of 120 km. The northern segment is zoned from equigranular biotite - hornblende granodiorite and quartz - diorite in the west (Grindley, 1971; Reid, 1972) to porphyritic biotite granite in the east (Henderson, 1950). Accessory minerals include; magnetite, epidote, apatite and abundant sphene.

Approximately two - thirds of the central segment comprises the Pearse Granodiorite. It is composed of plagioclase, hornblende and biotite, and minor pyroxene, K - feldspar and quartz. Accessory minerals include epidote and sphene (Grindley, 1980). The other third of this segment comprises a uniform (hornblende) biotite granodiorite varying to granite.

2.3.3 Tectonic history; Western Province

Early regional mapping by Henderson and co-workers in the 1920`s established four broad stratigraphic units; the Lower Aorere Series (now Aorere Group), the Mount Arthur Series (now equivalent to the Mount Arthur and Mount Patriarch Groups), the Haupiri Series (now Haupiri Group), and the Baton Series (now Ellis and Baton River Groups). Cooper (1989) established a general N-S trend of the belts and a right lateral offset of boundaries by NE-SW trending younger faults. Henderson (1923) regarded the Mount Arthur Series as the oldest (Ordovician) followed by the Aorere, Baton River, and Haupiri Series (Upper Devonian). No model of regional structural development was provided in this early work; that was not done until Grindley`s work in 1961.

Grindley (1961) proposed a model to explain the regional distribution of sedimentary

and volcanic terranes in the northwest Nelson region. The model is further discussed in Grindley's later work (1978; 1980). He suggested that the Central Sedimentary Belt was emplaced as an allochthonous stack of nappes and overthrust sheets across the autochthonous Western and Eastern Sedimentary Belts. The overthrusting was thought to have occurred during the first phase of the Tuhua Orogeny. Cooper (1989) however, suggested that there are major structural and stratigraphic problems with this model. He concluded that the later models proposed by Shelley (1975) and Crook and Feary (1982) are more enlightening.

Shelley (1975) proposed that the entire Phanerozoic development of New Zealand can be attributed to four eastward migrating cycles related to westward dipping Benioff zones, two of which were located within the Western Province. The first cycle represents a non - orogenic andesitic arc bordering the east side of the Buller terrane. Shelley (1975) described a pre - Tuhuan Orogeny (Greenland Event) during the Late Ordovician which produced paired metamorphic belts and a locus for granite intrusion. The Tuhuan Orogeny produced another paired metamorphic belt and more granites. The median boundaries lie progressively eastward (Figure 2.5).

Crook and Feary (1982) envisaged a similar model for the formation of the Western Province. However, they suggested that only one fore - arc environment existed (Takaka Terrane, Figure 2.2), and considered that the west facing Tuhua volcanic arc was active from the Late Proterozoic until the Middle or Late Cambrian. Post subduction sediments, neritic in the east and flyschoid in the west, accumulated on the Tuhua accretionary prism from Late Cambrian to Early Devonian. Metamorphism, granite plutonism and accompanying

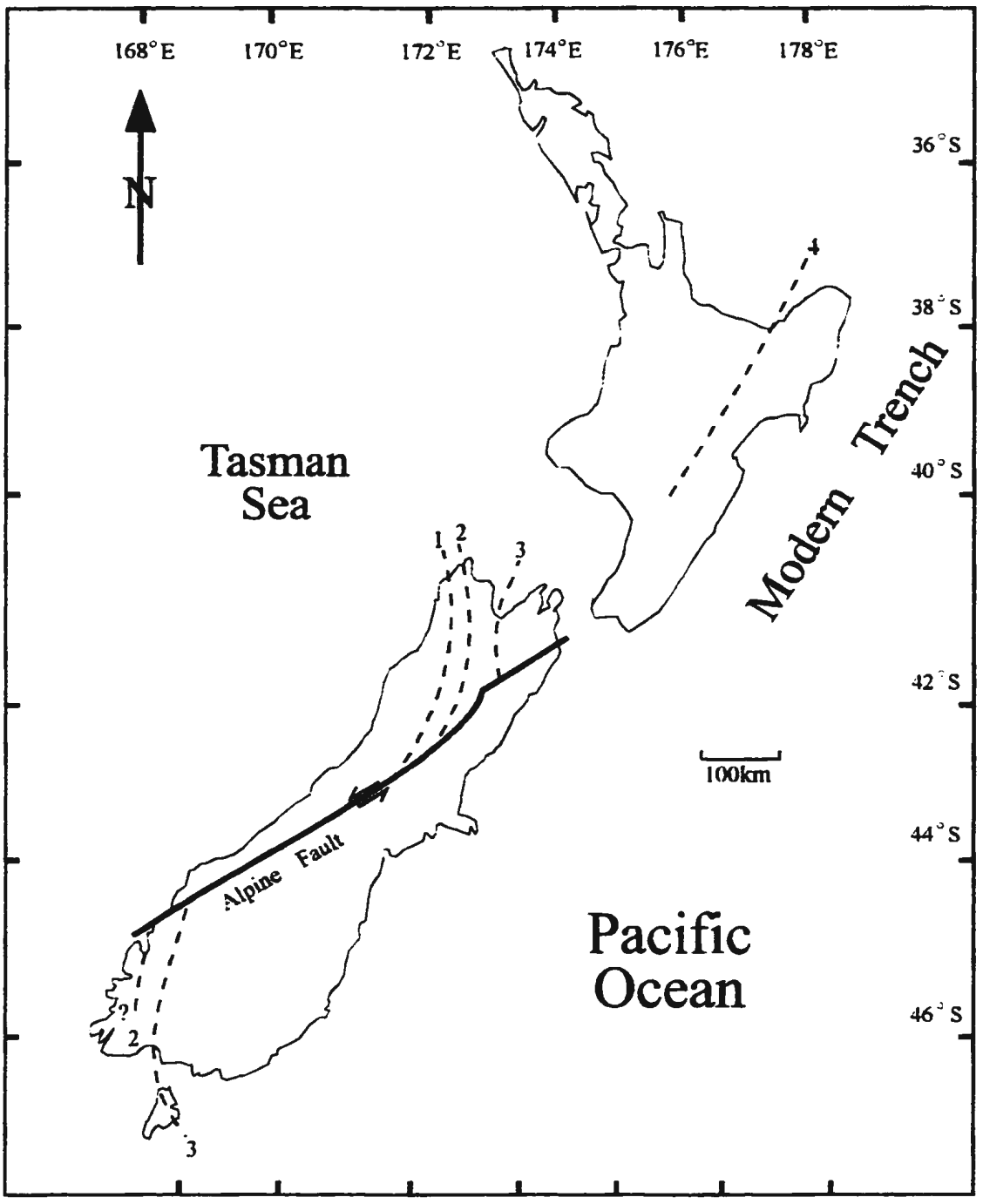

Figure 2.5 Median boundaries of paired metamorphic belts, separating low pressure granitic activity on the west from higher pressure metamorphism (without granites) on the east: 1. pre-Tuhua Orogeny; 2. Tuhua Orogeny; 3. Rangitata Orogeny; 4. Kaikoura Orogeny, after Shelley (1975).

deformation took place in the Middle to Late Devonian (Tuhua Orogeny).

2.4 Eastern Province

The Eastern Province consists of six subparallel geologic units (Figure 2.6) that are consistent with formation in a westward dipping subduction zone (Fleming, 1970; Landis and Bishop, 1972; Blake et al., 1974; Coombs et al., 1976; Carter et al., 1978; Sporli, 1978; Wood, 1978; Howell, 1980; Bradshaw et al., 1980; Dickinson, 1982; MacKinnon, 1983; and Malpas et al., 1994).

The six tectonostratigraphic units, from west to east, are:

1) Brooke Street magmatic arc

2) Maitai - Murihiku forearc basin

3) Dun Mountain Ophiolite

4) Caples terrane

5) Haast Schist

6) Torlesse terrane

The Brooke Street magmatic arc is made up of two parallel belts of extrusive rocks, including andesites and primitive island - arc tholeiites. It represents a magmatic arc (Korsch and Wellman, 1988).

The Maitai - Murihiku fore - arc basin deposits are mainly volcanic - derived siltstone

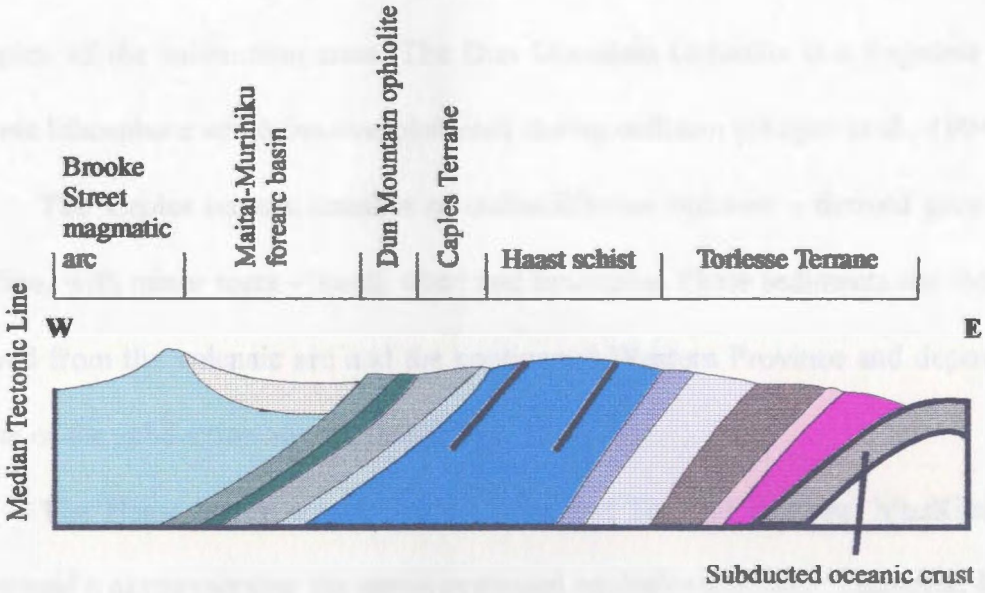

Figure 2.6 Sketch cross - section showing arrangement of Eastern Province units in South Island about 100ma (Korsch and Wellman, 1988).

with some turbiditic sandstone, conglomerate, breccia, limestone and non - volcanic derived sandstone. It was suggested by Carter et al. (1978), Landis (1980) and MacKinnon (1983) that the Brooke Street terrane was the source of sediment for these units.

The Dun Mountain Ophiolite, Caples terrane and the Haast Schist represent the trench complex of the subduction zone. The Dun Mountain Ophiolite is a fragment of ancient oceanic lithosphere which became obducted during collision (Malpas et al., 1994).

The Caples terrane consists of unfossiliferous volcanic - derived greywacke and argillite, with minor meta - basalt, chert and limestone. These sediments are thought to be derived from the volcanic arc and the continental Western Province and deposited in the trench of the subduction zone (MacKinnon, 1983).

The Haast Schist separates the Caples and Torlesse terranes. MacKinnon (1983) interpreted it as representing the metamorphosed equivalents of both. However, Korsch and Wellman (1988) considered it to be a deeply eroded part of the accretionary prism that was once more deeply buried and more strongly deformed by flowage than the rest of the prism.

The Torlesse terrane is made up of quartzo - feldspathic greywacke, argillite, with minor amounts of basalt, chert, conglomerate and limestone (Dickinson, 1971, 1982; Beggs, 1980; MacKinnon,1983). About 99 % of the exposed Torlesse terrane is greywacke and grey to black siltstone that is largely of flyschoid character (MacKinnon, 1983). The rocks of the Torlesse terrane and the Haast Schist form the basement to large parts of the North and South Islands.

It has been suggested by various workers (e.g. Blake et al., 1974; Coombs et al.,

1976; Andrews et al., 1976; Carter et al., 1978; Wood, 1978; Sporli, 1978; Bradshaw et al., 1980; Howell, 1980; Crook and Feary, 1982) that the sediments of the Torlesse terrane were tectonically juxtaposed outboard of the arc system. The origin of these sediments is, however, problematic. Bradshaw et al. (1980) suggested that the sediment was not derived from the Brooke Street terrane, but rather from a large continental source. Their source was Marie Byrd Land across a transcurrent section of the Gondwana - Pacific margin. Whatever the source, it is generally accepted that the Torlesse terrane is an accretionary prism that grew oceanward from the Caples terrane (Korsch and Wellman, 1988; MacKinnon, 1983).

2.4.1 Tectonic history; Eastern Province

As demonstrated above, the Eastern Province, most agree, originated at an active plate margin. During the Rangitata Orogeny these terranes were accreted to the eastern margin of the Cretaceous Western Province along the present day Median Tectonic Line.

2.5 Summary

The regional geology of the South Island of New Zealand consists of two main geological provinces; the older Western Province (Cambrian - Devonian), and the younger Eastern Province. Since this author's study area lies within the Western Province, the Eastern Province rocks will be discussed no further.

The Western Province consists of sedimentary and igneous rocks related to one or more subduction zone complexes. Metamorphic and intrusive rocks in the area are thought to be related to tectonic processes within these complexes.

CHAPTER 3

Field Relationships and Petrography

3.1 Introduction

Gill and Johnston (1970) introduced the revised term Riwaka Complex to represent the complex suite of intrusive mafic and ultramafic rocks extending from the Baton River north to the Riwaka River Valley (Figure 1.3). Also included are similar rocks mapped by Grindley (1961) as the Riwaka metavolcanics and Rameka intrusives. The present study concentrates on the Riwaka Complex and host rocks in the Graham Valley. Over two hundred samples were collected and these were petrographically studied, looking at silicate and sulphide phases under both transmitted and reflected light. Mineral chemistry was analysed by electron microprobe on selected samples and used in mineral classifications.

3.2 Intrusive History of Graham Valley Area

3.2.1 Basement rocks

The basement rocks found in the Graham Valley area consist of a variety of different metamorphic packages, the most prominent of which is the Arthur Marble which occurs

continuously along the north-western contact of the Riwaka Complex (Figure MA - 1; map appendix). The Arthur Marble varies from a very pure, cream to pale grey, calcite marble, to a siliceous, graphitic, dark grey marble (Plate 3.1) with minor interbedded schist and quartzite (Plate 3.2) (Suggate et al., 1978). Its thickness is estimated at approximately 1000 m and the unit has a Lower to Upper Ordovician age (Grindley, 1980).

Other metamorphic rocks which have been intruded by the Riwaka Complex include the Wangapeka Formation and Hailes Quartzite. The Wangapeka Formation conformably overlies the Arthur Marble. Its lower part is dominantly graphitic argillite, its upper section is a siliceous argillite with quartz greywacke units and thin quartzite bands toward the top. This formation is thought to be Upper Ordovician in age and its thickness has been estimated at 1200 m (Suggate et al., 1978; Grindley, 1980).

The Hailes Quartzite conformably overlies the Wangapeka Formation and the Arthur Marble. It is a grey to black quartzite, together with sandy shale, slate, and quartzose sandstone (Suggate et al., 1978). The unit has an age of Middle to Upper Silurian and its thickness is thought to be 1200 m (Grindley, 1980).

Grindley (1961) named the higher grade metamorphic equivalents of the Wangapeka Formation and Hailes Quartzite, the Onekaka Schist. It consists mainly of quartz - albite - biotite - clinozoisite - muscovite - garnet (staurolite) schist and quartzite (Suggate et al., 1978). It has a thickness of 1300 m (Grindley, 1980; Suggate et al., 1978). Several high grade mineral assemblages have been described, but the significance of these assemblages and the relative effects of the two intrusive igneous complexes (i.e. Riwaka Complex and Separation

Plate 3.1 Arthur Marble.

Plate 3.2 Arthur Marble with interbedded quartzite and schist.

Point Batholith) is not known (Gill and Johnston, 1970).

The eastern contact of the Riwaka Complex with the metamorphic sequences is intrusive and dips to the west. The wall rocks were metamorphosed to the upper "biotite zone" of the greenschist facies prior to the intrusion of the Riwaka Complex (Bates, 1980a).

The western contact is only exposed in one place where a west - dipping fault brings the Riwaka Complex into contact with the Wangapeka Formation. At this location quartzites lie against the Riwaka Complex; these grade rapidly westwards into impure marble and biotite schist (Bates, 1980a). The western contact is interpreted to be faulted along the entire length of the Graham Valley (Bates, 1980a).

3.2.2 Riwaka Complex

The geology of the Riwaka Complex in the Graham Valley has been mapped by previous workers, the most by Bates (1977, 1980a, 1980b) and Maxwell (1977). Bates (1980a) divided the area into three main units based on extensive mapping and petrological studies. The three units are; the Fractionation Suite, the Cumulus Gabbro, and the Late Stage Diorite.

Bates (1980a) further subdivided the Fractionation Suite into the Ultramafic Series, the Hornblende Series, and the Plagioclase Series. The Ultramafic Series includes the sub - units; dunite and peridotite, olivine - pyroxenite and pyroxenite. The Hornblende Series is divided into the units; hornblende - peridotite, hornblende - olivine - pyroxenite, poikilitic

hornblende - pyroxenite and hornblende - pyroxenite. In the Plagioclase Series he only differentiated two units in the field; undifferentiated Plagioclase Series and feldspathic pyroxenites.

The Cumulus Gabbro is made up of equal amounts of hypersthene gabbro and olivine gabbro. Cumulus textures are well developed (Maxwell, 1977).

The Late Stage Diorite has been divided into five mappable sub - units; 1) microdiorite, 2) dolerite, 3) granodiorite, mica diorite and quartz diorite, 4) hornblende diorite, hornblende gabbro and gabbro and 5) porphyritic diorite.

The present study suggests that sub - division of the three main lithologies (i.e. the Fractionation Suite, the Cumulus Gabbro and the Late Stage Diorite) into smaller units is not necessary. The sub - units make description much too complicated, especially when dealing with this type of intrusive complex that has modal mineralogy changing constantly and on a variety of scales. Therefore, the three main divisions put forward by Bates (1980a) (i.e. the Fractionation Suite, the Cumulus Gabbro, and the Late Stage Diorite), are used here.

The Fractionation Suite, the Cumulus Gabbro and the Late Stage Diorite are all thought to be intrusive. Firstly, the Fractionation Suite intruded the basement sediments. The Fractionation Suite was subsequently intruded by the Cumulus Gabbro, and both were then intruded by the Late Stage Diorite (Bates, 1980b).

3.2.3 Late intrusive rocks

The last intrusive rocks in the Graham Valley area are part of the Separation Point Batholith. This intrusive complex is a Lower Cretaceous (Grindley, 1980) batholith composed of three elongate segments which average 10 km in width and a total of 120 km in length (Tulloch, 1983). It intrudes the Riwaka Complex all along its southern contact. Within the Riwaka Complex it is seen in places as aplitic dikes (Plate 3.3).

3.3 Structure of the Riwaka Complex

3.3.1 Deformation within the Riwaka Complex

The structure of the Riwaka Complex is dominated by faulting, but folding is also present. Numerous high angle faults have been documented by various authors (i.e. Gill and Johnston, 1970; Maxwell, 1977; Bates, 1980a and 1980b). However, several low angle thrust faults have also been mapped in the present study (Plate 3.4) and although the amount of movement is not known, the Riwaka Complex appears to be overthrust toward the south. Folding in the area can be observed in well developed steeply dipping shear zones and it appears that the Fractionation Suite is isoclinally folded in places. Aplitic dikes in the area are more openly folded (Plate 3.5).

The relationship between the gabbro and the folded aplitic dikes indicates that

Plate 3.3 Aplitic dikes in the Late Stage Diorite of the Riwaka Complex.

Plate 3.4 Thrust fault in the Fractionation Suite (fault is denoted by the black line).

Plate 3.5 Folded aplitic dikes in isoclinally folded gabbros.

Plate 3.6 Well developed mylonite zone within the Separation Point Batholith.

deformation is post intrusion of the Separation Point Batholith. This is also supported by the development of a well defined mylonite zone within the granite (Plate 3.6). This deformation may have occurred during the Rangitata Orogeny and would thus indicate that the granite was emplaced prior to the end of this tectonic event, in agreement with previous workers results (Tulloch, 1983; Bradshaw, 1989). This is the only documented deformational phase within the Riwaka Complex. Although these features are not well understood, it is not within the scope of this thesis to provide a detailed structural analysis of the area.

3.3.2 Magmatic structure

The most prominent magmatic structure is igneous layering. This is best observed in the field within dioritic rocks (Late Stage Diorite), where layers contain different abundances of plagioclase. The scale of layering in these dioritic rocks ranges from less than a centimetre to several centimetres.

Modal layering is also developed within the ultramafic rocks of the Fractionation Suite. However, it is difficult to see in the field because all phases present (i.e. olivine, clinopyroxene, and amphibole) are very similar looking and due to the lack of outcrop. The layers observed in the field were from 0.5 m to 2 m. These layers could not be traced for more than several metres due to poor exposure, therefore the lateral extent and macroscopic nature of the layers is unknown. Nevertheless, detailed petrographic work reveals well developed modal layering over 10's of metres, with some layers up to 200 m in thickness.

A section was sampled perpendicular to the modal layering of the Fractionation Suite (cross-section A-B on Figure MA-1). The base of the layering was distinguished by the presence of more abundant olivine. Generally this is the earliest phase to crystallize from mafic melts (Campbell, 1977; Wager and Brown, 1968) and would therefore indicate the base of a mafic intrusion. The presence of the Late Stage Diorite at a low level within the stratigraphy of the Fractionation Suite supports Bates (1980a) suggestion that it was emplaced late in the history of the intrusion. However, as a result of poor exposure no intrusive relationships between the Late Stage Diorite and the ultramafic rocks were observed.

3.4 Petrography of the Riwaka Complex

3.4.1 Introduction

The petrography of approximately two hundred thin sections was examined in detail. The classification scheme of Maxwell (1977) and Bates (1980a) was initially used, but proved too specific and ambiguous for the wide variety of modal compositions encountered. Instead their broad classification has been adopted and a wide range of rock types included in each suite. The petrographic descriptions are however, new and may differ from the descriptions of Maxwell (1977) and Bates (1980a). The three broad suites used here include; the Fractionation Suite, the Cumulus Gabbro and the Late Stage Diorite.

Mineral compositions have been determined by use of a Cameca SX-50 electron microprobe. The data collected for the minerals of the Fractionation Suite, the Cumulus Gabbro and the Late Stage Diorite are located in Tables A1 - A9 (Appendix A).

3.4.2 The Fractionation Suite

The Fractionation Suite is dominated by ultramafic rocks. They have a simple mineralogy consisting mainly of medium - to coarse - grained anhedral clinopyroxene and olivine. The rock types range from clinopyroxene bearing dunites to olivine - hornblende clinopyroxenites. Primary amphibole is found in amounts up to 15 %. Accessory magnetite and minor pyrrhotite and chalcopyrite in two samples are also present. Orthopyroxene is noticably absent and plagioclase is very rare, being confined to pegmatitic patches.

The majority of the rocks are cumulate with poikilitic texture (Plate 3.7). In most places olivine crystals are found within clinopyroxene, but the opposite is also seen. Olivine exhibits consertal intergrowth when in contact with other olivine crystals. This also occurs with clinopyroxene in contact with clinopyroxene (Plate 3.8). The primary amphibole and the most of the feldspar are found as interstitial crystals. The crystallization sequence is; olivine and clinopyroxene, opaques, amphibole and feldspar.

The alteration varies widely from sample to sample (samples spaced 25 m apart), reflecting the fact that it is localized along fractures and minor faults.

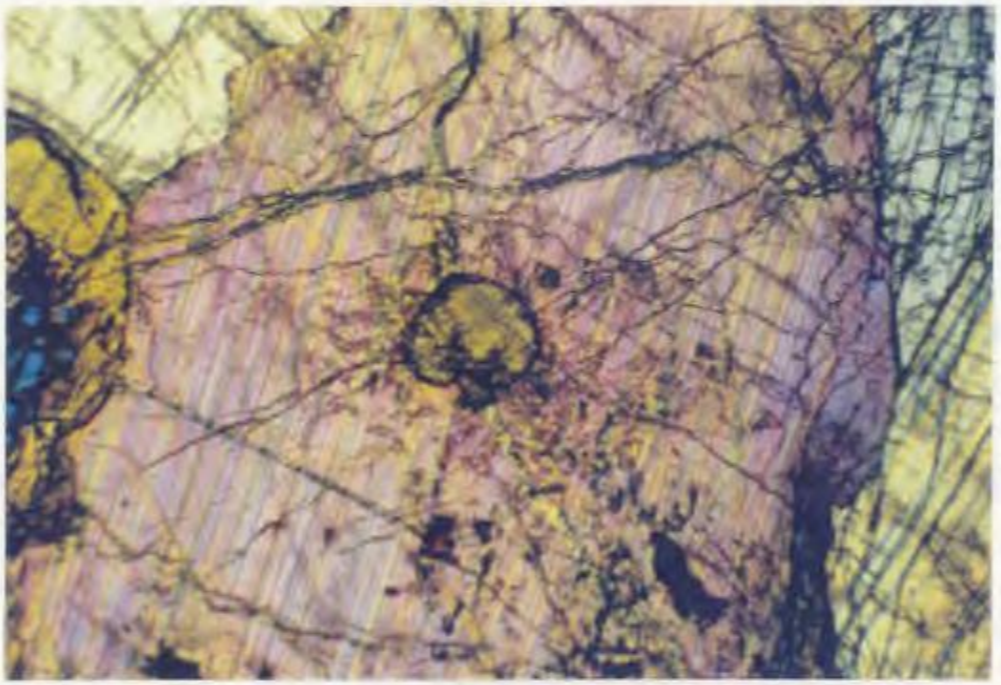

Plate 3.7 Poikilitic texture within the Fractionation Suite, olivine chadacryts inclosed by large oikocrysts of clinopyroxene (10.5 X magnification, XP).

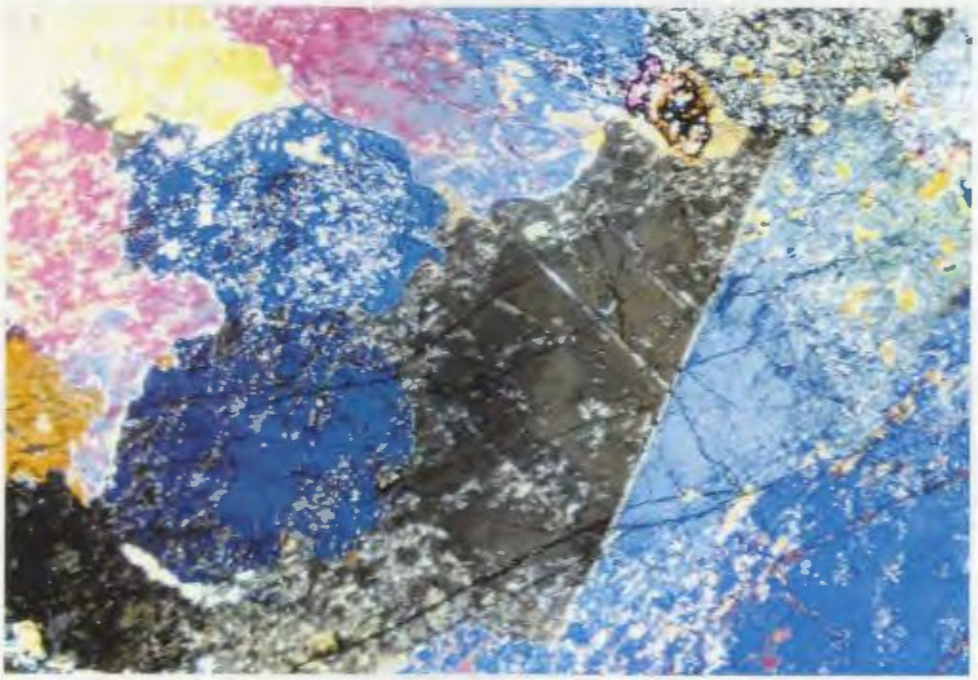

Plate 3.8 Consertal intergrowth of clinopyroxene (20.5 X magnification, XP).

3.4.2.1 Minerals of the Fractionation Suite

3.4.2.1.1 Olivine

Olivine within the Fractionation Suite is only found as a cumulate phase. Anhedral olivine crystals range in size from 0.2 to 1 cm and have a forsterite (Fo) content of 79 to 86. The lowest Fo content is found in olivines from hornblende - clinopyroxenites and the highest in the olivines of the wehrlites.

Olivine exhibits several alteration assemblages including; brucite, serpentine, iddingsite and an Fe oxide phase (Plate 3.9).

3.4.2.1.2 Clinopyroxene

The clinopyroxene in the Fractionation Suite is generally found as a cumulate phase, but can also be found as interstitial crystals. In places, a well developed poikilitic texture is developed with large oikocrysts of clinopyroxene containing olivine (Plate 3.7). The oikocrysts range in size from 0.5 mm to more than 1 cm and are anhedral to subhedral. They usually exhibit consertal intergrowth with other clinopyroxene crystals and twinning is a common feature.

Microprobe analyses indicate that the clinopyroxene crystals are diopside to salite (Figure 3.1) according to the classification of Poldervaart and Hess (1951). Their

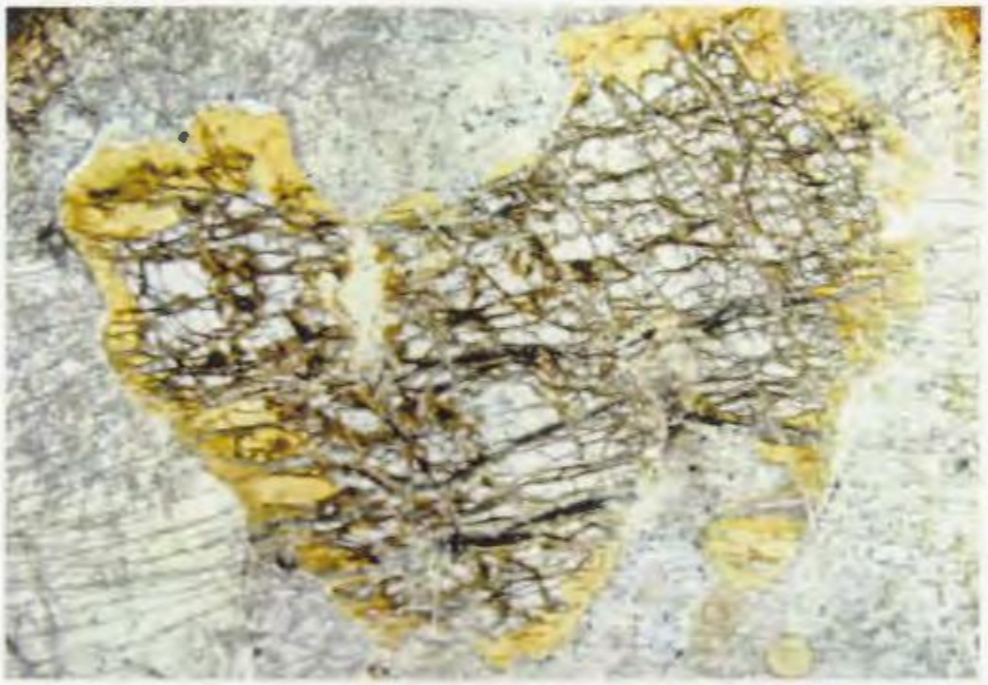

Plate 3.9 Corona alteration of olivine to yellow clay (10.5 X magnification, PPL).

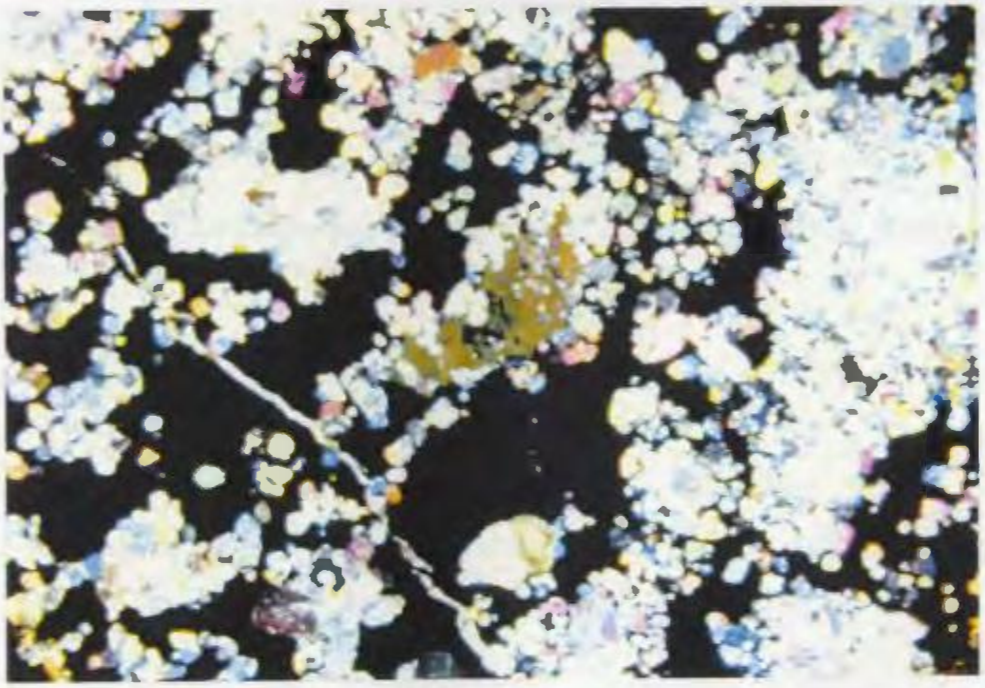

Plate 3.10 Interstitial sulphides (10.5 X magnification, XP).

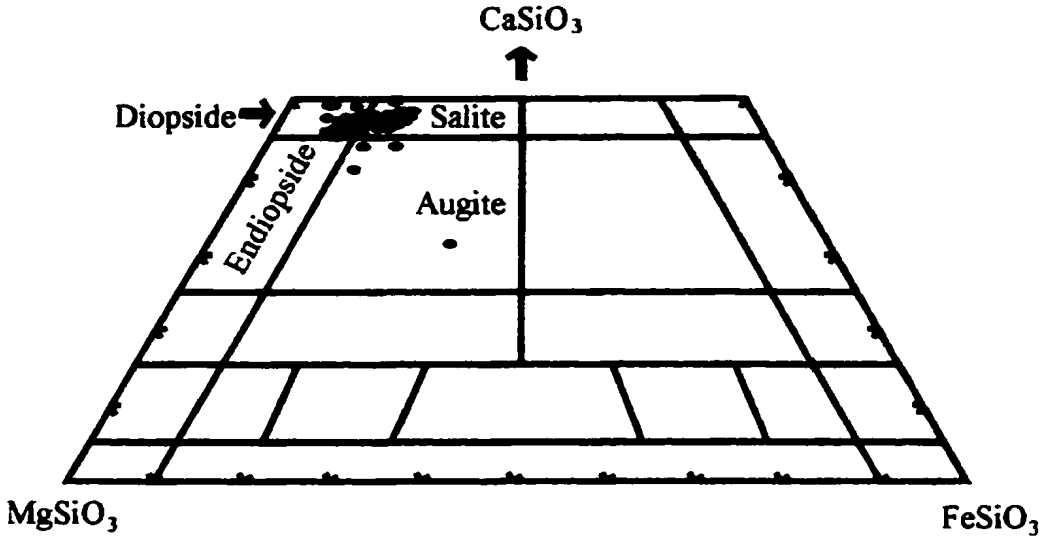

Figure 3.1 Clinopyroxene compositions of the Fractionation Suite based on the classification of Poldervaart and Hess (1951).

compositions average $Ca_{49-44}Mg_{49-44}Fe_{11.5-5.5}$. In Figure 3.1, clinopyroxene shows a slight Fe-enrichment, however, this is accompanied by a slight Ca-enrichment as opposed to the Ca-depletion that is observed in many tholeiitic intrusions.

3.4.2.1.3 Amphibole

Two phases of amphibole are present within the Fractionation Suite, an early primary amphibole and secondary amphibole produced by the alteration of clinopyroxene. The two phases are easily distinguished, the primary phase is dark green to dark brown pleochroic ferroan pargasite to magnesic taramite (classification according to Leake, 1978) and is everywhere found as anhedral interstitial crystals enclosing clinopyroxene and olivine (Plate 3.11). The secondary phase is light green, columnar to fibrous actinolite, in parallel to sub-parallel or radial aggregates (Plate 3.11). This actinolite can have the appearance of being subhedral and cumulate because it has replaced clinopyroxene.

Microprobe analysis of both phases indicates that the primary amphiboles are pargasite and pargasitic hornblende and the secondary phase is actinolitic hornblende (Leake, 1978).

3.4.2.1.4 Accessory minerals

Accessory minerals in the Fractionation Suite are; magnetite, plagioclase, pyrrhotite and chalcopyrite. The magnetite is found only in trace amounts and appears to be a primary

Plate 3.11 Two phases of amphibole; the dark pargasite is primary, the light green actinolite replacing clinopyroxene is secondary (10.5 X magnification, PPL).

phase as it is euhedral. Pyrrhotite and chalcopyrite are found in minor amounts in two samples and appear to be a primary interstitial phase. The plagioclase was only found in a small pegmatitic patch within one sample.

3.4.3 Cumulus Gabbro

No field evidence was seen by the author to suggest that a separate suite of Cumulus Gabbro outcrops in the Graham Valley area. However, Bates (1980b) suggested that it is a restricted suite and might only be recognized in drill core. He believed it to be of particular importance because it is host for significant copper - nickel sulphide accumulations.

Gabbros described from drill core contain 20 to 80 % clinopyroxene, depending on the amount of sulphide mineralization present. The amount of sulphide mineralization ranges from 5 to 65 %, increasing at the expense of clinopyroxene. The other main phases present include: up to 15 % olivine, 5 to 10 % primary amphibole and up to 20 % plagioclase. Phases that are found in minor amounts include: orthopyroxene, biotite, magnetite and apatite. All phases with the exception of clinopyroxene, plagioclase and apatite are anhedral, with the apatite in some places being found as subhedral crystals.

This lithology has well developed cumulate textures with olivine and clinopyroxene as cumulus phases. The sulphides, amphibole and plagioclase are everywhere found as interstitial phases (Plate 3.10). Clinopyroxene crystals mostly exhibit consertal texture and in some places have blebby intergrowths of amphibole. The crystallization sequence appears to

be olivine followed by clinopyroxene, then plagioclase and sulphides, and always amphibole last.

As in the Fractionation Suite, varying amounts of alteration are seen, likewise considered to be localized effects. The main alteration phases present are: amphibole, an Fe oxide phase, serpentine and brucite after clinopyroxene; clay, iddingsite, serpentine, brucite and an Fe oxide phase after olivine; and sausseritization of plagioclase.

3.4.3.1 Minerals of the Cumulus Gabbro

3.4.3.1.1 Olivine

Olivine found within the Cumulus Gabbro is generally anhedral 0.1 - 0.6 mm cumulate crystals. It is forsteritic with a Fo content that ranges from 75 - 83. The lowest value is found within a hornblende-gabbro that has olivine only as an accessory phase. The highest value is from an olivine-gabbro that contains up to 15 % olivine by volume. The olivines of the Cumulus Gabbro have an alteration assemblage that is similar to that of the Fractionation Suite.

3.4.3.1.2 Clinopyroxene

The clinopyroxene of the Cumulus Gabbro is found as an anhedral phase that nearly

everywhere exhibits consertal intergrowth. The clinopyroxenes are diopside to salite, they range in size from 0.5 mm to 0.5 cm and have a composition in the range $Ca_{48-40}Mg_{52-41}Fe_{15-9}$.

3.4.3.1.3 Amphibole

The amphibole in the Cumulus Gabbro is always found as primary anhedral interstitial crystals ranging in size from 1mm to 1cm. The amphibole from the Cumulus Gabbro is classified as ferroan pargasite to magnesic taramite according to the classification of Leake (1978).

3.4.3.1.4 Plagioclase

The plagioclase in the Cumulus Gabbro ranges in size from less than 1mm to 5mm. It is always found as an anhedral interstitial phase. Much of the plagioclase exhibits slight sausseritization. Plagioclases from the Cumulus Gabbro are classified as bytownites.

3.4.3.1.5 Sulphide minerals

The main sulphide minerals present are pyrrhotite, pyrite and chalcopyrite. Minor pentlandite is also present. These minerals will be described in detail in Chapter 5.

3.4.3.1.6 Accessory minerals

Accessory minerals in the Cumulus Gabbro include; apatite, biotite, orthopyroxene and magnetite. Orthopyroxenes range in size from 2mm to 6mm and appears to be an early cumulate phase. Much of the orthopyroxene has been altered to iddingsite. The biotite and magnetite range in size from less than 1mm to 7mm. These phases are anhedral and interstitial. The apatite ranges in size from less than 1mm to 5mm and is generally euhedral.

3.4.4 Late Stage Diorite

The dioritic rocks have a mineralogy that is dominated by amphibole and plagioclase, with lesser amounts of apatite, clinopyroxene, biotite, quartz and opaques. Amphibole makes up 20 to 60 % of the LSD, the primary amphibole is interstitial and ranges from 5 to 10%, the remainder of the amphibole is a result of clinopyroxene alteration. Only minor amounts of primary clinopyroxene remain unaltered. The abundances of the other phases present are: 15 to 30% plagioclase, 3 to 15% apatite, 2 to 6% biotite, up to 6% pyrite. Other alteration assemblages include sausseritized plagioclase and Fe oxide rims around opaque crystals. Unlike the FS and the CG, the LSD does not appear to be cumulate, but exhibits a subhedral granular texture.

3.4.4.1 Minerals of the Late Stage Diorite

3.4.4.1.1 Clinopyroxene

Most clinopyroxene in the LSD has been altered to actinolite. The subhedral crystals range in size from 0.5 to 2.5 mm.

3.4.4.1.2 Amphibole

The amphiboles of the LSD are made up of two phases, a primary actinolitic hornblende and a secondary actinolite after clinopyroxene (Leake, 1978). The amphibole are generally anhedral and range in size from 0.5 to 4.0 mm.

3.4.4.1.3 Plagioclase

The plagioclase of the LSD is anorthite and the subhedral crystals range in size from 0.5 to 1.5mm.

3.4.4.1.4 Apatite

The LSD contains up to 15% modal apatite. This apatite is easily identified because

of its euhedral shape and high relief. The apatite crystals range in size from 0.25 to 2.0 mm and it appears to occur as a primary phase.

3.4.4.1.5 Accessory minerals

The main accessory minerals in the LSD are biotite, quartz and pyrite. These phases range from subhedral to anhedral and from 0.1 to 2.0 mm in size.

3.5 Separation Point Batholith

The portion of the Separation Point Batholith in the Graham Valley area comprises a hornblende-biotite granodiorite / granite (Tulloch, 1983). This particular section of the batholith contains calcic oligoclase, quartz, biotite, interstitial microcline, epidote, Fe oxide, sphene and minor muscovite (Grindley, 1980). Sheets of metasomatized foliated granite intrude the border zone of the Riwaka Complex in the Rocky River area and elsewhere. This foliated granite has higher contents of muscovite and microcline microperthite at the expense of plagioclase while coarse sphene, apatite, epidote and allanite are produced by metasomatic interchange with marble rafts within the granite and contact rocks (Grindley, 1980).

3.6 Discussion

3.6.1 Introduction

This discussion will review the dominant field and petrological relationships of some of the main global occurrences of mafic to ultramafic intrusive bodies and their comparison with the Riwaka Complex. These other occurrences include; ophiolites, layered intrusions and Alaskan - type ultramafic complexes.

3.6.1.1 Ophiolites

Ophiolite complexes represent portions of ancient oceanic lithosphere that have formed at oceanic spreading centres. The term ophiolite refers to a distinctive assemblage of mafic to ultramafic rocks and associated sediments. In a completely developed ophiolite, rock types in the following sequence occur, starting from the bottom and working up (Nicolas, 1989):

- Ultramafic complex, consisting of variable proportions of harzburgite, lherzolite and dunite, usually with a tectonic fabric;

- Gabbroic complex, ordinarily with cumulus textures commonly containing cumulus peridotites and pyroxenites and usually less deformed than the ultramafic complex;

- Mafic sheeted dike complex;

- Mafic volcanic complex, commonly pillowed;

- Associated rock types include (1) an overlying sedimentary section typically including ribbon cherts, thin shale interbeds, and minor limestones; (2) podiform chromite bodies, generally associated with the dunites; (3) sodic felsic intrusive and extrusive rocks.

The ultramafic complex of the Semail Ophiolite is predominantly composed of harzburgite, olivine (Fo_{90-91}) 74%, orthopyroxene (En_{90-91}) 24% and spinel 2%. The peridotite section also contains bands of dunite through out the section (Pallister and Hopson, 1981; Hopson et al., 1981).

The ultramafic complex of the Halmahera Ophiolite in eastern Indonesia is predominantly harzburgites with rare occurrences of lherzolites (Ballantyne, 1992).

The ultramafic complex in the Bay of Islands ophiolite is composed of harzburgite, spinel lherzolites, dunites and feldspathic dunites (Malpas, 1978).

Structurally, the upper sections of the gabbros, dikes and basalts generally contain abundant normal faults, often the result of amagmatic extension (Alexander and Harper, 1992). The peridotites and lower-most gabbros exhibit a high-temperature plastic deformation and the boundary of the peridotites and gabbros is a serpentinized zone of low-temperature shearing or thrusting due to the contrast in rheology between the two lithologies (Nicolas, 1989). Ophiolites that are found in alpine regions and on continental margins have been emplaced by obduction producing a sole thrust between the ophiolitic rocks and the country rocks (Alexander and Harper, 1992; Nicolas, 1989; Malpas, 1979).

3.6.1.2 Layered intrusions

Layered intrusions represent cooled bodies of magma of various sizes. The rocks within layered intrusions are dominantly cumulate, containing varying amounts of cumulate minerals and crystallized intercumulate liquid. The distinguishing feature of layered intrusions is the occurrence of igneous layering defined by one or more cumulus minerals. Layers are sheet-like units that are characterized by distinct mineralogy, composition and/or textural features (Hess, 1989).

The Stillwater Complex in southwestern Montana is a example of a layered intrusion. It is made up of three main units; the Basal Series (10s meters thick), the Ultramafic Series (2000 meters thick), the Layered Banded Series (approximately 4700 meters thick).

The Basal Series is composed of norite and two - pyroxene gabbros. These rocks have been contaminated by the assimilation of footwall sedimentary rocks.

The Ultramafic Series is composed of a lower peridotite zone and an upper orthopyroxenite zone. The crystallization sequence for the Ultramafic Series is cumulate chromite + olivine and intercumulate olivine + orthopyroxene + plagioclase + augite. The lower-most layers of the peridotite zone exhibit a Mg enrichment in the orthopyroxenes from the base of the series to a height of about 500 meters. The Mg numbers increase from 0.76 to 0.86 over this interval (Raedeke and McCallum, 1985).

The Banded Series is dominated by plagioclase-rich rocks; anorthosite, norite, troctolite and gabbro. It is divided into three zones; the lower, middle and upper banded zones

(McCallum et al., 1980; Todd et al., 1982). The lower banded zone contains troctolite, anorthosite, norite and gabbronorite with a crystallization sequence of cumulate olivine + plagioclase and intercumulate plagioclase + orthopyroxene + augite (Todd et al., 1982). The middle zone is composed of anorthosite, troctolite and olivine gabbro. The crystallization sequence for the middle zone is cumulate olivine + plagioclase and intercumulate olivine + plagioclase + augite + orthopyroxene. Most of the upper zone is composed of a uniform gabbronorite (Hess, 1989).

The Bushveld Complex in South Africa is the largest recognized layered intrusion. It is divided into five main sections as described in the table below:

Table 3.1 Geological description of the Bushveld Complex.

Series	Depth(m)	Description
Upper	9000-6800	Anorthosite, gabbro and ferrodiorite. Base defined by the first appearance of cumulus magnetite. Extreme iron enrichment and occurrence of cumulus apatite, minor amounts of quartz, alkali feldspar, biotite and hornblende.
Main	6800-3000	Anorthosite, norite and hypersthene gabbro. Chromite and olivine absent. Thick monotonous sections of hypersthene gabbro. Layering not well developed.
Critical	3000-1800	Norite, orthopyroxenite and anorthosite with chromitite, dunite and

		harzburgite layers.
Lower	1800-0	Thick, nearly monolithic units of bronzite containing 95-99% pyroxene. Macro - rhythmic layering of units of dunite, harzburgite and orthopyroxenite.
Basal	0	Norite with many xenoliths of country rock.

The crystallization sequence for the ultramafic rocks of the Bushveld intrusion is chromite + olivine + orthopyroxene.

The Skaergaard Intrusion is a layered intrusion that occurs on the east coast of Greenland. A large part of this intrusion is the Layered Series, it is subdivided into the lower, middle and upper zones. The crystallization sequence for the layered series is; cumulate olivine + plagioclase and intercumulus augite + pigeonite + magnetite - olivine disappears - iron-rich olivine reappears - pigeonite disappears + apatite + alkali-feldspar + quartz.

3.6.1.3 Alaskan - type ultramafic complexes

Irvine (1974) used the term Alaskan - type ultramafic complexes to describe mafic to ultramafic intrusions from Alaska that were recognized as being distinctive. These intrusions are spatially related to subduction - zone environments (Murray, 1972; Irvine, 1974; Tistl et al., 1994) and are unique in several aspects. Firstly, many exhibit crude concentric zoning, featuring a dunite core surrounded by successive rings of olivine - clinopyroxenite, magnetite

- rich clinopyroxenite and hornblendite. Secondly, Alaskan - type ultramafic complexes are distinguished from other mafic to ultramafic intrusions in having highly calcic clinopyroxenes, virtually no orthopyroxene or plagioclase, abundant magnetite and Fe - rich chromite (Irvine, 1974).

Some examples of Alaskan - type ultramafic complexes are the Duke Island ultramafic complex, the Union Bay ultramafic complex and the Blashke Islands complex along with approximately 30 others along the Alaskan pan handle (Irvine, 1974). On the Kamchatka Peninsula of Russia the Seinav massif, the Galmoenan massif and the Snegovoy pluton are similar to Alaskan - type ultramafic complexes (Batanova and Astrakhantsev, 1994). In Columbia, the Condoto complex is a example of an Alaskan - type ultramafic complex (Tistl et al., 1994). Of these intrusions only the Blashke Islands complex, the Condoto complex and the Snegovoy pluton exhibit well defined concentric zoning. The Alaskan intrusions range in size from 3 to 20 km^2 (Irvine, 1974), the Condoto complex has a diameter of approximately 6 km (Tistl et al., 1994), the Snegovoy pluton has a diameter of approximately 4 km. The Seinav and the Galmoenan massifs are linear intrusions up to 3 km wide and 20 km in length (Batanova and Astrakhantsev, 1994).

All these intrusions are found in areas of plate convergence and all are mineralogically very similar, with calcic clinopyroxenes, little or no orthopyroxene or plagioclase and abundant hornblende.

3.6.2 The Riwaka Complex in perspective

The basement rocks of the Graham Valley area are made up of a variety of metamorphosed sedimentary rocks including a thick sequence of marble, graphitic argillite and quartzite. These rocks were deposited in one or more subduction zone complexes (Shelley, 1975; Crook and Feary, 1982). This package of metamorphosed sedimentary rocks is subsequently intruded by the Riwaka Complex.

The vast majority of the Riwaka Complex is made up of the Fractionation Suite. The Cumulus Gabbro and the Late Stage Diorite make up only about 5-10% of the rocks in the Graham Valley area. This is an interesting fact as most layered tholeiitic intrusions such as the Skaergaard and the Stillwater intrusions are dominated by gabbroic rocks with minor zones of ultramafic rocks (Irvine, 1974) and there is no field evidence to suggest that these rocks were structurally removed as is the case with some fragmented ophiolites.

The mineralogy of the Riwaka Complex is dominated by olivine, clinopyroxene and amphibole. Minor amounts of plagioclase, magnetite, apatite, biotite, quartz, orthopyroxene, serpentine, brucite, iddingsite, pentlandite, pyrrhotite, chalcopyrite and pyrite are also found. The mineralogy of the Riwaka Complex is interesting because it is different from most tholeiitic layered intrusions. Orthopyroxene is nearly absent and plagioclase is only found in the Cumulus Gabbro and the Late Stage Diorite. The crystallization sequence in most layered tholeiitic intrusions is olivine followed by orthopyroxene, clinopyroxene, plagioclase and amphibole (Irvine, 1979). The Fractionation Suite's crystallization sequence is olivine

followed by clinopyroxene and amphibole. There is no orthopyroxene or plagioclase crystallization. Of interest is the fact that, Alaskan - type ultramafic complexes have this same crystallization sequence (Irvine, 1974; Batanova and Astrakhantsev, 1994; Tistl et al, 1994).

The clinopyroxene chemistry does not show a Fe - enrichment trend as would be expected from clinopyroxenes in a layered tholeiitic intrusion (Hess, 1989). Instead they exhibit a slight Ca - enrichment (Figure 3.1). Tistl et al. (1994) suggest that with increasing Ca in the magma, orthopyroxene crystallization is prohibited because of clinopyroxene crystallization. The absence of orthopyroxene crystallization makes available much more Mg that can be incorporated into the clinopyroxene, thus cancelling any Fe enrichment. According to Loucks (1990) this feature is typical for clinopyroxenes of intra oceanic arc cumulates, and can be explained by the considerable water content of arc-related melts. This high water pressure in the magma can also hinder the crystallization of plagioclase (Conrad and Kay, 1984; Debari and Kay, 1987). The Ca - enrichment is similar to that exhibited by clinopyroxenes from Alaskan - type ultramafic complexes (Figure 3.1) (Irvine, 1974). Therefore, because the Riwaka Complex is clearly intruded into country rocks (unlike ophiolites) and because of the high percentage of ultramafic rocks with a distinctive mineralogy (unlike layered intrusions), it appears that the Riwaka Complex is most similar to Alaskan - type ultramafic complexes.

Chapter 4

Mineral and Whole Rock Geochemistry

4.1 Introduction

The purpose of this chapter is to characterize the geochemistry of the Riwaka Complex and to use this data in conjunction with field relationships to infer its petrogenesis. Major elements, trace elements, rare earth elements and mineralogical data were determined for the Fractionation Suite, the Cumulus Gabbro and the Late Stage Diorite. Some geochemical analyses of the Separation Point Batholith, the Arthur Marble and the Onekaka Schist were also collected for comparison purposes. Analytical methods are discussed in Appendix B.

4.2 Whole Rock Geochemistry

4.2.1 Major elements

The major element data are presented in Table A10 - A15 (Appendix A). Bowen diagrams are plotted for 16 samples of the Fractionation Suite (FS), 6 of the Cumulus Gabbro

(CG), 8 of the Late Stage Diorite (LSD), 2 of the Arthur Marble (AM), 2 of the Onekaka Schist (OS) and 1 of the Separation Point Granite (SPG). The AM, OS and the SPG samples were analysed for comparison with the Riwaka Complex rocks.

When MgO is used as the discriminant, it is seen to decrease from approximately 36 wt% in the most MgO - rich rocks of the FS to approximately 4 wt% in rocks of the LSD (Figures 4.1 a - i). Samples of the CG can not geochemically be discriminated from the FS here. There is a noticeable gap between 7.2 wt% and 10.8 wt% MgO. This gap separates the FS and CG rocks from those of the LSD. Other major element oxide plots that show a similar gap between FS and CG rocks and LSD rocks include; P_2O_5 - 0.2 to 0.9 wt%, and Al_2O_3 - 12 to 15 wt%. Also, for MgO versus SiO_2, TiO_2, Fe_2O_3, FeO, K_2O and P_2O_5, the overall geochemical trends for the FS and CG rocks are different from the trend of the LSD rocks. The trends for MgO versus Na_2O, CaO, MnO and Al_2O_3 are not effectively distinguishable.

TiO_2, Al_2O_3, Fe_2O_3, FeO, CaO, Na_2O, K_2O and P_2O_5 all exhibit an overall increase from the FS and CG to the LSD. SiO_2 and MnO show an overall decrease.

The AM contains less than 1 wt% MgO, the SPG contains 5 wt% and the OS contains between 3 - 6 wt% MgO.

The geochemical trend of the data for the LSD is different than the geochemical trend of the FS and CG rocks.

Figure 4.1 a - i Bowen diagrams for the major elements of the Fractionation Suite, the Cumulus Gabbro and the Late Stage Diorite with MgO used as a discriminant (all values are in wt%). The geochemical trend is indicated with a black line.

KEY

- ♦ Separation Point Granite
- ▲ Late Stage Diorite
- ● Cumulus Gabbro
- ■ Fractionation Suite
- – Onekaka Schist
- ● Arthur Marble

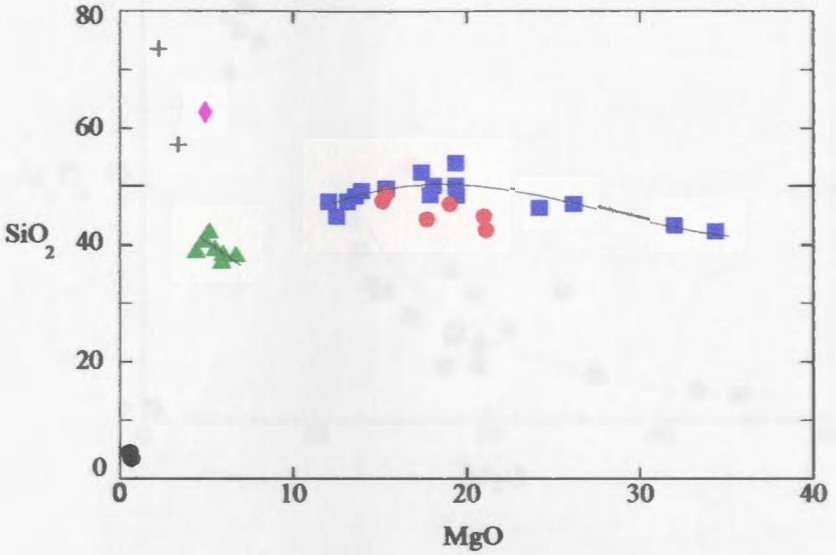
80
60
40
20
0
SiO2
0
10
20
30
40
MgO

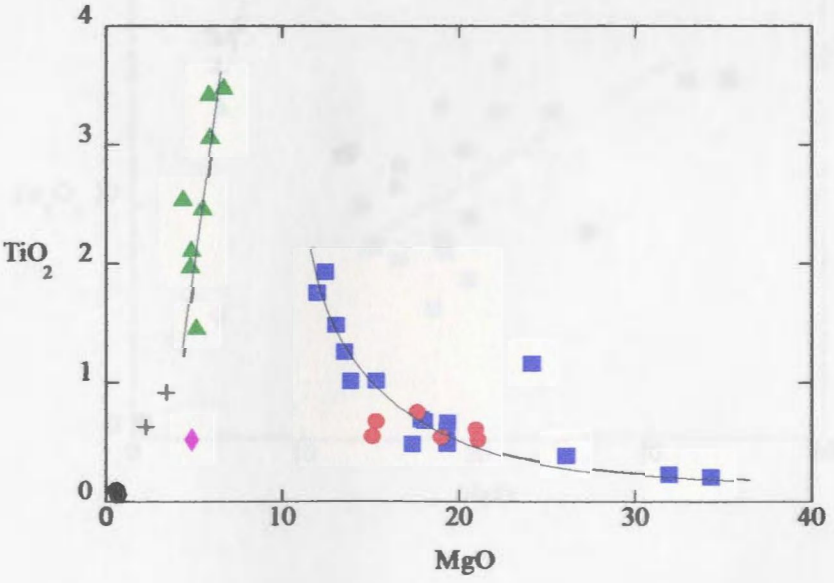
4
3
2
1
0
TiO2
0
10
20
30
40
MgO

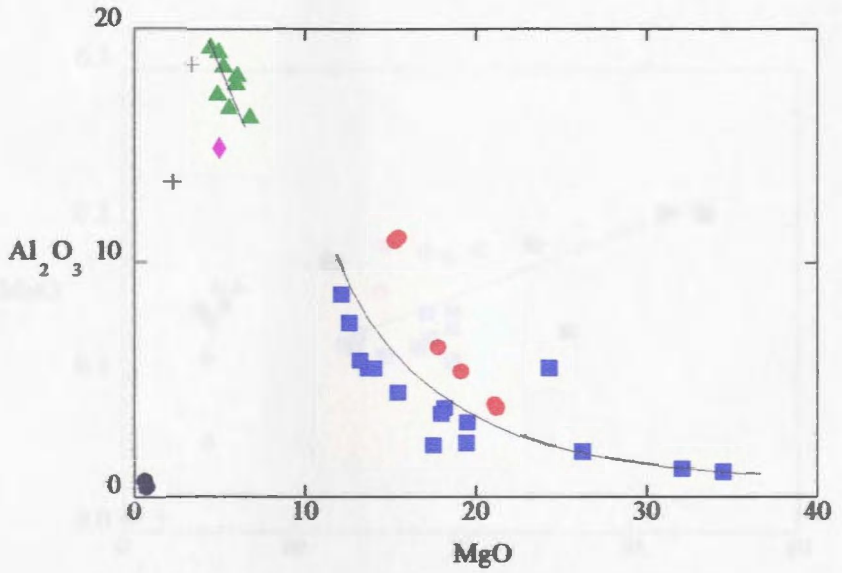
20
Al2O3 10
0
0
10
20
30
40
MgO

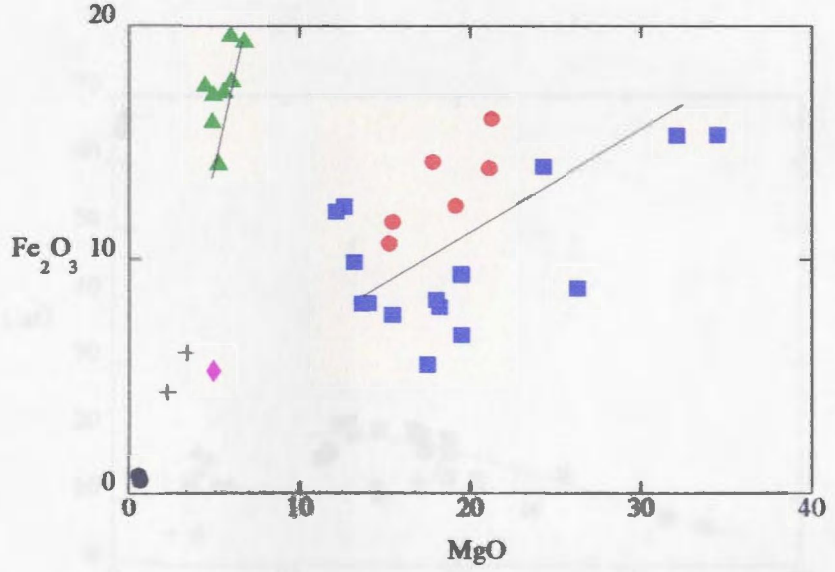
20
Fe2O3 10
0
0
10
20
30
40
MgO

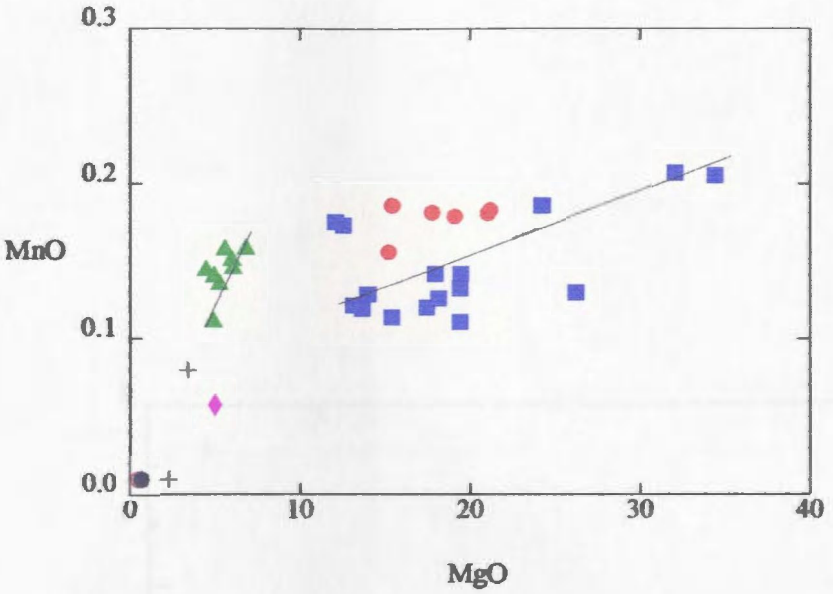
0.3
0.2
0.1
0.0
MnO
0
10
20
30
40
MgO

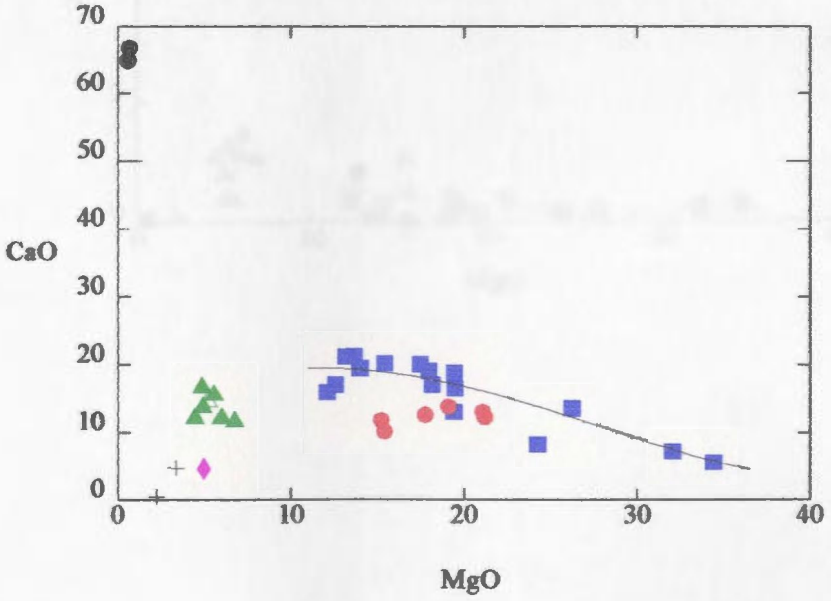
70
60
50
40
30
20
10
0
CaO
0
10
20
30
40
MgO

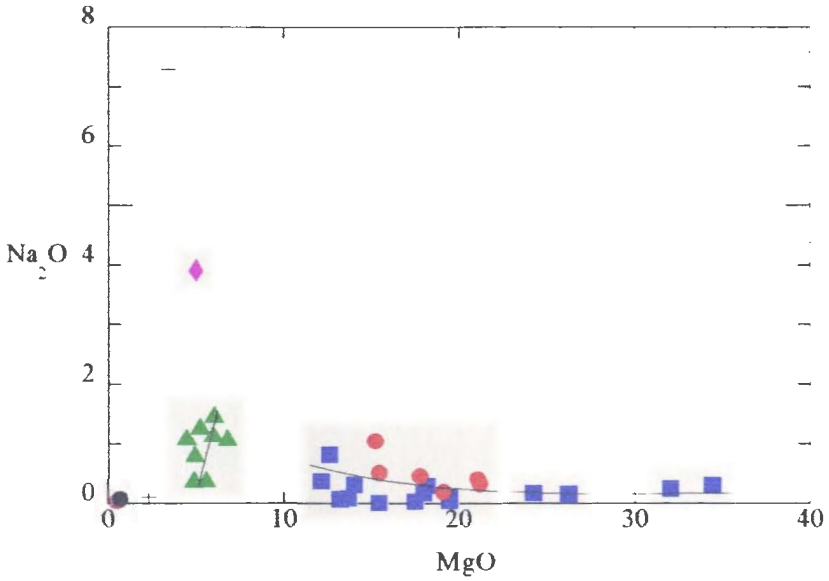
8
6
4
2
0
Na2O
0
10
20
30
40
MgO

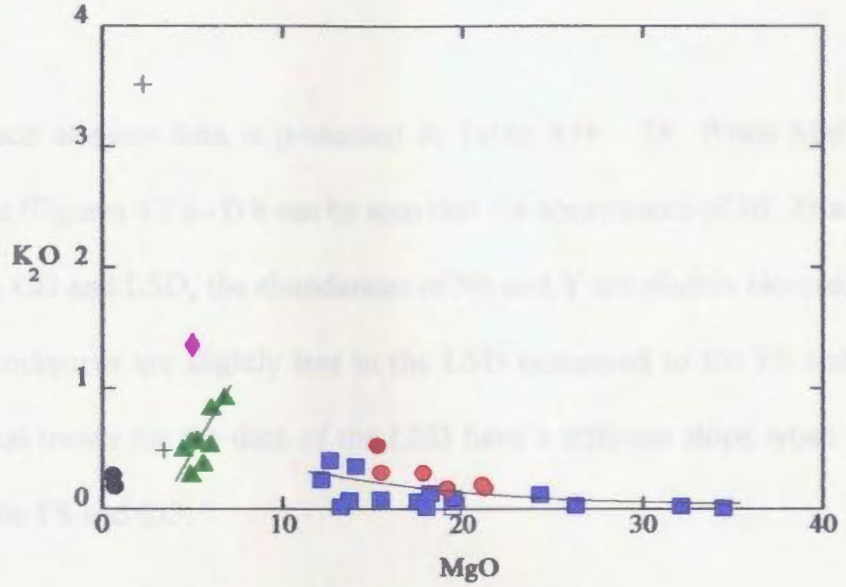
4
3
2
1
0
K_2O
0
10
20
30
40
MgO

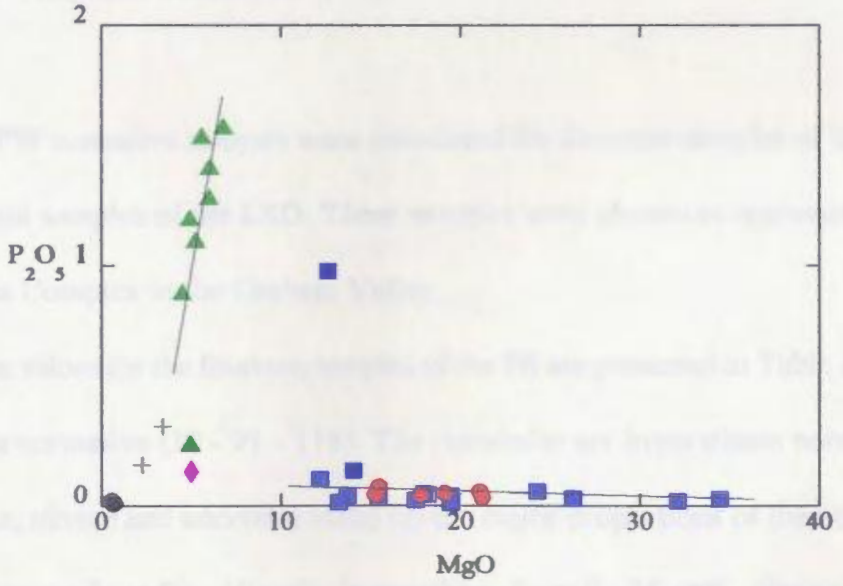
2
1
0
P_2O_5
0
10
20
30
40
MgO

4.2.2 Trace elements

Trace element data is presented in Table A16 - 18. When MgO is used as the discriminant (Figures 4.2 a - f) it can be seen that the abundances of Hf, Zr and Ta are similar for the FS, CG and LSD, the abundances of Nb and Y are slightly elevated in the LSD and the Cr abundances are slightly less in the LSD compared to the FS and CG rocks. The geochemical trends for the data of the LSD have a different slope when compared to the trends of the FS and CG.

4.3 Normative Analysis

CIPW normative analysis were calculated for fourteen samples of the FS, five of the CG and eight samples of the LSD. These samples were chosen as representative samples of the Riwaka Complex in the Graham Valley.

The values for the fourteen samples of the FS are presented in Table A23. One sample is nepheline normative (JS - 91 - 118). The remainder are hypersthene normative. Diopside, hypersthene, olivine and anorthite make up the major proportions of the normative analysis. Diopside ranges from 20 - 69 wt%, hypersthene from 0 - 35 wt%, olivine from 0 - 54 wt% and anorthite from 3 - 15 wt%. Minor phases include: orthoclase 0.1 - 2.5 wt%, albite 0 - 7 wt%, magnetite 2.5 - 6 wt%, ilmenite 0.4 - 3.5 wt% and apatite 0.05 - 2.3 wt%.

The values for the five samples of the CG are presented in Table A24. All samples are

Figure 4.2 a - f Bowen diagrams for selected trace elements of the Fractionation Suite, the Cumulus Gabbro and the Late Stage Diorite with MgO used as a discriminant (all trace element values are in ppm). The geochemical trend is indicated with a black line.

KEY

- ♦ Separation Point Granite
- ▲ Late Stage Diorite
- ● Cumulus Gabbro
- ■ Fractionation Suite
- + Onekaka Schist
- ● Arthur Marble

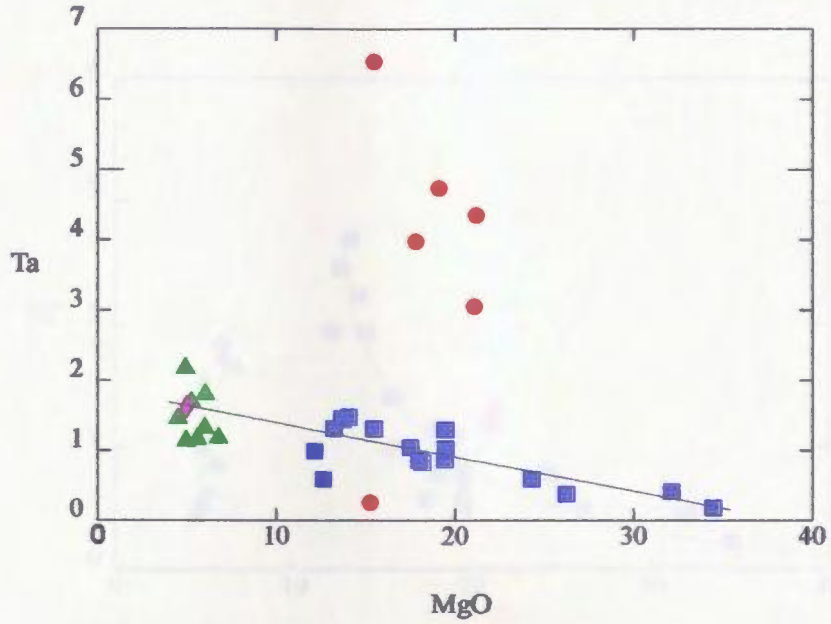
7
6
5
4
3
2
1
0
Ta
0
10
20
30
40
MgO

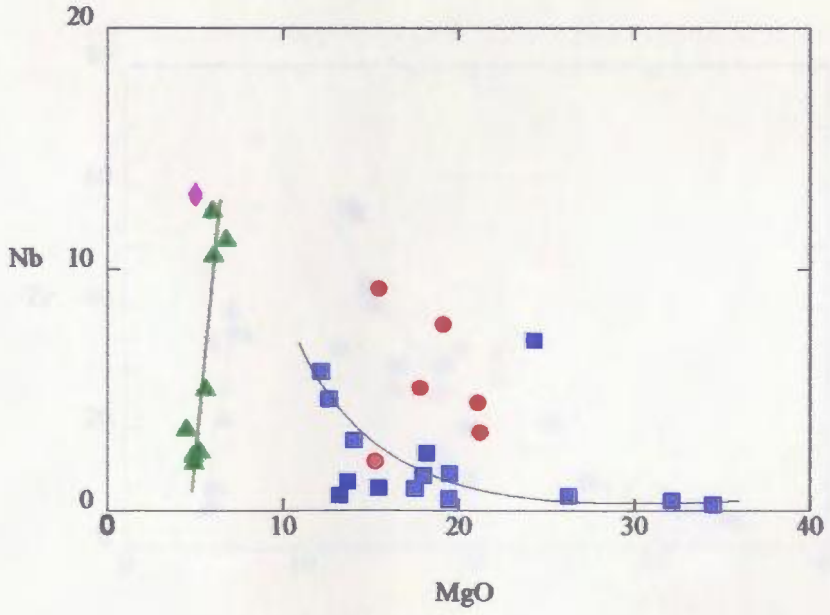
20
10
0
Nb
0
10
20
30
40
MgO

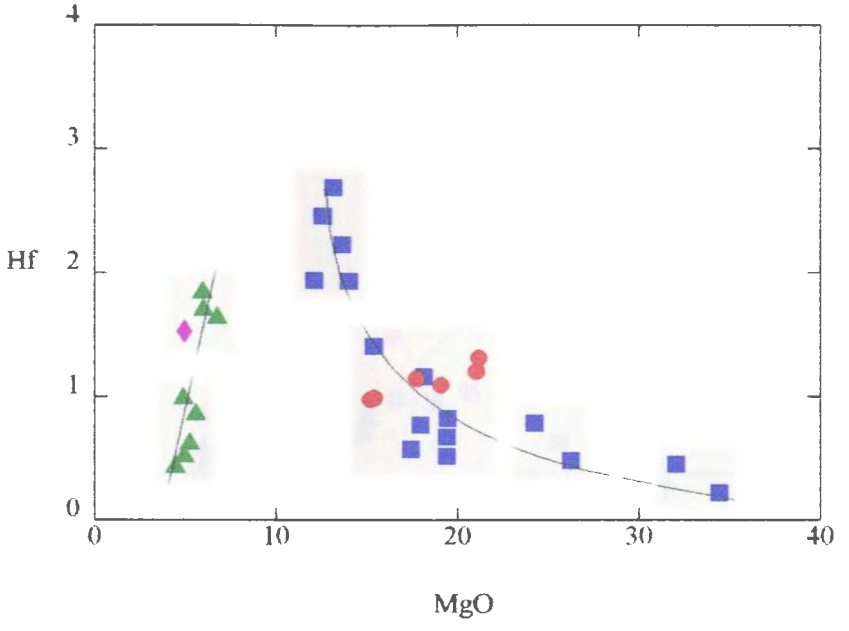
Hf
MgO
0
1
2
3
4
0
10
20
30
40

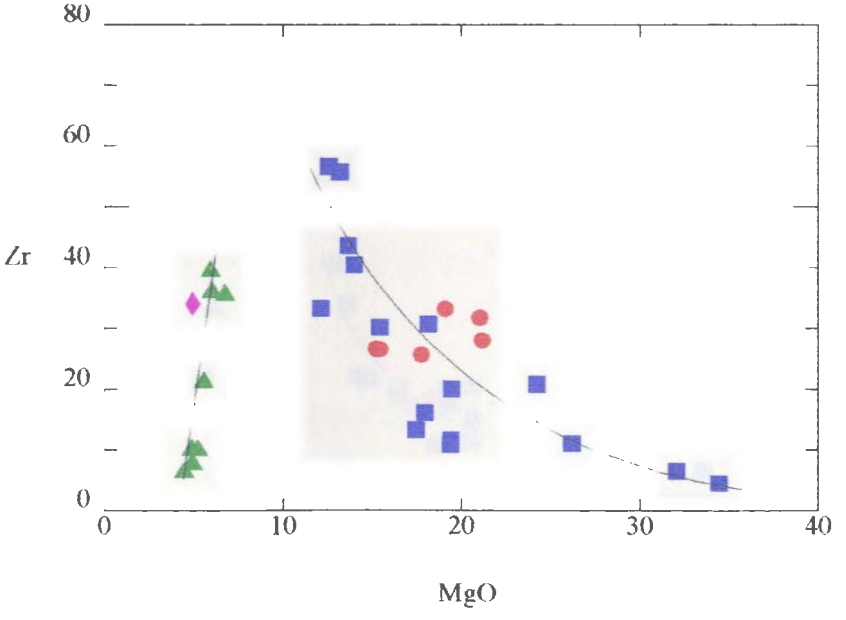
Zr
MgO
0
20
40
60
80
0
10
20
30
40

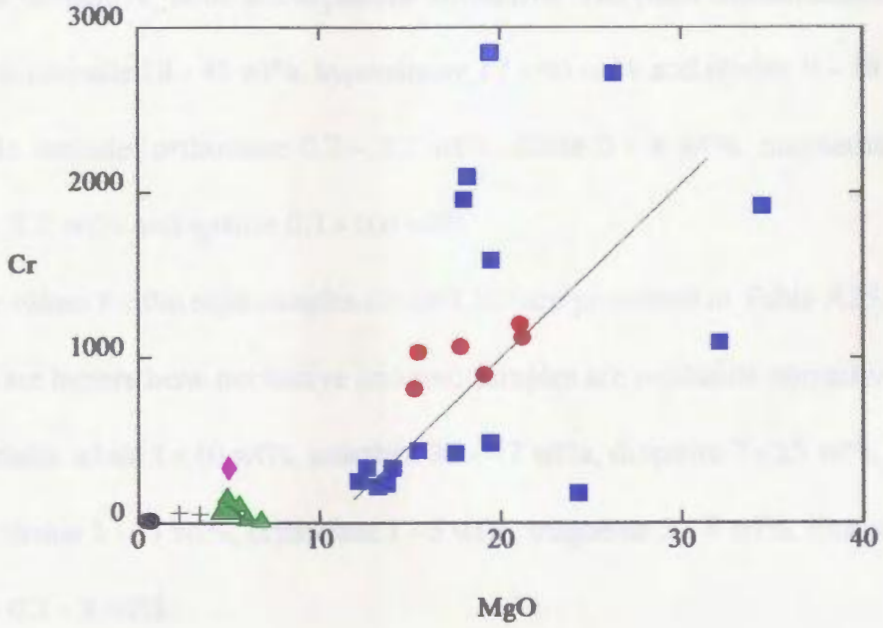
3000
2000
1000
0
Cr
0
10
20
30
40
MgO

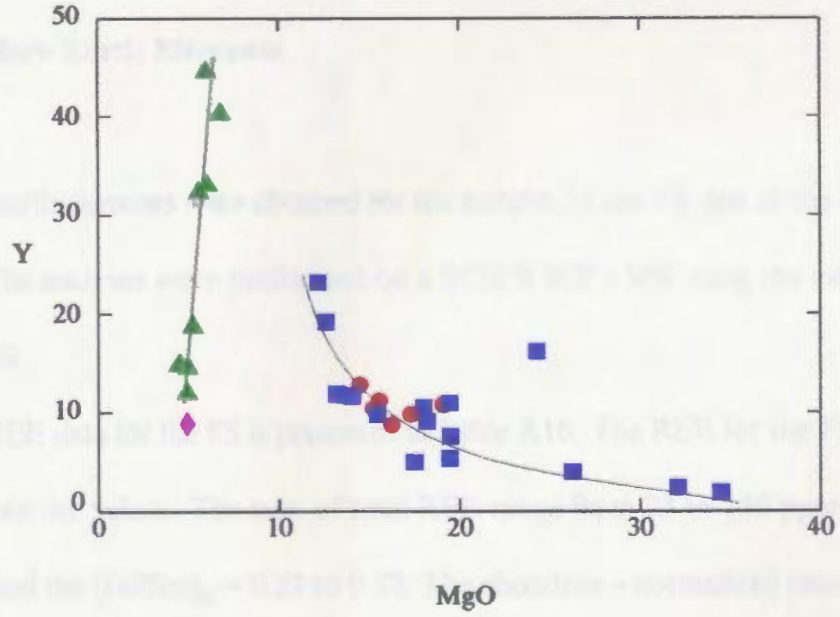
50
40
30
20
10
0
Y
0
10
20
30
40
MgO

hypersthene normative, none are nepheline normative. The main constituents are: anorthite 13 - 27 wt%, diopside 18 - 45 wt%, hypersthene 17 - 40 wt% and olivine 0 - 18 wt%. Minor components include: orthoclase 0.7 - 3.2 wt%, albite 0 - 8 wt%, magnetite 4 - 7 wt%, ilmenite 1 - 3.3 wt% and apatite 0.1 - 0.6 wt%.

The values for the eight samples of the LSD are presented in Table A25. Six samples of the LSD are hypersthene normative and two samples are nepheline normative. The major minerals include: albite 3 - 10 wt%, anorthite 36 - 47 wt%, diopside 7 - 25 wt%, hypersthene 0 - 8 wt%, olivine 3 - 17 wt%, orthoclase 1 - 5 wt%, magnetite 5 - 8 wt%, ilmenite 2 - 7 wt% and apatite 0.5 - 4 wt%.

4.4 Rare Earth Elements

Rare earth elements were obtained for ten samples of the FS, ten of the CG and seven of the LSD. The analyses were performed on a SCIEX ICP - MS using the method outlined in Appendix B.

The REE data for the FS is presented in Table A16. The REE for the FS are enriched relative to chondrite values. The sum of total REE range from 23 to 140 ppm; the $(La/Lu)_{cn}$ = 3.7 to 9.3; and the $(Eu/Sm)_{cn}$ = 0.23 to 0.32. The chondrite - normalized rare earth element (CNREE) diagram has an overall negative slope (Figure 4.3 A). The light rare earth elements show a slight enrichment from La to Nd, with values of approximately 5 to 50 times chondrite values. The middle and heavy rare earth elements (MREE & HREE, respectively)

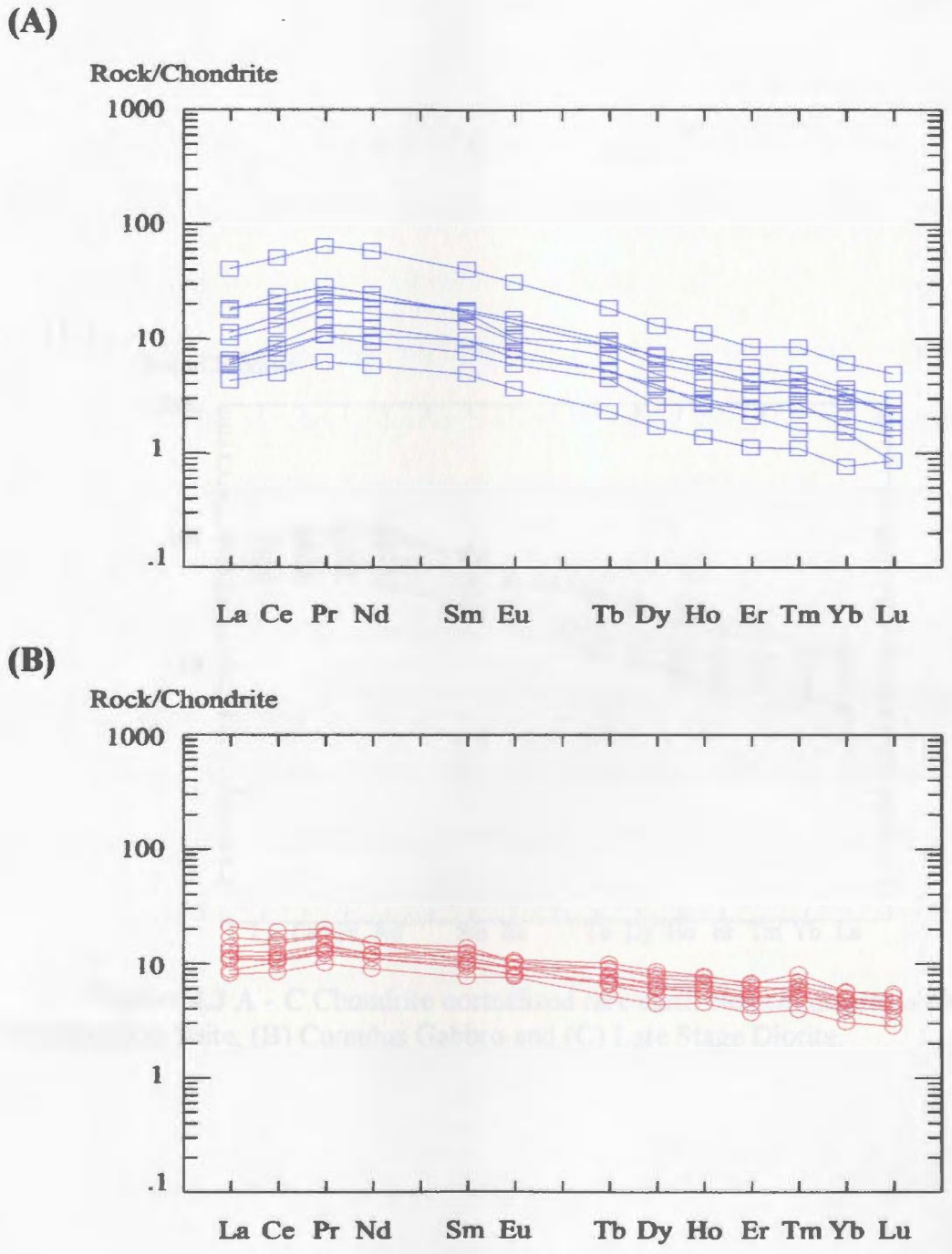

Figure 4.3 A - C Chondrite normalized rare earth element diagrams for the (A) Fractionation Suite, (B) Cumulus Gabbro and (C) Late Stage Diorite.

(C)

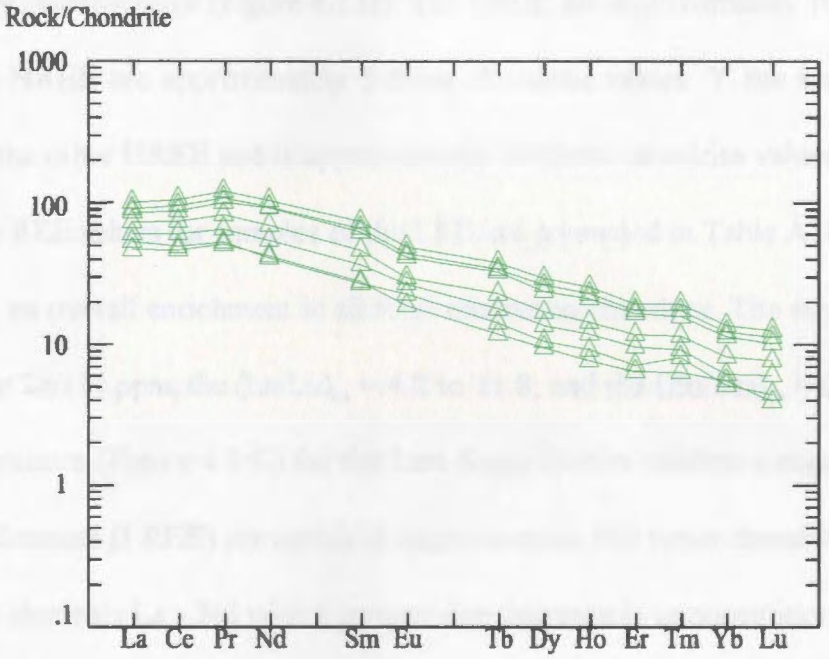

Figure 4.3 A - C Chondrite normalized rare earth element diagrams for the (A) Fractionation Suite, (B) Cumulus Gabbro and (C) Late Stage Diorite.

progressively decrease from Sm to Lu, with values that are 1 to 10 times chondrite. Y shows a slight enrichment relative to the other HREE; it has values 1 to 10 times chondrite.

The REE values for samples of the CG are presented in Table A17. The REE for the CG all show an enrichment relative to chondrite. Total REE abundances range from 26.3 to 47.6 ppm; the $(La/Lu)_{cn}$ = 1.7 to 3.6; and the $(Eu/Sm)_{cn}$ = 0.29 to 0.38. The (CNREE) pattern has a slightly negative slope (Figure 4.3 B). The LREE are approximately 10 times chondrite values, the HREE are approximately 5 times chondrite values. Y has a slight enrichment relative to the other HREE and is approximately 10 times chondrite values.

The REE values for samples of the LSD are presented in Table A18. The LSD suite also shows an overall enrichment in all REE relative to chondrite. The sums of all REE are from 71.7 to 246.11 ppm; the $(La/Lu)_{cn}$ = 4.2 to 11.8; and the $(Eu/Sm)_{cn}$ = 0.24 to 0.33. The (CNREE) pattern (Figure 4.3 C) for the Late Stage Diorite exhibits a negative slope. Light rare earth elements (LREE) are enriched approximately 100 times chondrite. The pattern is flat for the elements La - Nd with a progressive decrease in concentration from Sm to Lu, which is enriched approximately 5 - 10 times chondrite, and a Y enrichment of 10 - 20 times chondrite.

4.5 Mineral Chemistry vs Stratigraphic Height

Within the Riwaka Complex 18 samples were collected through the FS perpendicular to observed phase layering, but because of poor exposure in the field, correlations between

similar units was difficult. The section collected did not have a recognizable structural orientation (top or bottom), but simply represents a transect across the entire Riwaka Complex along section A - B (Figure MA - 1). The first four hundred metres from the eastern boundary of the Riwaka Complex contained the most abundant olivine and is here considered to be the base of the section. This part of the section was sampled at 25m intervals as to better ascertain the initial properties of the magma. The CG was not included because its position in the section was difficult to ascertain as most of the CG samples were collected from drill core. The LSD is here considered a separate intrusive event, and is not therefore part of the layered section.

The main objective was to determine how the composition of minerals in the FS changed as a function of position in the section. The phases probed were olivine and clinopyroxene. The mineral data collected is presented in Table A1 - A2, A4 - A5.

The forsterite (Fo) content in olivines from the section collected through the FS range from Fo_{79} to $Fo_{85.5}$. It appears from Figure 4.4 (a) that the Fo content in olivines undergoes three compositional resettings, the first is at approximately 125m, the second at approximately 225m and the third at 350m. The overall trend of the Fo content in olivines is shown by line A (Figure 4.4 (a)). It exhibits an overall decrease in Fo content from approximately Fo_{85} at 25m to Fo_{80} at 400m.

The enstatite (En) composition in clinopyroxenes from the FS ranges from $En_{41.2}$ to $En_{49.3}$. The En in clinopyroxenes has been reset significantly four times; at approximately 75m, 125m, 350m and 725m (Figure 4.4 (b)). There also appears to be a slight resetting at 225m,

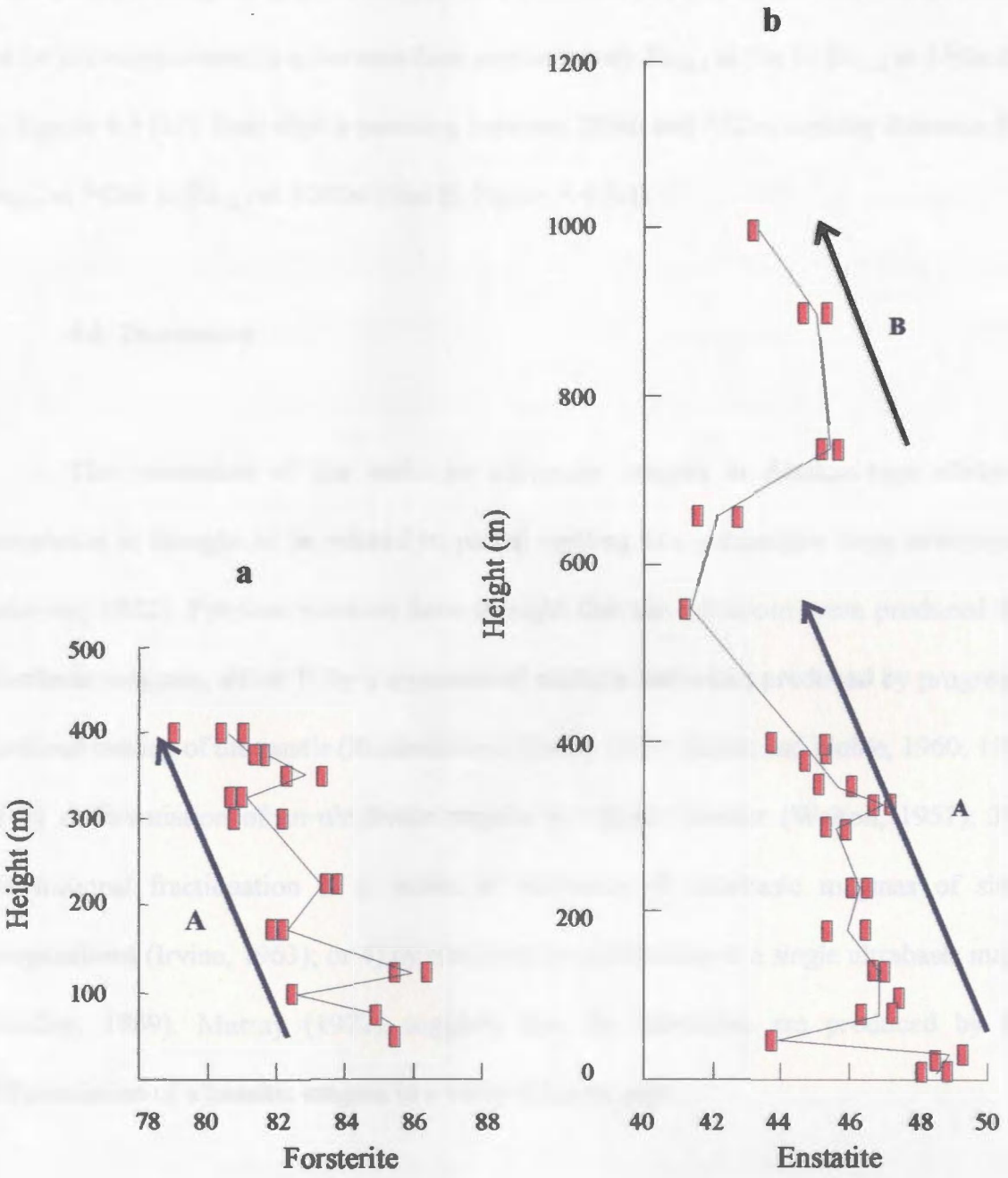

Figure 4.4 a - b Forsterite and enstatite compositions versus stratigraphic height for olivines and clinopyroxenes of the Fractionation Suite. Lines **A** and **B** represent overall geochemical trends of the data over indicated intervals.

which would correspond to a resetting in the Fo content of the olivines. The overall trend of the En in clinopyroxenes is a decrease from approximately $En_{48.5}$ at 0m to $En_{41.2}$ at 550m (line A, Figure 4.4 (b)), then after a resetting between 550m and 742m, another decrease from $En_{45.5}$ at 742m to $En_{43.2}$ at 1002m (line B, Figure 4.4 (b)).

4.6 Discussion

The generation of the mafic or ultramafic magma in Alaskan-type ultramafic complexes is thought to be related to partial melting in a subduction zone environment (Murray, 1972). Previous workers have thought that the intrusions were produced from ultrabasic magmas, either 1) by a sequence of multiple intrusions produced by progressive fractional melting of the mantle (Ruckmick and Noble, 1959; Taylor and Noble, 1960, 1969); 2) by differentiation of an ultrabasic magma by vapour transfer (Walton, 1951); 3) by gravitational fractionation of a series of intrusions of ultrabasic magmas of similar compositions (Irvine, 1963); or 4) by fractional crystallization of a single ultrabasic magma (Findlay, 1969). Murray (1972) suggests that the intrusions are produced by flow differentiation of a basaltic magma in a vertical feeder pipe.

4.6.1 Major and trace elements

In magmatic intrusions fractional crystallization plays an important role in the

development of different lithologies and their resultant geochemistries. Where mineral chemistry is plotted together with whole rock chemistry (Figure 4.5 a - e) it appears that olivine is the first cumulate phase to crystallize in the FS, this forces the composition of the magma crystallizing the earliest FS rocks to move away from the olivine composition. At approximately 17 wt% MgO, clinopyroxene becomes the dominant cumulate phase. Again, the crystallization of cumulate clinopyroxene is able to move the major oxide composition of the magma away from the crystallizing clinopyroxene composition and toward the composition of the LSD. The trend change (i.e. slope) of the LSD compared to the FS and CG may be attributed to mixing of the remaining magma with either the AM, the OS or both. A mixing line can be drawn between these lithologies. A comprehensive trace element study on the minerals of the Riwaka Complex was not carried out here, however the model of crystallization outlined for the major oxides can also be applied to the trace elements. This model would explain the trace element variation and trend difference between the FS, CG and the LSD.

4.6.2 Normative analyses

The normative analyses indicate that the majority of samples (all except 1 from the FS and 2 from the LSD) of the Riwaka Complex are hypersthene normative and therefore silica saturated, indicating that the parental magma for the Riwaka Complex was a tholeiitic magma (Hughes, 1982).

Figure 4.5 a - e Bowen diagrams of selected whole rock and mineral major elements using MgO as a discriminant (all major element values are wt%, all trace element values are ppm). Line **A** represents the direction the magma composition will move in when olivine is removed, line **B** represents the direction the magma composition will move in when clinopyroxene is removed and line **C** represents the direction that the magma composition will move in when amphibole is removed.

KEY

- Plagioclase (CG and LSD)
- Amphibole (FS, CG and LSD)
- Clinopyroxene (FS and CG)
- Olivine (FS and CG)
- Separation Point Granite
- Late Stage Diorite
- Cumulus Gabbro
- Fractionation Suite
- Onekaka Schist
- Arthur Marble

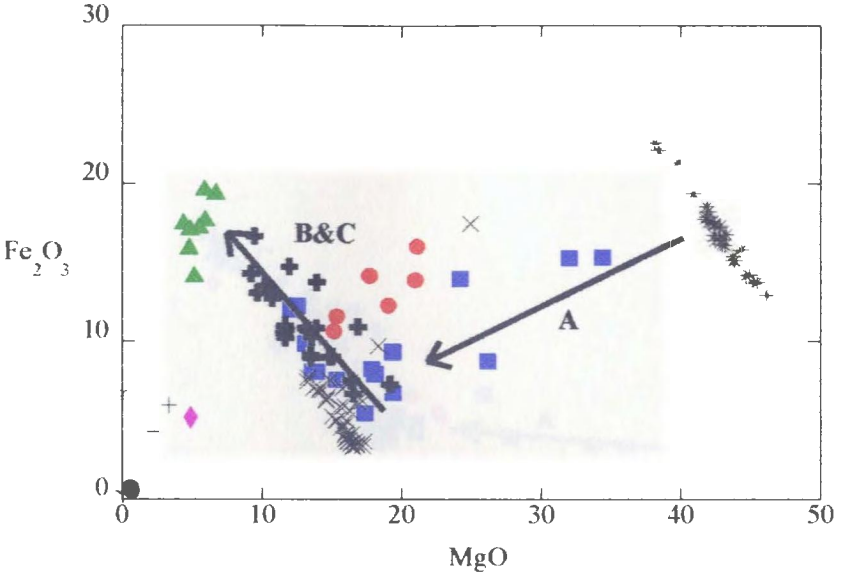
30
20
10
0
Fe2O3
B&C
A
0
10
20
30
40
50
MgO

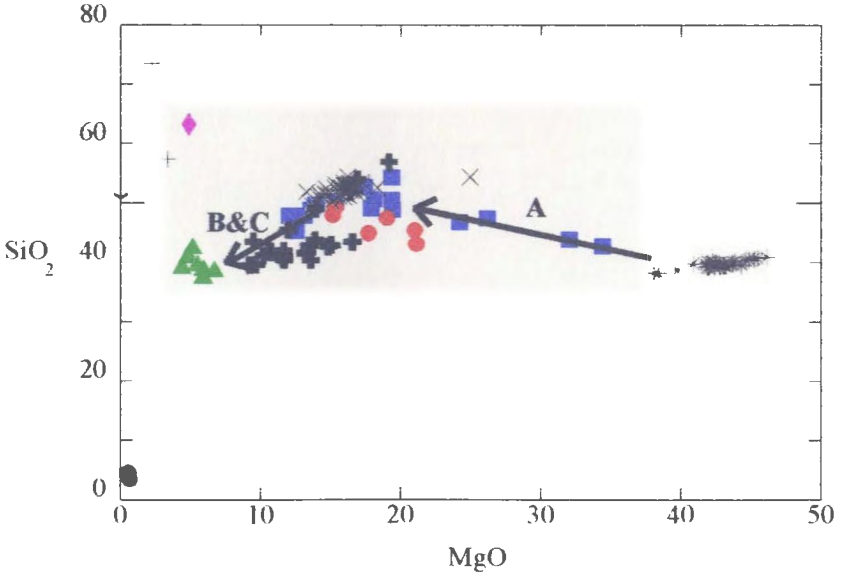
80
60
40
20
0
SiO2
B&C
A
0
10
20
30
40
50
MgO

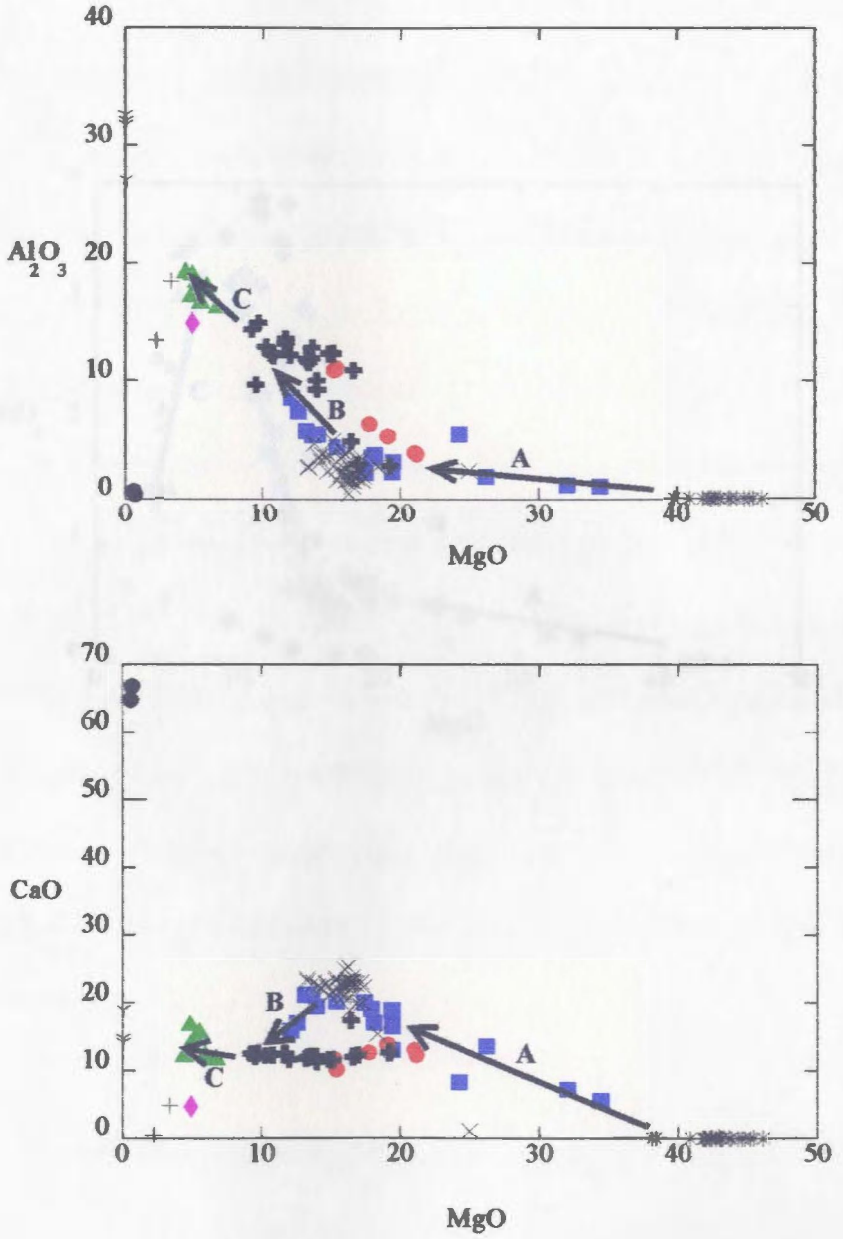
40
30
20
10
0
Al_2O_3
C
B
A
0
10
20
30
40
50
MgO
70
60
50
40
30
20
10
0
CaO
B
C
A
0
10
20
30
40
50
MgO

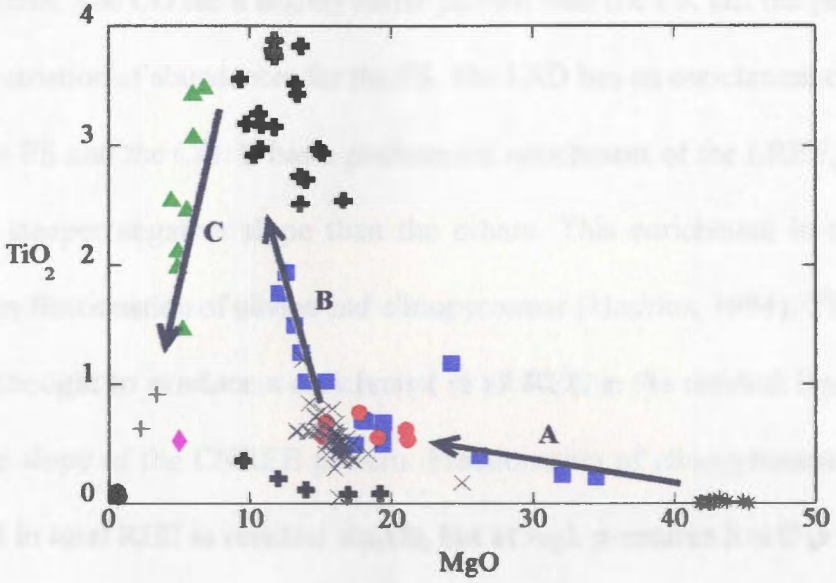
4
3
2
1
0
TiO2
0
10
20
30
40
50
MgO
A
B
C

4.6.3 Rare earth elements

The CNREE diagrams for the FS, CG and LSD (Figure 4.3 A, B and C) have very similar patterns. The CG has a slightly flatter pattern than the FS, but the pattern is contained within the variation of abundances for the FS. The LSD has an enrichment of all REE relative to both the FS and the CG. It has a preferential enrichment of the LREE, giving its pattern a slightly steeper negative slope than the others. This enrichment in total REE can be explained by fractionation of olivine and clinopyroxene (Haskins, 1984). The fractionation of olivine is thought to produce a enrichment in all REE in the residual liquid, but it will not change the slope of the CNREE pattern. Fractionation of clinopyroxene will also cause a enrichment in total REE in residual liquids, but at high pressures it will preferentially enrich the LREE causing an increase in a negative slope (Haskins, 1984). No Eu anomalies are observed in these CNREE diagrams indicating that the crystallization and fractionation of plagioclase did not play an important role during the formation of the Riwaka Complex (Haskins, 1984).

4.6.4 Mineral chemistry versus stratigraphic height

The Fo composition of olivines and the En compositions in clinopyroxenes both exhibit compositional resettings and an overall fractionation throughout the section of the FS. In the 400m section that contains olivine and clinopyroxene three resetting events occurred,

at 125m, 225m and 350m, that have affected the chemistry of both phases. At 400m olivine disappears from the section, but this does not appear to have affected the composition of the clinopyroxenes. Between 550m and 742m the En composition in clinopyroxenes is significantly reset, but olivine does not reappear. The resettings in composition are likely caused by injections of a less fractionated magma to the crystallizing magma chamber.

The overall trend in the first 400m and the remainder of the section is that of "normal fractionation" (i.e. the magma is evolving from a liquid that has a high MgO content to one with a lower content). It is here speculated that the sampled magma chamber was replenished by "fresh" unfractionated magma as many as five times.

4.7 Summary

The Riwaka Complex formed from a tholeiitic magma, that underwent olivine fractionation, producing the earliest rocks of the FS. At approximately 17 wt% MgO clinopyroxene became the dominant cumulate phase producing the late FS and CG rocks. The chemical trends exhibited by the FS and the CG are consistent with magmatic fractionation. The trend shown by the LSD does not initially appear to be the result of straight forward differentiation. However, it is thought that because there was likely little melt left when the LSD crystallized, amphibole fractionation and possible assimilation of marble and schist country rocks was enough to give the LSD a different crystallization history compared with the FS and CG. Hence, the LSD was the last lithology to crystallize and was the result of

magma differentiation and country - rock assimilation.

Olivine and clinopyroxene of the Riwaka Complex exhibit cryptic variation across a 1000 m section of the Fractionation Suite. There appear to be up to five periods of magma replenishment. These periods of replenishment indicate that the Riwaka Complex was possibly formed from multiple intrusions derived from a larger magma source.

Geochemical evidence from the Riwaka Complex indicates that it may have been produced by either a sequence of multiple intrusions produced by progressive fractional melting of the mantle as was proposed by Ruckmick and Noble, 1959; Taylor and Noble, 1960, 1969, for other Alaskan - type ultramafic complexes; or by gravitational fractionation of a series of intrusions of ultrabasic magmas of similar compositions (Irvine, 1963).

Chapter 5

Economic Mineralization and Potential

5.1 Introduction

In 1967, Mike Johnston, later of the Geological Survey of New Zealand, discovered an outcrop of semi - massive sulphides near Prospect Creek in the Graham Valley area of the Riwaka Complex while mapping for his M.Sc. thesis. This discovery led to considerable exploration in the area for Cu - Ni deposits. The exploration was begun in 1968 by McIntyre Mines (NZ) Limited. Their exploration included stream sampling and regional prospecting which located Cu - Ni sulphides at Prices and Field Creeks. They drilled a total of 22 diamond drill holes (ddh), 16 in the Graham Valley and three each at Prices and Field Creeks. McIntyre withdrew from New Zealand in 1970 and farmed out their holdings to Western Compass N.L., who drilled an additional four ddh in the Prospect Creek area with no substantial discoveries.

From 1974 to 1979 the area was explored under a joint venture between Otter Minerals Exploration Limited and Gold Mines of New Zealand Limited. They carried out additional mapping, soil sampling and geophysical surveys on the property. No work was done between 1979 and 1987.

In 1987 Sigma Resources NL took over the mineral rights to the property. They sampled mineralized outcrops and previously drilled core, and did some shallow trenching. They also initiated sampling for precious metals (platinum - group elements (PGE)).

A complete history of work done in the area is given in Table 5.1 (after Cowden et al., 1988).

Table 5.1

The main targets of exploration include; Prospect Creek, Thorns Creek, Prices Creek, North Graham Valley and Field Creek (Figure MA - 1).

1. Thorns Creek

(a) McIntyre Mines New Zealand Limited (1967 - 1970)
- Minor stream sediment sampling

(b) Otter Minerals and Gold Mines of New Zealand Limited (1975 - 1978)
- Minor stream sampling
- Extension of Prospect Creek grid, 1000 ft long base line, 800 ft cross - lines at 100 ft intervals
- Copper and nickel soil survey, samples at 50 ft spacings on cross lines
- Ground magnetic survey
- Seven Crone EM traverses
- Geological mapping
- Petrology

(c) Sigma Resources
- Sampling of mineralized outcrop, minor shallow trenching

2. Prospect Creek (Central Graham Valley)

(a) McIntyre Mines New Zealand Limited (1967 -1970)
- Stream sediment sampling
- Established a grid, 5000 ft base line, 3000 ft cross - lines at 200 ft intervals
- Geological mapping
- Copper, lead, nickel, cobalt and zinc in soil survey, samples at 50 ft spacing.
- IP survey on all lines

- Ground magnetic survey
- Drilling of 16 diamond drill holes (ddh)
- Metallurgical testwork

(b) Western Compass Minerals NL (1971 - 1978)
- Construction of Prospect Creek road
- Drilling of 4 ddh in the Prospect Creek area

(c) Otter Minerals and Gold Mines of New Zealand Limited (1975 - 1978)
- Re - establishment of McIntyre grid, establishment of an intermediate (100 ft) lines along the eastern contact. Extension of grid south and west.
- Construction of 'Newmans' road
- Copper and nickel in soil survey over eastern contact and grid extensions, 50 ft sample spacing, 50 ft line spacing in the Prospect Creek area
- Ground magnetic survey
- Crone EM survey over entire grid
- Drilling of one ddh
- Metallurgical testwork
- Petrology
- Geological mapping

(d) Sigma Resources (1987 - 1988)
- Re - establishment of Gold Mines - McIntyre grid over eastern contact zone
- Geological mapping
- Sampling of mineralized outcrop
- Sampling of drill core for PGE assay

3. North Graham

(a) McIntyre Mines New Zealand Limited (1967 - 1970)
- Minor stream sediment sampling

(b) Mineral Deposits Limited (1970 - 1972)
- Extension of Prospect Creek Road
- Soil survey
- Geological mapping
- Drilling of 3 ddh

(c) Otter Minerals and Gold Mines of New Zealand Limited (1975 - 1978)
- Stream sediment sampling
- Geological mapping
- Petrology

(d) Sigma Resources (1987 - 1988)
- No work

4. Field Creek

(a) McIntyre Mines New Zealand Limited (1967 - 1970)
- Stream sediment sampling
- Establishment of grid, 4400 ft long base line, cross lines at 200 ft intervals
- Copper, nickel and cobalt in soil survey, samples at 50 ft spacing
- IP survey on every alternate line
- Ground magnetic survey on every alternate line
- Drilling of 3 ddh

(b) Otter Minerals and Gold Mines of New Zealand Limited (1975 - 1978)
- Ridge and spur soil sample traverses
- Establishment of new grid
- Soil survey over new grid
- Geological mapping

(c) Sigma Resources (1987 - 1988)
- Limited outcrop sampling

5. Prices Creek

(a) McIntyre Mines of New Zealand Limited (1967 - 1970)
- Stream sediment sampling
- Establishment of grid, 3400 ft long base line, cross - lines at 200 ft intervals
- Copper, nickel and cobalt in soil survey, samples at 50 ft intervals
- Ground magnetic survey
- Some IP surveys
- Geological mapping
- Outcrop sampling
- Drilled 3 ddh

(b) Otter Minerals and Gold Mines of New Zealand Limited (1975 - 1978)
- Ridge and spur soil sample traverses
- Geological mapping
- Petrology

6. North Riwaka Complex

(a) McIntyre Mines of New Zealand Limited (1967 - 1970)

- Stream sediment sampling

(b) Otter Minerals and Gold Mines of New Zealand Limited (1975 - 1978)
- Stream sediment sampling
- Limited ridge and spur soil sample traverses

This chapter will describe the main mineralized showings and the economic potential of the area by examining the petrography and geochemistry of collected mineralized samples. This information is then further used to help understand the petrogenesis of the Riwaka Complex.

5.2 Cu - Ni Mineralization

The author's work on mineralized samples is confined to the Prospect Creek and Thorns Creek showings. Descriptions of other showings are taken from Cowden et al. (1988).

5.2.1 Prospect Creek showing

The mineralized samples at Prospect Creek contain up to 65 % sulphides, dominantly pyrrhotite with lesser amounts of pyrite, chalcopyrite, pentlandite and minor mackinawite. The mineralization occurs in the Cumulus Gabbro and is thought to represent a trapped interstitial phase that occurred between cumulate pyroxenes in the gabbro.

5.2.2 Beau's Creek

Outcrops are of gossanous pyroxenite and gabbro with sulphide contents up to 20 %. The sulphides present are pyrrhotite, pentlandite and chalcopyrite. The mineralized outcrops extend over an area 150 m in length and 22 m in width. This prospect contains anomalous Cu - Ni and PGE (Cowden et al., 1988).

5.2.3 Thorns Creek

Samples here contain up to 80 % sulphides, but the best copper and nickel values are obtained where 15 - 30 % sulphides are present. The sulphides are pyrite, chalcopyrite, minor pyrrhotite and pentlandite. They are found within a magnetite - bearing, poikilitic, pyroxene - hornblendite (Cowden et al., 1988).

5.2.4 North Graham

North of Prospect Creek an area of copper - rich mineralization occurs within a hornblendite host (Cowden et al., 1988).

5.2.5 Field Creek

Samples of gossanous pyroxenite and hornblendite contain minor pyrrhotite - pyrite, chalcopyrite and pentlandite (Cowden et al., 1988).

5.2.6 Prices Creek

Mineralization occurs here in a magnetite - bearing, poikilitic, pyroxene - hornblendite. It consists of pyrite, chalcopyrite, minor pyrrhotite and pentlandite (Cowden et al., 1988).

5.3 Petrography of the Sulphide Phases

The majority of sulphides present within the Riwaka Complex consist of pyrrhotite, chalcopyrite, pentlandite and minor pyrite. These minerals are found dominantly within samples of Cumulus Gabbro. The Late Stage Diorite contains only very minor pyrite and the ultramafic rocks of the Fractionation Suite contain minor sulphides in two samples. The pyrrhotite, pentlandite and chalcopyrite are interstitial and appear to have crystallized by sulphur saturation of original magma resulting in a trapped immiscible sulphide phase between the cumulate pyroxene.

5.3.1 Pyrrhotite

Pyrrhotite is the most abundant sulphide mineral; it can make up to 35 % of the mode. It is always found as an interstitial phase and anhedral crystals range from 0.5 to 5 mm in size. A variety of textures are well developed including monoclinic pyrrhotite replacement of hexagonal pyrrhotite along fractures (Plate 5.1) and (Figure 5.1). Crystals also have well developed twins, indicating the sulphides have experienced some deformation (Plate 5.2). The extent of this deformation is not well documented, but it does not appear to have affected the silicate phases. Therefore it is not thought to have mobilized the sulphides or affected the nature of mineralization.

5.3.2 Chalcopyrite

Chalcopyrite is a common phase in the samples that contain abundant sulphides and some samples contain up to 5 % of anhedral, 0.5 to 5 mm crystals. The chalcopyrite appears to have crystallized at the same time as the pentlandite with which it is spatially closely related (Plate 5.3). The chalcopyrite can be seen as thin wisps within the pyrrhotite, similar to the pentlandite (Plate 5.4).

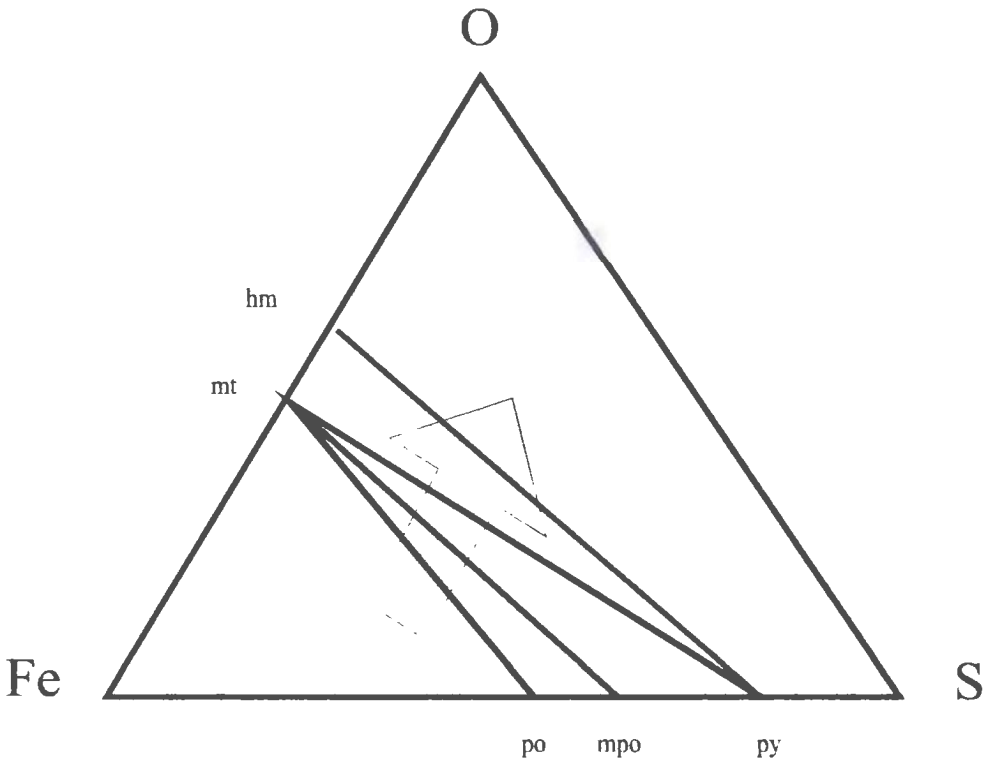

Figure 5.1 Diagrammatic low - temperature phase relations in the Fe - S - O system showing oxide and sulphide minerals. Oxidation of mineral assemblages, as indicated by the shaded arrow, results in the change of hexagonal pyrrhotite (po) into monoclinic pyrrhotite (mpo) and pyrite (py) (Craig, 1990).

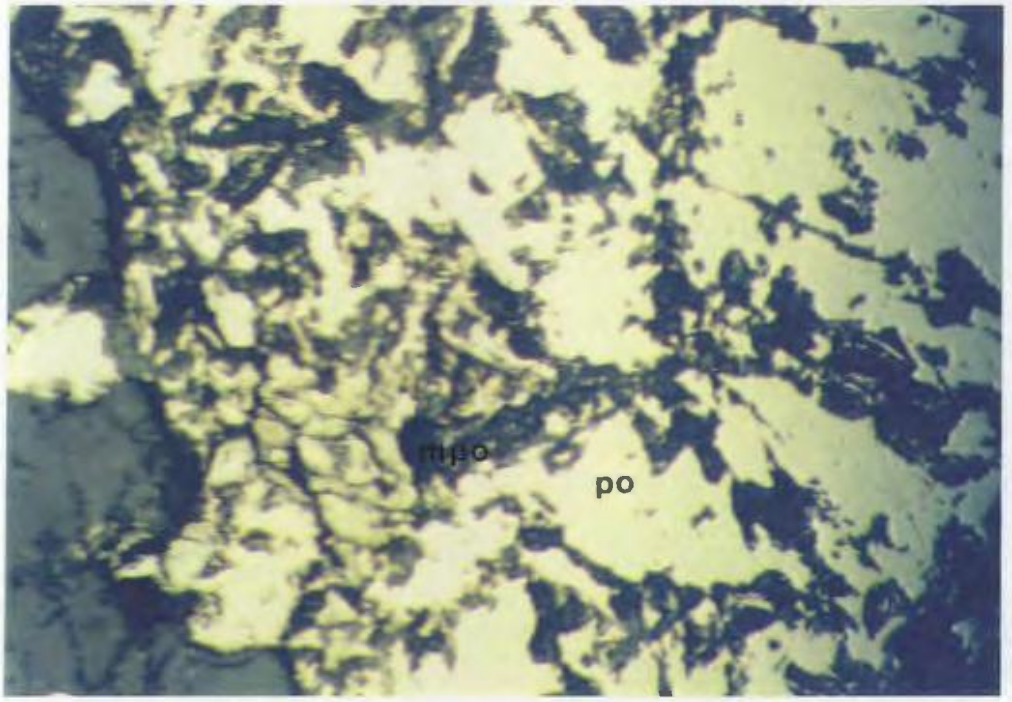

Plate 5.1 Monoclinic pyrrhotite (po) replacement of hexagonal pyrrhotite along fractures (32X magnification, PPL).

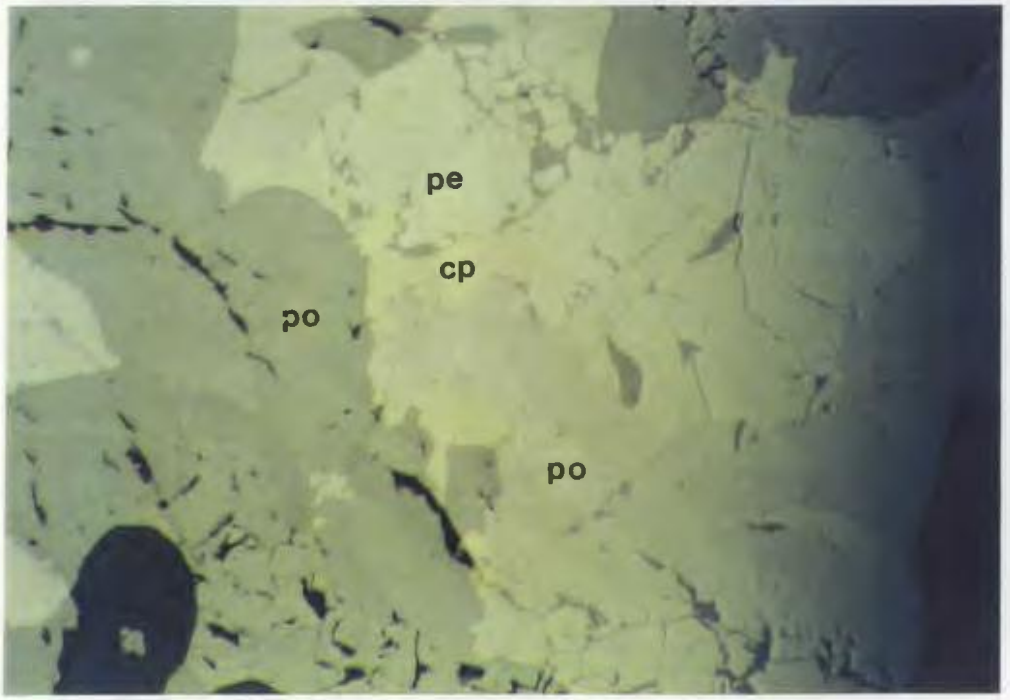

Plate 5.2 Twinning in pyrrhotite (po) (32X magnification, XP).

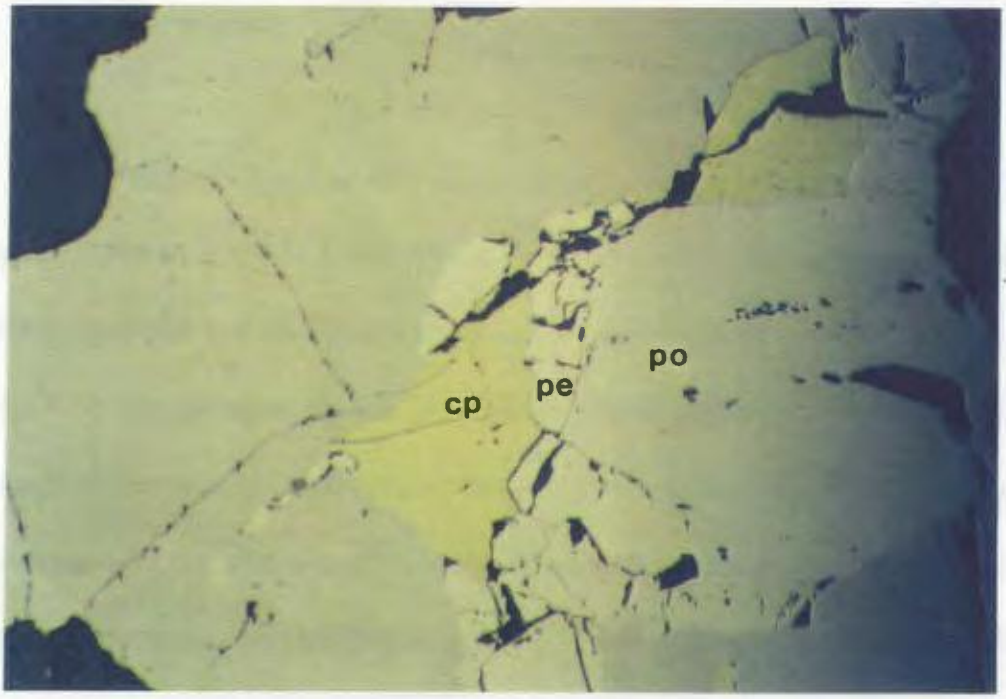

Plate 5.3 Spatial relationship of pyrrhotite (po), pentlandite (pe) and chalcopyrite (cp) (32X magnification, PPL).

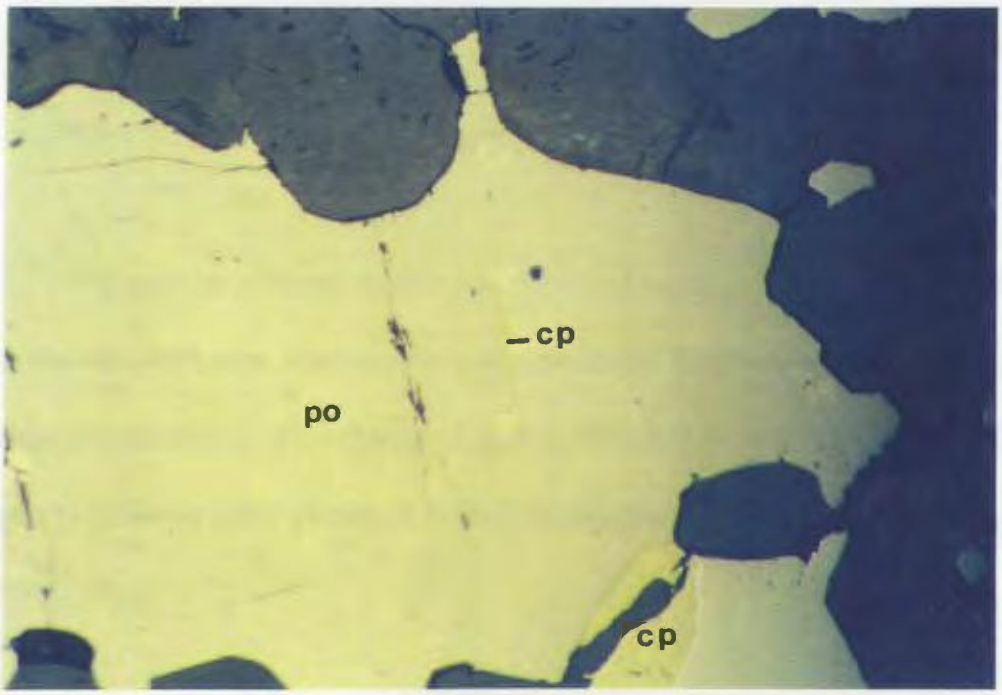

Plate 5.4 Thin wisps of chalcopyrite (cp) within pyrrhotite (po) (32X magnification, PPL).

5.3.3 Pentlandite

Pentlandite is found as thin wisps within pyrrhotite and as distinct anhedral crystals ranging in size from 0.1 to 1 mm. The crystals are concentrated along boundaries between grains of pyrrhotite and are thought to be due to coalescesence of early exsolved pentlandite (Plate 5.5). The anhedral crystals of pentlandite form highly fractured chain - like veinlets. This pull - apart texture is attributable to the high coefficient of thermal expansion (i.e. 2 to 10 times greater than that of pyrrhotite and chalcopyrite) causing shrinkage of pentlandite that formed by coalescence of early exsolved lamellae at high temperatures (300 - 600 °C). The crystals of pentlandite are typically fractured because they have undergone much greater shrinkage than the surrounding pyrrhotite (Craig, 1990) (Plate 5.5).

5.3.4 Pyrite

The majority of the pyrite found within the Riwaka Complex appears to have formed later than the pyrrhotite, chalcopyrite and pentlandite. Its formation maybe due to oxidation during remobilization of pyrrhotite (Figure 5.1) as it is mostly found in small veinlets that appear to cross-cut other phases. It is found within the Cumulus Gabbro and the Late Stage Diorite.

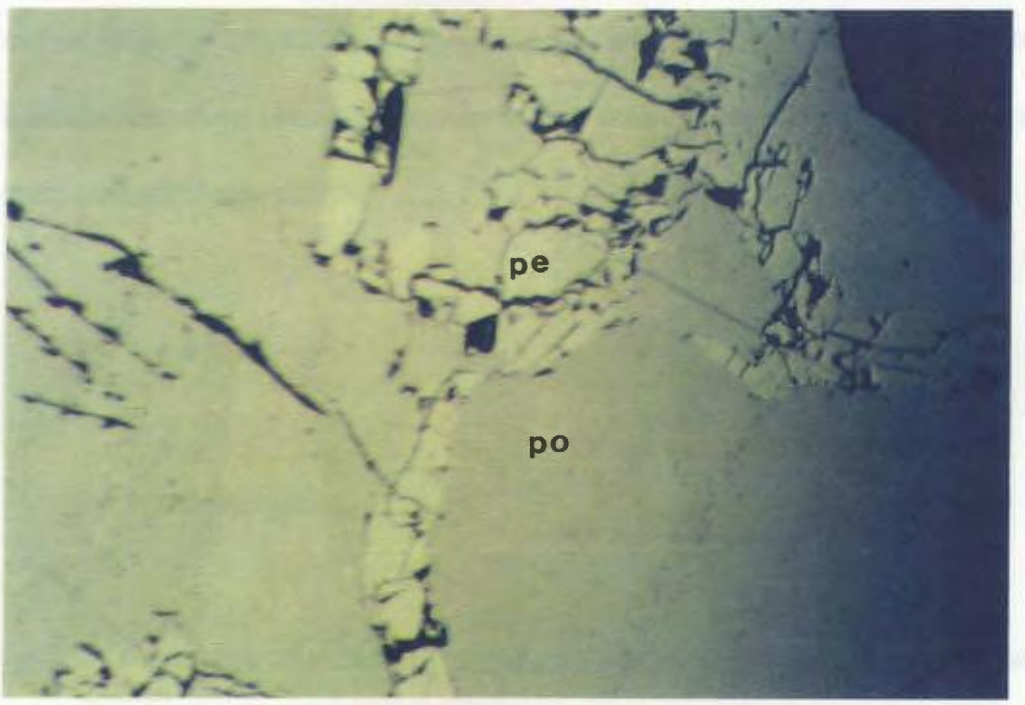

Plate 5.5 Pentlandite (pe) concentrated along grain boundaries of pyrrhotite (po) (32X magnification, PPL).

5.3.5 Alteration

The petrography of sulphide phases in the Riwaka Complex suggests that they have undergone some hydrothermal alteration as have the silicate phases (Chapter 3) as indicated by local pyrite veinlets. The alteration is thought to be related to localized faulting. It has not significantly remobilized the sulphides as they still exhibit primary interstitial igneous textures. However, in some samples the chalcopyrite has undergone remobilization due to alteration, as it can be seen along cleavage fractures within biotite. This occurs in the same samples that contain monoclinic pyrrhotite.

5.4 Geochemistry

5.4.1 Introduction

The elements considered in this chapter are economically important and have historically been found associated with lithologies similar to those present in the Riwaka Complex. They include Ni, Cu and the platinum group elements (PGE) (Ir, Os, Ru, Rh, Pt, Pd and for the purpose of this study Au). The Ni and Cu concentrations were measured by X-ray fluorescence spectrometry on pressed pellets; the PGE were measured by Inductively Coupled Plasma Mass Spectrometry (Table A19 - A22).

Samples of all three suites have been analyzed for Ni and Cu. However, only

representative samples of the most mineralized sections of the Cumulus Gabbro and two samples of the Fractionation Suite have been analyzed for their PGE as they represent the best targets for these metals. The Cumulus Gabbro samples are sections of drill core taken from diamond drill holes GV - 1, GV - 4 and GV - 5 which intersected mineralization at the Prospect Creek and Beau's Creek showings. A listing of the sample numbers, drill holes and intervals, as well as geological maps of the drill hole areas are given in Appendix C.

Naldrett and Duke (1980) normalized their values of Ni, Cu and PGE values to 100% sulphides. However, Barnes (1987) did not believe that this process is appropriate. She suggested that a number of the assumptions made when normalizing are not necessarily valid. Firstly, normalizing to 100% sulphides assumes that during crystallization of the rocks, all precious metals entered a sulphide liquid containing 36 - 38% sulphur. In rocks containing chromite or olivine some of the Os, Ir and Ru may be present in these phases, or as platinum - minerals. Secondly, Balhaus and Stumpfl (1986) suggested that under certain circumstances the precious metals partition into a fluid phase rather than a sulphide phase. Thirdly, the normalization assumes that the present sulphur content of the rock is the same as the original or primary value, but sulphur is an extremely mobile element during hydrous alteration of rocks. Naldrett and Duke (1980) do recognize that there are inherent problems with their method, and for these reasons, the data collected in this study have not been normalized to 100% sulphides.

5.4.2 The Fractionation Suite

The Fractionation Suite rocks are for the most part unmineralized with the exception of two samples (JS - 91- 122, JS - 91 - 149). These samples contained trace pyrrhotite and chalcopyrite. Samples taken in this study were collected through a section perpendicular to layering. Table A19 lists the Ni and Cu values along with the Ni/Cu ratios. The Ni values range from 105 to 1129 ppm and Cu values range from 8 ppm to 311 ppm. The Ni/Cu ratios range from 0.34 to 94. Samples JS - 91 - 122 and JS - 91 - 149 were analyzed for PGE. Values are reported in Table A22.

5.4.3 The Late Stage Diorite

Samples of the Late Stage Diorite were randomly collected. They are essentially unmineralized, although very minor pyrite occurs. Table A21 gives the Ni and Cu concentrations in these rocks. The Ni ranges from 0 to 144 ppm and the Cu from 26 to 174 ppm, the Ni/Cu ratios range from 0 to 1.34. No PGE analyses were performed on these rocks.

5.4.4 Cumulus Gabbro

All Cumulus Gabbro samples were collected from diamond drill holes GV - 1, GV - 4 and GV - 5. They represent heavily mineralized sections (pyrrhotite, pentlandite and

chalcopyrite). Table A20 and A22 presents the Ni, Cu and PGE values for samples of the Cumulus Gabbro. The Ni ranges from 231 ppm to 0.9 wt%, the Cu from 139 ppm to 4.2 wt%. The Ni/Cu ratios range from 0.23 to 5.54. The large variation in Ni/Cu ratios indicates that the mineralizing process preferentially enriched neither Ni nor Cu.

The Pt+Pd/(Ru+Ir+Os) ratios (Table A22) for the Cumulus Gabbro are all above 20 with the exception of two samples (JS-91-122 and JS-91-203). This is reflected in the chondrite normalized PGE (CNPGE) pattern in Figure 5.2 (after Naldrett and Duke, 1980), which has a positive slope, indicating an enrichment of Pt, Pd and Au relative to Os, Ir and Ru. If the PGE pattern is mantle normalized (MNPGE) (Figure 5.3; values from Barnes et al., 1987) the samples again have a positive slope. The Os, Ir and Ru values are similar to mantle and the Pd and Au values have an enrichment of 10 to 100 times mantle. When Ni and Cu are added to the same CNPGE pattern diagram (figure 5.4; after Barnes, 1987) a trough - shaped curve results. The samples from the Cumulus Gabbro plot in the layered intrusion and the flood basalt field on the metal ratio diagrams of Ni/Cu versus Pd/Ir (Figure 5.5) and Cu/Ir versus Ni/Pd (Figure 5.6)

5.5 Metallogeny

5.5.1 Introduction

The metallogeny of Cu-Ni and PGE deposits within mafic intrusions has been well

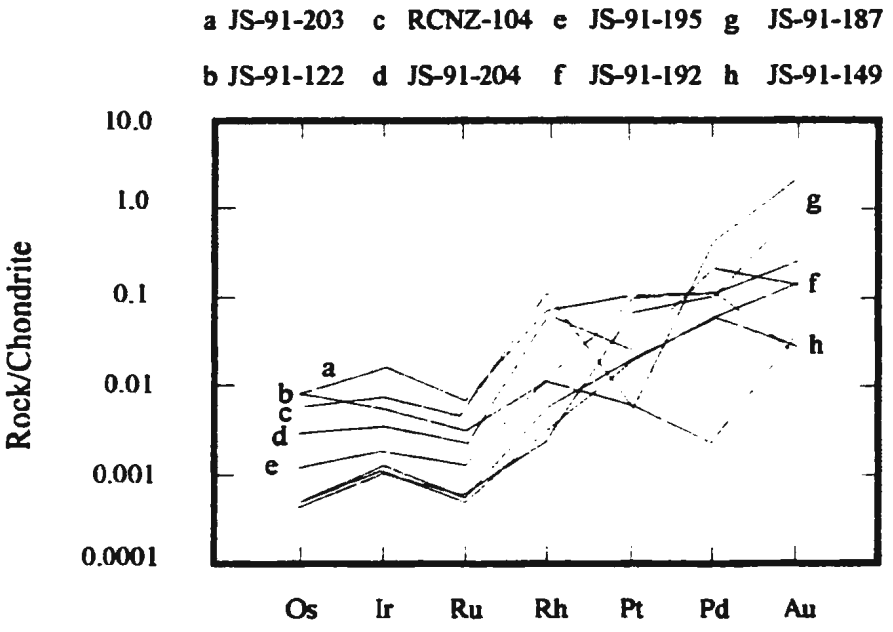

Figure 5.2 Chondrite - normalized PGE pattern diagram.

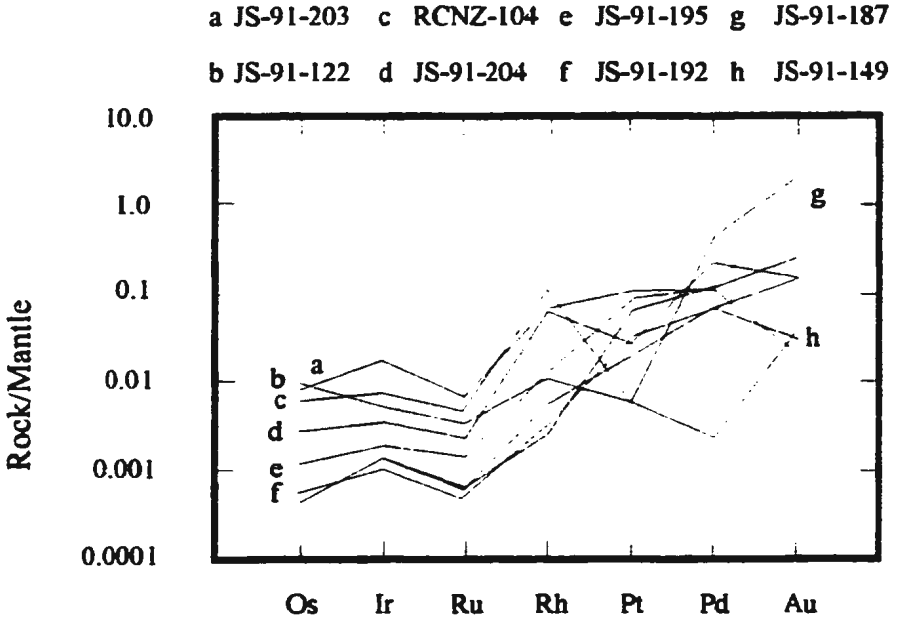

Figure 5.3 Mantle - normalized PGE pattern diagram.

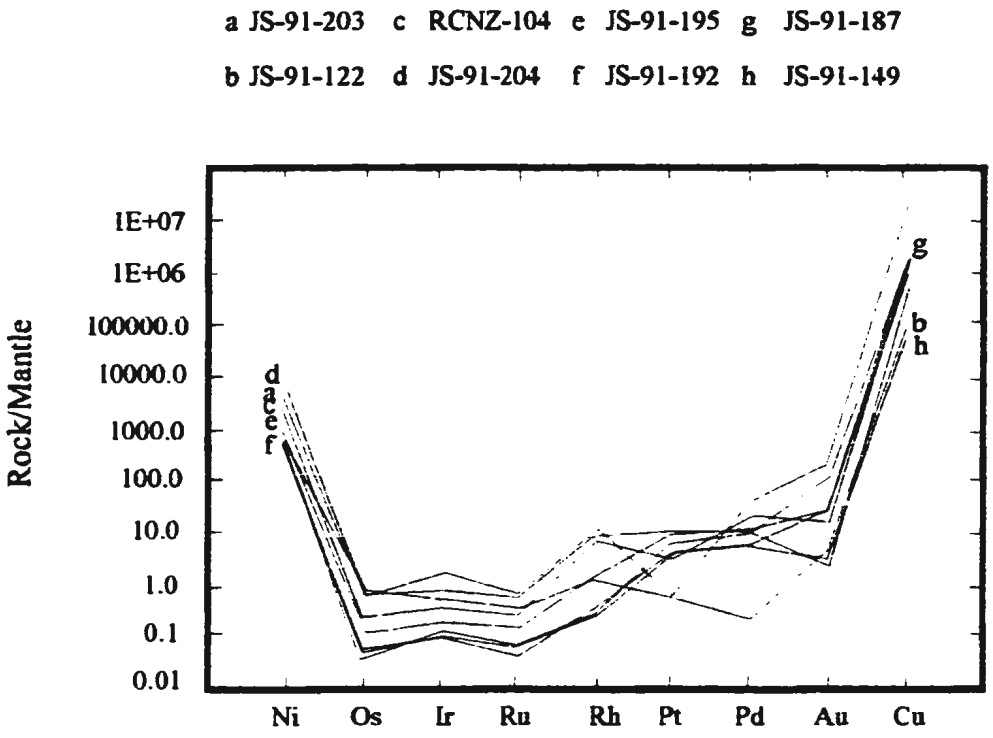

Figure 5.4 Mantle - normalized PGE pattern diagram with Ni and Cu added.

Figure 5.5 (a). Metal ratio diagram of Pd/Ir versus Ni/Cu based on literature data for discriminating between the compositional fields of: mantle, komatiites and sulphides associated with them, high MgO - basalts and associated sulphides, ocean - floor basalts, boninites and low TiO_2 basalts, flood basalts and sulphides associated with them, ophiolites and podiform chromites from ophiolites, Pt - reefs, layered intrusions of unknown affinity and Cu - rich sulphides. D = dunites from Thetford ophiolite, B = B - zones of komatiites and C = Cliff locality from Unst. The inset shows the displacement vectors on the diagram for the affects of partial melting of mantle, olivine removal or addition and chromite removal or addition (after Barnes et al., 1987). (b) Diagram of Pd/Ir versus Ni/Cu for the Cumulus Gabbro of the Riwaka Complex compared with selected fields.

a

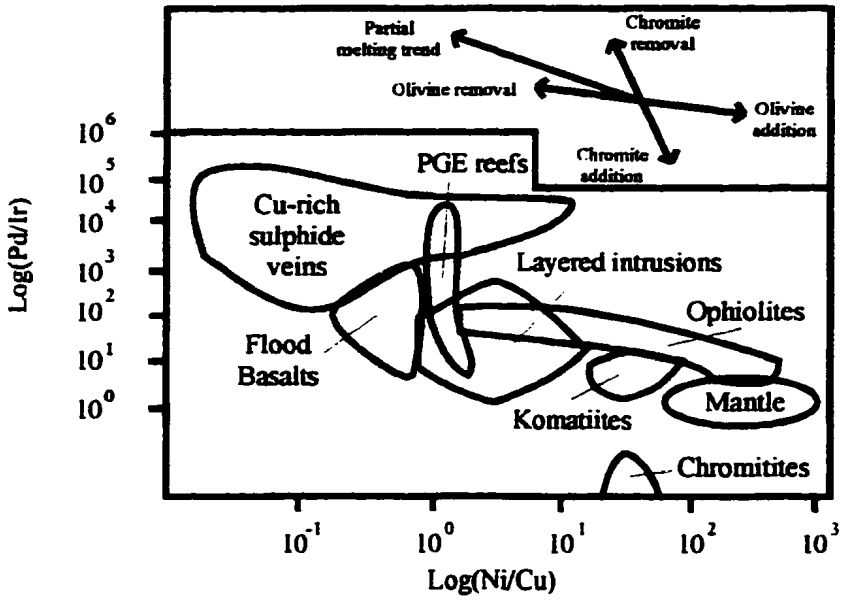
Partial melting trend
Chromite removal
Olivine removal
Olivine addition
Chromite addition
PGE reefs
Cu-rich sulphide veins
Layered intrusions
Ophiolites
Flood Basalts
Komatiites
Mantle
Chromitites
Log(Pd/Ir)
Log(Ni/Cu)

b

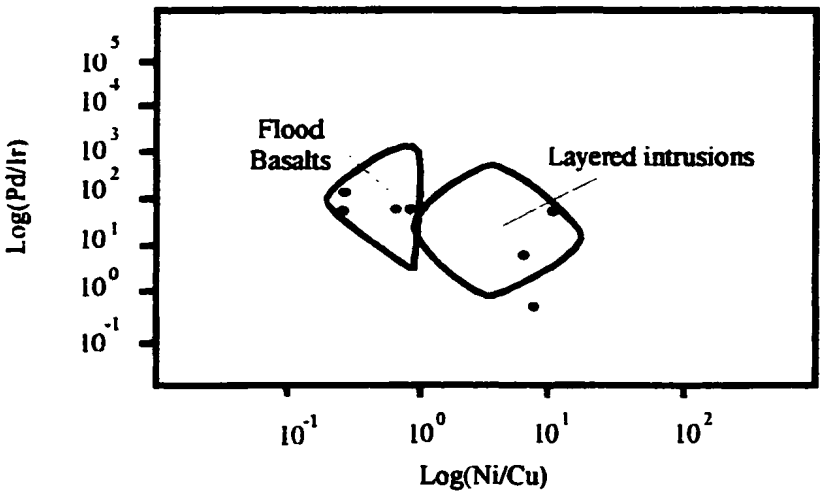
Flood Basalts
Layered intrusions
Log(Pd/Ir)
Log(Ni/Cu)

Figure 5.6 (a) Metal ratio diagram of Ni/Pd versus Cu/Ir based on the literature data base. Compositional fields are as on Figure 5.5 (a). Inset shows the displacement vectors for olivine removal or addition, chromite removal or addition and sulphide removal, the partial melting trend has been left off for clarity (after Barnes et al., 1987). Symbols as on Figure 5.5 (a). (b) Diagram of the Ni/Pd versus Cu/Ir for the Cumulus Gabbro of the Riwaka Complex compared with selected compositional fields.

a

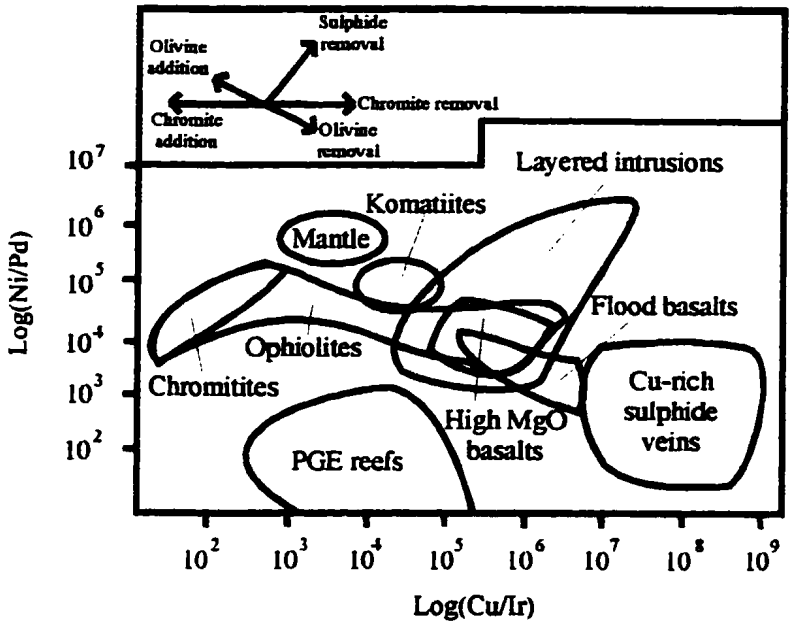
Sulphide removal
Olivine addition
Chromite removal
Chromite addition
Olivine removal
Layered intrusions
Komatiites
Mantle
Flood basalts
Ophiolites
Chromitites
Cu-rich sulphide veins
High MgO basalts
PGE reefs
Log(Ni/Pd)
Log(Cu/Ir)

b

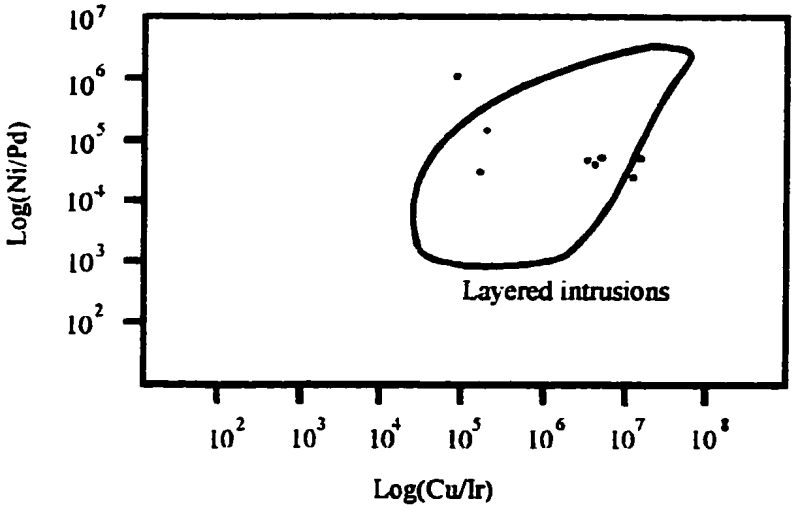
Layered intrusions
Log(Ni/Pd)
Log(Cu/Ir)

documented (Naldrett and MacDonald, 1980; Naldrett and Duke, 1980; Naldrett, 1981; Barnes et al., 1987; Barnes, 1987). The majority of Cu - Ni and PGE deposits are regarded as magmatic in origin (Vogt, 1918; Souch et al, 1969; and Naldrett and MacDonald, 1980), forming from immiscible sulphur droplets in a mafic to ultramafic magma. These droplets partition and concentrate the metals.

Naldrett and Duke (1980) describe the steps in the formation of a magmatic Cu-Ni and PGE deposit as:

1. Generation of a mafic or ultramafic magma within the mantle.

2. Ascent of the magma into the crust.

3. Cooling and the onset of crystallization within or on the crust preceded, accompanied, or succeeded by the segregation of immiscible sulphide into which Ni, Cu and PGE's can partition readily, thus acting as a collector for these elements.

4. Concentration of the sulphides, commonly by gravitational settling (specific gravity of sulphide liquid approximately 3.9 g/cc, specific gravity of silicate melt approximately 2.6-3.0 g/cc).

5. Crystallization of the sulphide liquid into the main sulphide minerals pyrrhotite, pentlandite, chalcopyrite and pyrite, all of which can contain PGE in solid solution. This may be accompanied or followed by the crystallization of platinum minerals.

6. Redistribution of ore minerals by hydrothermal solutions.

Mafic to ultramafic magmas can occur in a variety of locations including; major layered intrusions, minor differentiated sills and dikes, concentrically zoned intrusions,

ophiolites, minor associates of batholithic complexes, alkalic ultrabasic rocks in ring complexes, kimberlites, ultrabasic lavas and ultrabasic nodules (Wyllie, 1967).

Naldrett (1981) developed a classification scheme for magmatic sulphide deposits. It has three main subdivisions based on paleotectonic setting. The three divisions are; 1) syn - volcanic bodies, 2) intrusions in cratonic areas and 3) bodies emplaced during orogenesis. The last of these divisions is of interest to this study as the geological history of this part of New Zealand has been dominated by orogenic events. It has three sub - categories including; 1) synorogenic intrusions, 2) tectonically emplaced bodies (i.e. ophiolites and possibly mantle diapirs) and 3) Alaskan - type ultramafic complexes.

5.5.2 Bodies emplaced during orogenesis

As outlined in the previous two chapters, the Riwaka Complex is here thought to represent an Alaskan - type ultramafic complex. The genesis of the Riwaka Cu-Ni and platinum rich sulphides is related to the emplacement of a mafic to ultramafic magma into carbonaceous sediments, and the processes for the formation of Cu - Ni and PGE deposits is thought to be very similar to those of deposits in other mafic intrusions. A study of Cu-Ni and PGE mineralization can however, be used to help interpret the nature of the parental magma.

Several processes can take place to produce the immiscible sulphur droplets needed to absorb the Ni, Cu and PGE from the surrounding mafic to ultramafic magma in Alaskan -

type ultramafic complexes.

1) Simple cooling of a magma (Haughton et al., 1974).

2) Mixing of two magmas, one primitive, the other more evolved (Irvine, 1977).

3) Addition of sulphur and silica by contamination (Irvine, 1975; Naldrett and MacDonald, 1980).

Any of these processes may have produced the sulphide phase in the Riwaka Complex. However, it is possible that sulphur and silica contamination occurred through assimilation of surrounding carbonaceous sediments. Sulphur isotopes may be necessary to confirm or disprove this, but were beyond the scope of this preliminary work.

Some minor localized hydrothermal alteration has occurred within the Riwaka Complex, however, it is not thought to have remobilized any of the ore minerals, as they exhibit primary igneous textures.

5.5.3 Metallogeny of the Riwaka Complex

5.5.3.1 Nickel/Copper ratios

Nickel/copper ratios have been extensively described from a number of deposit types (Naldrett, 1981). Each deposit type has a unique ratio related to the evolution of the parental magma. Barnes (1987) suggested that as a magma becomes more evolved, the Ni/Cu ratio will decrease. This is logical because the early fractionation of olivine and chromite in a

primary magma will decrease the concentration of Ni in the liquid causing a decrease in the ratio. Hence, suites with the most primitive composition (mantle material) will have high ratios, and the more evolved (continental flood basalts), lower ratios (Table 5.2).

Table 5.2 Ni/Cu ratios for selected rock types (Barnes et al., 1987).

Rock type	Ni/Cu ratio
Mantle	100 - 1000
Komatiite	10 - 100
Ophiolites	0 - 750
Layered intrusions	0 - 10
Flood basalts	0.1 - 0

The Ni/Cu ratios for the Riwaka Complex cover a range of values. The olivine - rich ultramafic rocks of the Fractionation Suite are seen to have the highest values ranging from 0.34 to 94. The Cumulus Gabbro samples range from 0.23 to 5.54. These rocks contain some olivine, but it is much less abundant than in the Fractionation Suite. The Late Stage Diorite has the lowest Ni/Cu ratios ranging from 0 to 1.34. These values correlate well with what is expected as the Fractionation Suite has the most primitive mineralogy, the Cumulus Gabbro slightly more evolved and the Late Stage Diorite the most evolved. Table 5.2 shows that the

Ni/Cu ratios are intimately related to the MgO content of the rocks.

The highest Ni/Cu ratios in the Fractionation Suite correspond to primitive rocks such as komatiites and some rock types found in ophiolites. However, the lower Ni/Cu ratios of the Fractionation Suite are similar to those found in layered intrusions (Table 5.2). The values of the Cumulus Gabbro and the Late Stage Diorites are much lower than those of these primitive rocks and are similar to values found for evolved portions of layered intrusions or those of high MgO basalts (Figure 5.5). This data is not entirely demonstrative of a particular parental magma, but seems to indicate that it began as a relatively primitive magma similar to komatiites and evolved into a basaltic magma.

5.5.3.2 Chondrite - normalized PGE pattern diagrams

Naldrett and Duke (1980) and Barnes et al. (1985) suggested that PGE fractionate in a systematic fashion. Barnes et al. (1985) described PGE as fractionating in order of descending melting point (Os, Ir, Ru, Rh, Pt, Pd and Au). They noted that Pd/Ir and (Pt+Pd)/(Ru+Ir+Os) ratios, reflected by their slopes in chondrite normalized patterns, differ according to the amount of fractionation that has occurred in the parental magma. Mantle derived material (garnet lherzolite and spinel lherzolite xenoliths) have unfractionated PGE patterns (i.e. flat patterns). Peridotitic komatiites have mildly fractionated patterns, pyroxenitic komatiites slightly more fractionated. Both continental and ocean - floor basalts are highly fractionated (Figure 5.7, after Barnes et al., 1985). Mantle derived material has low

Figure 5.7 **a - c**, Chondrite - normalized PGE's: (a) mantle nodules, A, E and F = garnet lherzolite, B and D = spinel lherzolite, C = harzburgite, G = estimate; (b) alpine complexes, A = lherzolite, B, C, E, F and H = harzburgite, D and G = dunite; and (c) chromites from ophiolites.

d - e. Chondrite - normalized PGE's: (d) ophiolites, A and D = dunite, B and E = pyroxenite, C and F = gabbro, G and H = basalt; and (e) ocean floor, A = lower - limit MORB's, B = upper - limit MORB's, C = estimate of MORB's, D = oceanic islands.

f - g. Chondrite - normalized PGE's: (f) komatiites A and C = A - zones of olivine spinifex flows, B = clinopyroxene spinifex flow, D and E = B - zone of olivine spinifex flows; and (g) sulphides from komatiites A = upper limit, D = lower limit, I = Ungava.

h. Chondrite - normalized PGE continental tholeiites: A = Karroo, B = estimate, C = Archean tholeiite, D = Great Lakes, E = Insizwa, Karroo, F = Duluth.

i - j. Chondrite - normalized PGE's: Bushveld, A = lower - zone marginal rock, B = main - and critical - zone marginal rock, C = UG - 2 Reef, D = Merensky Reef; and (j) Stillwater, A = basal zone, B = chromitites, C = JM Reef.

k. Alkali rocks, A and B = kimberlites, C = basanite.

l. Alaskan rocks, A = dunite, B = ultramafic (St. Louis et al., 1986).

m. Riwaka Complex, Cumulus Gabbro.

a to l after Barnes et al., 1985.

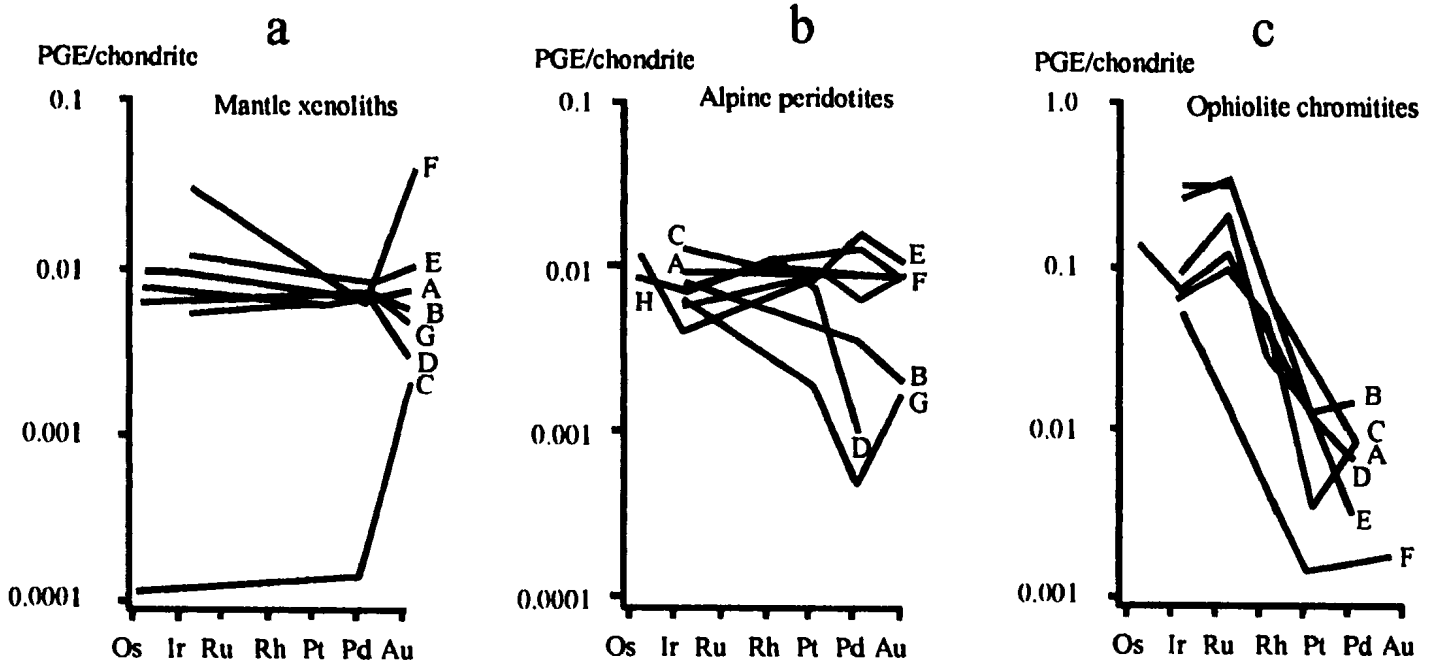
a
PGE/chondrite
Mantle xenoliths
0.1
0.01
0.001
0.0001
F
E
A
B
G
D
C
Os Ir Ru Rh Pt Pd Au
b
PGE/chondrite
Alpine peridotites
0.1
0.01
0.001
0.0001
C
A
H
E
F
B
G
D
Os Ir Ru Rh Pt Pd Au
c
PGE/chondrite
Ophiolite chromitites
1.0
0.1
0.01
0.001
B
C
A
D
E
F
Os Ir Ru Rh Pt Pd Au

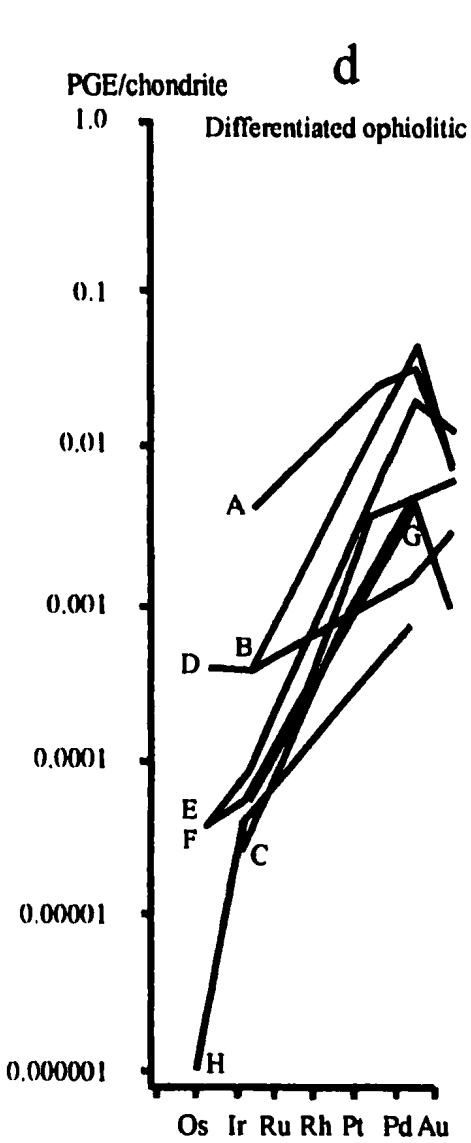
d
PGE/chondrite
Differentiated ophiolitic rocks
1.0
0.1
0.01
0.001
0.0001
0.00001
0.000001
A
B
C
D
E
F
G
H
Os Ir Ru Rh Pt Pd Au

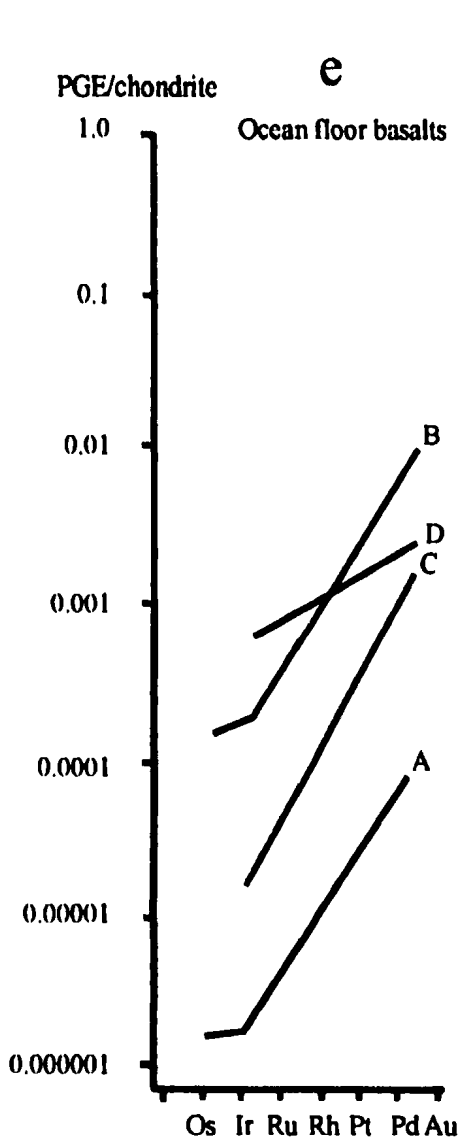
e
PGE/chondrite
Ocean floor basalts
1.0
0.1
0.01
0.001
0.0001
0.00001
0.000001
A
B
C
D
Os Ir Ru Rh Pt Pd Au

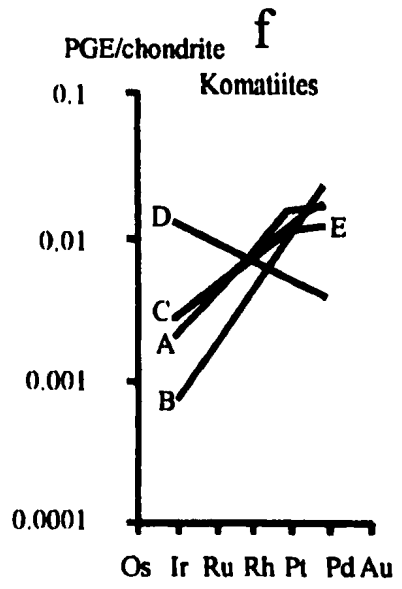
f
PGE/chondrite
Komatiites
0.1
0.01
0.001
0.0001
A
B
C
D
E
Os Ir Ru Rh Pt Pd Au

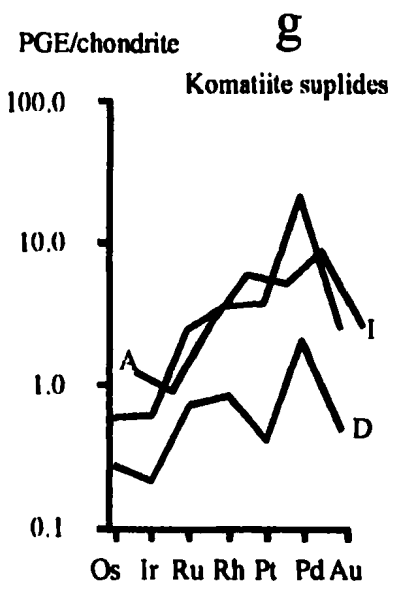
g
PGE/chondrite
Komatiite suplides
100.0
10.0
1.0
0.1
A
D
I
Os Ir Ru Rh Pt Pd Au

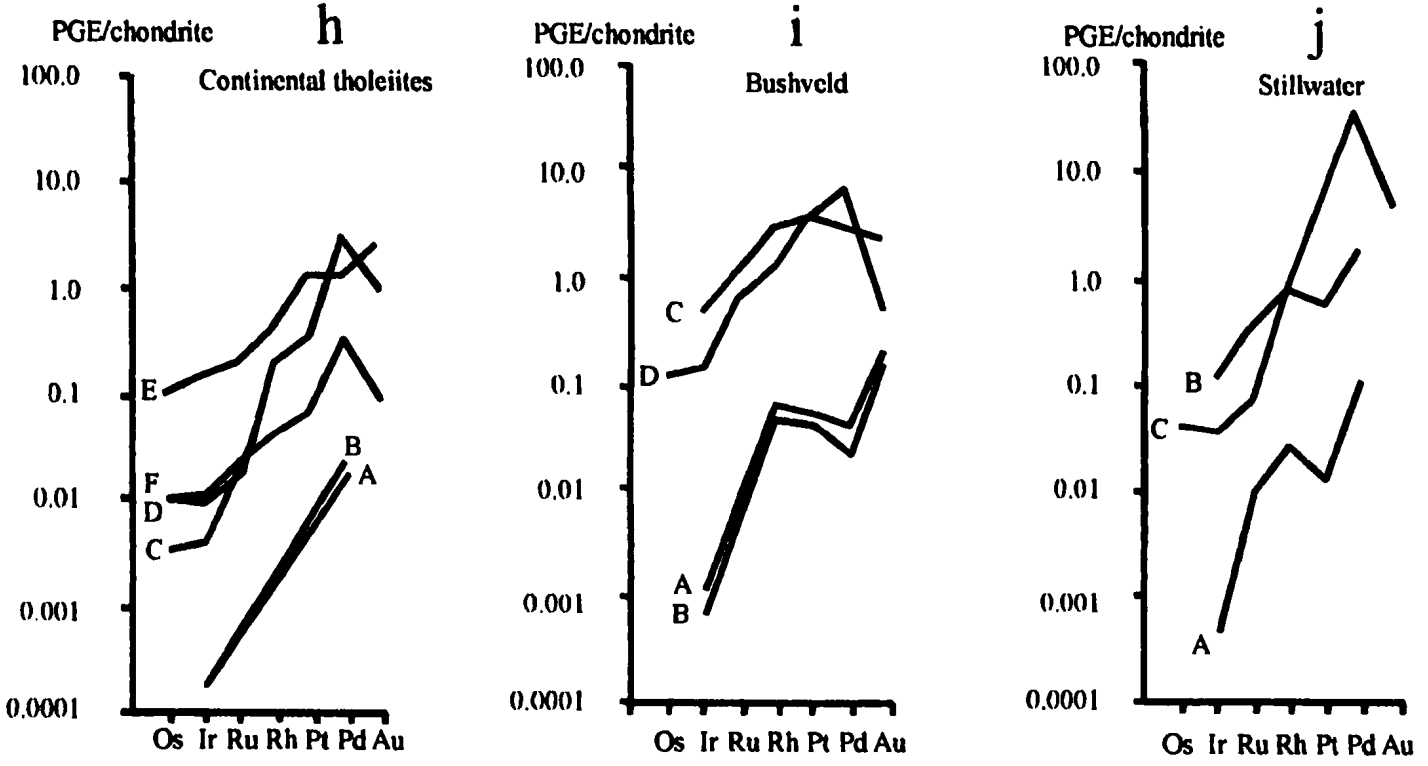
h
PGE/chondrite
Continental tholeiites
100.0
10.0
1.0
0.1
0.01
0.001
0.0001
E
F
D
C
B
A
Os Ir Ru Rh Pt Pd Au
i
PGE/chondrite
Bushveld
C
D
A
B
j
PGE/chondrite
Stillwater
B
C
A

k

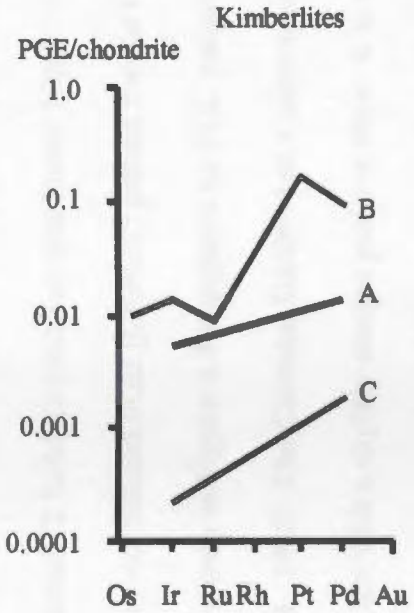
Kimberlites
PGE/chondrite
1.0
0.1
0.01
0.001
0.0001
B
A
C
Os Ir Ru Rh Pt Pd Au

l

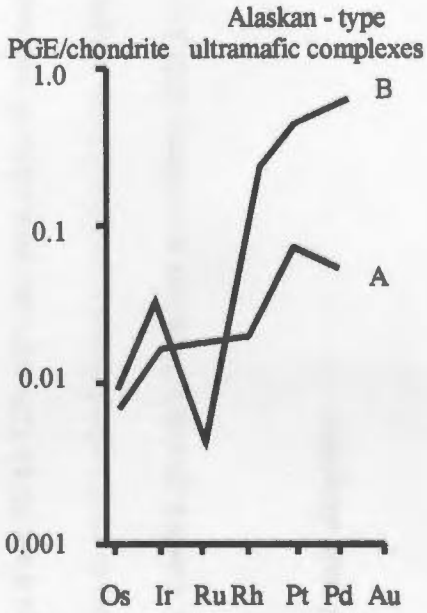
Alaskan - type
ultramafic complexes
PGE/chondrite
1.0
0.1
0.01
0.001
B
A
Os Ir Ru Rh Pt Pd Au

m

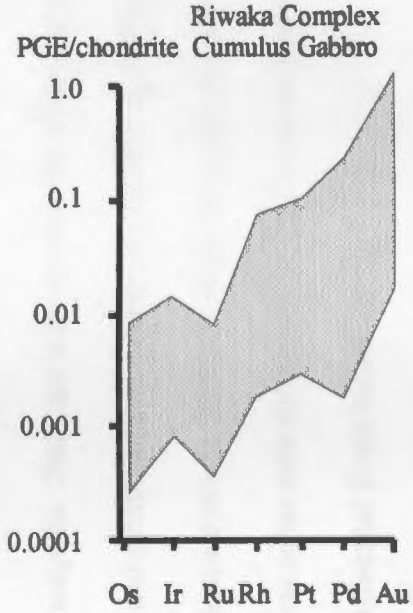
Riwaka Complex
Cumulus Gabbro
PGE/chondrite
1.0
0.1
0.01
0.001
0.0001
Os Ir Ru Rh Pt Pd Au

(Pt+Pd)/(Ru+Ir+Os) ratios and ratios of 13 or more are characteristic of gabbroic magmas containing less than about 12 % MgO (Naldrett and Duke, 1980).

The chondrite - normalized PGE (CNPGE) pattern for the Cumulus Gabbro of the Riwaka Complex is shown in Figure 5.7 compared to PGE patterns from other types of intrusions (Barnes et al., 1985). The Cumulus Gabbro has a pattern similar to Alaskan - type ultramafic complexes, but with a slightly steeper positive slope. It is also similar to tholeiitic intrusions (i.e. continental tholeiites and Stillwater), which are thought to have crystallized from a basaltic parental magma (Hughes, 1982). The (Pt+Pd)/(Ru+Ir+Os) ratios of the Cumulus Gabbro range from 50 to 120 with the exception of two samples. These values are characteristic of gabbroic rocks which have crystallized from magmas containing less than about 12 % MgO (i.e. basaltic parent) (Naldrett and Duke, 1980).

5.5.3.3 Metal ratio diagrams

Metal ratio diagrams have been used by Barnes et al. (1987) in conjunction with mantle - normalized PGE (MNPGE) patterns to investigate petrological problems related to mafic and ultramafic magmas. They can help resolve the effects of partial melting, sulphide segregation, chromite and olivine crystallization. In Figure 5.5, Ni/Cu versus Pd/Ir ratios are used because as a magma evolves the Pd/Ir ratio increases and the Ni/Cu decreases. This separates various magma suites with the most primitive (mantle material) at one extreme and the most evolved (continental flood basalts) at the other.

The Ni/Pd versus Cu/Ir (Figure 5.6) can be used to determine if a sulphide liquid has segregated from a magma or if a sulphide phase has been added to the cumulate. Because the partition coefficients for Cu and Ni into sulphides are much less than for PGE, the segregation of sulphides from a silicate magma causes the silicate liquid to become depleted in PGE relative to Ni and Cu. Therefore, any cumulate containing these sulphides will become enriched in PGE relative to Ni and Cu.

Figures 5.5 and 5.6 are two metal ratio diagrams (after Barnes et al., 1987). The first has Ni/Cu versus Pd/Ir. Samples from the Cumulus Gabbro fall into the layered intrusion field and this is also the case in Figure 5.6 (Cu/Ir versus Ni/Pd). These figures indicate that the Cumulus Gabbro crystallized from a tholeiitic magma with a similar composition found in layered intrusions. It is thought to represent an evolved magma and not a primitive picritic parent.

5.5.3.4 Mantle - normalized PGE patterns

The mantle - normalized PGE (MNPGE) patterns (after Barnes et al., 1987) can be used in a similar manner to chondrite - normalized diagrams. The MNPGE pattern diagrams have Ni added to the left end of the diagram with the PGE that have the highest melting point and Cu to the other end with the PGE with the lowest melting points. This is based on the hypothesis that Ni is compatible with high temperature phases such as olivine and chromite and that Cu acts incompatibly. When early high temperature phases crystallize the remaining

liquid will become enriched in Cu and PGE's with a lower melting point.

The MNPGE pattern diagram (Figure 5.4) exhibits a trough shape. It is enriched in Ni; Os, Ir and Ru are low; there is a marked enrichment of Rh through to Cu. The Ni values are 1000 to 10000 times mantle values; the Os, Ir and Ru are 0.1 to 1 times mantle values; Rh, Pt and Pd range from 1 to 100 times mantle values; and the Au and Cu are from 10 to 10000 times mantle values. Barnes et al. (1987) suggested that this type of pattern is indicative of a magma that has had a sulphide phase removed by fractionation. This would result in the PGE being depleted relative to Cu and Ni. Again this figure supports the theory that the Cumulus Gabbro crystallized from an already fractionated liquid. The sulphides and PGE's may have fractionated out of the magma before crystallization in the Fractionation Suite. If such were the case, the Fractionation Suite would represent a good exploration target for these elements.

5.5 Summary

The Riwaka Complex is a mafic to ultramafic intrusion that has associated primary sulphide phases. The petrography indicates the phases present are pyrrhotite, pentlandite, chalcopyrite and pyrite and that these phases have not undergone significant remobilization due to hydrothermal alteration. These minerals are almost exclusively found within the Cumulus Gabbro suite and this suite represents a good potential target for economic concentrations of Ni and Cu. The largest values are; 0.9 % for Ni, 4.2 % for Cu and 99 ppb

for Pt.

The Ni/Cu ratios and metal ratio diagrams indicate that the parental magma for the Fractionation Suite was a magma with a composition similar to that of a komatiite. This magma then evolved into a basaltic type composition that gave rise to the Cumulus Gabbro and lastly the Late Stage Diorite.

The CNPGE and MNPGE diagrams indicate that the rocks which contain the PGE (Cumulus Gabbro) have undergone fractionation. The trough - shaped pattern of the MNPGE diagram is thought to indicate an earlier segregation of a sulphide phase rich in the high melting point PGE (Os, Ir and Ru) (Barnes et al., 1987). Although these sulphides have not been yet located in the Riwaka Complex, the early crystallized Fractionation Suite rocks may represent a good target for mineral exploration.

CHAPTER 6

Discussion and Conclusions

6.1 Introduction

This study has examined; previous work, the field relationships, petrography and geochemistry of the Graham Valley area of the Riwaka Complex in order to determine the petrogenesis, geochemical evolution and the economic viability of the mafic to ultramafic intrusion. The conclusions of this study are summarized in this chapter.

6.2 Field Relationships

The Riwaka Complex is a linear tholeiitic igneous intrusion (40km long, up to several km wide) that is part of New Zealand's geologic Western Province. This Province is older (Lower Paleozoic) than the Eastern Province (Upper Carboniferious to Middle Cretaceous) and it is separated from the Eastern Province by the Median Tectonic Line (Landis and Coombs, 1967).The Western Province is thought to represent a remnant of the super continent Gondwana that separated from Australia in the Early Tertiary with the formation of the Tasman sea (Korsch and Wellman, 1988). This Province consists of an assemblage of sedimentary, volcanic, intrusive and metamorphic rocks that were formed in a fore - arc

environment associated with either two westward dipping Benioff zones (Shelley, 1975) or one westward dipping Benioff zone (Crook and Feary, 1982).

The Riwaka Complex intruded a portion of the Takaka Terrane that is a conformable package of Lower Ordovician to Upper Silurian sedimentary rocks represented by the Arthur Marble, the Wangapeka Formation and the Hailes Quartzite. The Riwaka Complex is intruded by the Cretaceous Separation Point Batholith.

The Riwaka Complex is linear and there is no evidence of concentric zoning, however all other features of classic Alaskan - type ultramafic complexes match well with the Riwaka Complex. Linear intrusions without concentric zoning, but with other features of Alaskan - type ultramafic complexes have been described by Batanova and Astrakhantsev (1994) on the Kamchatka Peninsula. They believe that these intrusions form from a similar magma and undergo similar magmatic processes as 'classic' Alaskan -type ultramafic complexes, but that they are formed earlier in convergent margin history from deeper seated magma chambers.

6.3 Petrography

The Riwaka Complex can be divided into three main suites of rocks: the Fractionation Suite; the Cumulus Gabbro; and the Late Stage Diorite. The FS is made up of rock types ranging from clinopyroxene - bearing dunites to olivine - hornblende clinopyroxenites. Orthopyroxene is absent from these rocks and plagioclase is very rare. The olivine is only

found as a cumulate phase and has a Forsterite content of 79 to 86. The clinopyroxene is dominantly a cumulate phase, but is in some places found interstitially. The clinopyroxenes range from diopside to salite. Clinopyroxene analyses through a section of the Riwaka Complex reveal only a very slight Fe - enrichment as opposed to the significant Fe - enrichment that generally occurs in clinopyroxenes of tholeiitic layered intrusions (Hess, 1989). In the Riwaka Complex, what little Fe - enrichment there is, is accompanied by a Ca - enrichment as opposed to a Ca - depletion that generally occurs in tholeiitic layered intrusions (Hess, 1989). The lack of a significant Fe - enrichment is attributed to the fact that no orthopyroxene crystallized, and more Mg substitutes in clinopyroxenes (Tistl et al., 1994). The Ca - enrichment, as opposed to depletion, is thought to be caused by the lack of plagioclase crystallization. High aqueous fluid pressure hinders the crystallization of plagioclase (Batanova and Astrakhantsev, 1992). The Ca - enrichment and the lack of plagioclase are uncommon in tholeiitic layered intrusions, but are generally seen in Alaskan - type ultramafic complexes. High water contents in primitive magmas suppress the crystallization of orthopyroxene and plagioclase allowing clinopyroxenes to incorporate the excess Mg and Ca in the melt (Loucks, 1990). The FS rocks also can contain up to 15% modal amphibole. This amount of amphibole also suggests that the FS rocks crystallized from a relatively hydrous magma. This would be compatible with a parent magma derived in the mantle wedge above a dehydrating subducted lithospheric slab.

The Cumulus Gabbro does not appear to outcrop in the Graham Valley and is restricted to drill core samples only. It is thought to represent a very small volume of the

Riwaka Complex in the Graham Valley area. However, it is an economically important suite of rocks as it hosts significant copper-nickel sulphide accumulations. The CG contains 20 to 80% cumulus clinopyroxene, up to 65% interstitial sulphides, 0 to 15% cumulus olivine, 5 to 10% interstitial amphibole and up to 20% interstitial plagioclase. Unlike the FS, the CG does contain small amounts of orthopyroxene. Other minor phases include; biotite, magnetite and apatite.

The CG represents a magma that was produced by olivine and clinopyroxene fractionation of the same magma that gave rise to the FS rocks. The CG represents only a small volume of the Riwaka Complex and these conditions may have enabled the magma to assimilate enough sedimentary country rocks locally (namely the Arthur Marble) to become sulphur saturated and crystallize primary pyrrhotite, pentlandite, chalcopyrite and pyrite.

The Late Stage Diorite represents only a very small amount of the rocks of the Riwaka Complex in the Graham Valley. Its mineralogy consists dominantly of ; amphibole, plagioclase, apatite, biotite and minor amounts of quartz, clinopyroxene and pyrite. The presence of abundant apatite may be used as further evidence that the magma from which the Riwaka Complex crystallized was volatile rich.

6.4 Geochemistry

The rocks of the Riwaka Complex can be attributed to the differentiation of a tholeiitic magma. Major element chemistry and REE data indicates that crystallization of cumulate

olivine and clinopyroxene produced the FS and CG rocks and gave rise to differentiated magma that mixed with the country rocks to produce the LSD.

Mineral chemistry indicates that there may have been as many five as pulses of more primitive magma while the FS rocks of the Riwaka Complex were crystallizing.

Nickel and copper ratios indicate that the composition of the parental magma was similar to that of a komatiite. This magma evolved with olivine and clinopyroxene fractionation into a basaltic type composition which gave rise to the Cumulus Gabbro and Late Stage Diorite rocks.

Metal ratio patterns of the PGE for the Riwaka Complex are very similar to patterns found in other Alaskan - type ultramafic complexes.

6.5 Economic Potential

The Riwaka Complex in the Graham Valley area has undergone extensive exploration for a massive sulphide deposit of copper, nickel and PGE. To date concentrations of metals significant enough to warrant a mine have not been located. The majority of the sulphides, which include; pyrrhotite, chalcopyrite, pentlandite and pyrite, appear to be restricted to the Cumulus Gabbro. Petrography of the sulphides indicate that they are primary and crystallized from a sulphur saturated interstitial melt within the Cumulus Gabbro.

Geochemistry of the sulphides and PGE suggest that the high temperature PGE were fractionated prior to the crystallization of the Cumulus Gabbro. The early crystallized FS

rocks may represent a good target for exploration for both PGE and massive sulphides.

6.6 Conclusions

The Riwaka Complex is here thought to represent a tholeiitic intrusion in a supra - subduction zone setting. A model of its intrusion may be similar to that proposed by Bates (1980a) (Figure 2.4). The Riwaka Complex intruded sediments deposited in an arc environment. The magma differentiated primarily by olivine and clinopyroxene fractionation giving rise to firstly the FS, then the CG, finally when only a small amount of magma remained, it assimilated some of the country rocks to give rise to the LSD.

During crystallization of the CG the magma became sulphur saturated, at least locally, producing Ni - Cu and PGE rich sulphides. The PGE from these sulphides have already undergone a previous fractionation which may have occurred in the crystallization of the FS rocks.

The Riwaka Complex's field relationships, petrography and geochemistry are very similar to Alaskan - type ultramafic complexes, especially the tholeiitic, linear intrusions that have been documented by Batanova and Astrakhantsev (1994) on the Kamchatka Peninsula.

REFERENCES

Adams, C. J. D., 1975. Discovery of Precambrian rocks in New Zealand. Age relations of the Greenland Group and Constant Gnesiss, West Coast, South Island. Earth and Planetary Science Letters 28(1): 98-104.

Alexander, R. J. and Harper, G. D., 1992. The Josephine ophiolite: and ancient analogue for slow to intermediate - spreading ridges.In Parson, L. M. and Murton, B. J. (eds). Ophiolites and their Modern Analogues. Geological Society Special Publication No. 60: 3-38.

Andrews, P. B., Speden, I. G. and Bradshaw, J. D., 1976. Lithological and paleontological content of the Carboniferious - Jurassic Canterbury suite, South Island, New Zealand. New Zealand Journal of Geology and Geophysics, (19): 791-819.

Aronson, J.L., 1968. Regional geochronology of New Zealand. Geochimica et Cosmochimica Acta, 32(7): 669-98.

Ballantyne, P., 1992. Petrology and geochemistry of the plutonic rocks of the Halmahera ophiolite, Eastern Indonesia, an analogue for modern oceanic forearcs. In Parson, L. M. and Murton, B. J. (eds). Ophiolites and their Modern Analogues. Geological Society Special Publication No. 60: 179-202.

Ballhaus, C. G. and Strumpfl, E. F., 1986. Sulphide and platinum mineralization in the Merensky Reef: evidence from hydrous silicates and inclusions. Contributions to mineralogy and Petrology, (94): 193-204.

Barnes, S. J., Naldrett, A. J. and Gorton, M. P., 1985. The origin of the fractionation of platinum - group elements in terrestrial magmas. Chemical Geology, (53): 303-323.

Barnes, S. J., 1987. Unusual nickel and copper to noble - metal ratios from the Rana Layered Intrusion, northern Norway. Norsk Geological Tidsskr., (67): 215-231.

Barnes, S. J., Boyd, R. Korneliussen, A., Nilsson, L-P., Often, M., Pedersen, R. B. and Robins, B., 1987. The use of mantle normalization and metal ratios in discriminating between the effects of partial melting, crystal fractionation and sulphide segregation on platinum group elements, gold, nickel and copper: examples from Norway. In Prichard, H. M., Potts, P. J., Bowles, J. F. W. and Cribb, S. J. (eds). Geo - Platinum 87: 113-141.

Batanova, V. G. and Astrakhantsev, O. V., 1992. Island - arc mafic - ultramafic plutonic complexes of North Kamchatka. In Ishiwatari et. al. (eds). Proceedings of the 29th

International Geological Congress. Part D: 129-143.

Bates, T. E., 1977. Geology of the southern part of the Riwaka Complex and comments on techniques used during exploration for copper and nickel there. Annual Conference N. Z. branch Australian Institute of Mining and Metallurgy, Nelson.

Bates, T. E., 1980a. The origin, distribution and geological setting of copper and nickel sulphides in the Riwaka Complex, Northwest Nelson, New Zealand. Proceedings of the Annual Conference of the Australian Institute of Mining and Metallurgy, New Zealand: 35-51.

Bates, T. E., 1980b. Copper and nickel mineralisation in the Riwaka Complex Northwest Nelson. Mineral Deposits of New Zealand: 119-123.

Beggs, J. M., 1980. Sedimentology and paleogeography of some Kaihikuan Torlesse rocks in mid - Canterbury. New Zealand Journal of Geology and Geophysics, (23): 439-445.

Blake, M. C., Jr., Jones, D. L. and Landis, C. A., 1974. Active continental margins: Contrasts between California and New Zealand. In Burk, C. A. and Drake, C. L. (eds.). The Geology of Continental Margins. Springer - Verlag, Berlin: 853-872.

Bradshaw, J. D., Adams, C. J. and Andrews, P. B., 1980. Carboniferious to Cretaceous on the Pacific margin of Gondwana: The Rangitata phase of New Zealand. In Cresswell. M. M. and Vella, P. (eds.). Gondwana Five. A. A. Balkema, Rotterdam: 217-221.

Bradshaw, J. D., 1989. Origin and metamorphic history of an Early Cretaceous polybaric terrain, Fiordland, southwest New Zealand. Contributions to Mineralogy and Petrology, (103): 346-360.

Cambell, I. H., 1977. A study of cumulate processes and macrorythmic layering in the Jimberlana intrusion of western Australia. Part I: The upper layered series. Journal of Petrology, (18): 183-215.

Carter, R. M., Hicks, M. D., Norris, R. J. and Turnbull, I. M., 1978. Sedimentation patterns in an ancient arc - trench - ocean complex: Carboniferious to Jurassic Rangitata Orogen, New Zealand. In Stanley, D. J. and Kelling, G. (eds.). Sedimentation in Submarine Canyons, Fans and Trenches. Dowden, Hutchinson and Ross, Stroudsburg, PA.: 340-361.

Coombs, D. S., Landis, C. A., Norris, R. J., Sinton, J.A., Borns, D. J. and Craw, D., 1976. The Dun Mountain Ophiolite Belt, New Zealand, its tectonic setting, construction,

and origin, with special reference to the southern portion. American Journal of Science, (276): 561-603.

Cooper, R. A., 1965. Lower Paleozoic rocks between upper Takaka and Riwaka, North-west Nelson. New Zealand Journal of Geology and Geophysics, 8 (1): 49-61.

Cooper, R.A. 1974. Age of the Greenland and Waiuta Groups, South Island, New Zealand. New Zealand Journal of Geology and Geophysics, 17(4): 955-62.

Cooper, R. A. 1979. Lower Paleozoic rocks of New Zealand. Journal of the Royal Society of New Zealand, 9 (1): 29-84.

Cooper, R. A. 1989. Early Paleozoic terranes of New Zealand. Journal of the Royal Society of New Zealand, No. 1, (19): 73-112.

Cowden, A., Bawden, P. and Inger, M., 1988. Assessment of the nickel - copper - platinum group element mineralisation of the Riwaka Complex, exploration licence 33 - 335 volume 1. Sigma Resources N. L. Unpublished report.

Cox, S. H., 1881. On certain mines in the Nelson Collingwood districts, and the geology of the Riwaka Range. New Zealand Geological Survey Report Geological Exploration 1879-80, (13): 1-11.

Craig, J. R., 1990. Textures of the ore minerals. In Jambor, J. L. and Vaughn, D. J. (eds.). Short course on advanced microscopic studies of ore minerals. Mineralogical Association of Canada, Toronto: 213-261.

Crook, K. A. W. and Feary, D. A., 1982. Development of New Zealand according to the fore - arc model of crustal evolution. Tectonophysics, (87): 65-107.

Conrad, W.R. and Kay, R.W., 1984. Ultramafic and mafic inclusions from Adak Island. Crystallization history and implication for the nature of primary magmas and crustal evolution in the Aleutian arc. Journal of Petrology, No. 1, (25): 88-125.

Debari, S. and Kay, R.W., 1987. Ultramafic xenoliths from Adagdak volcano, Aleutian Islands arc. Journal of Geology, (95): 329-341.

Dickinson, W. R., 1971. Detrital modes of New Zealand greywackes. Sedimentary Geology, (5): 37-56.

Dickinson, W. R., 1982. Compositions of sandstones in Circum - Pacific Subduction Complexes and fore - arc basins. American Association of Petroleum Geologists,

Bulletin, (66): 121-137.

Findley, D. C., 1969. Origin of the Tulameen ultramafic - gabbro complex, southern British Columbia. Canadian Journal of Earth Sciences, (6): 399-425.

Fleming, C. A., 1970. The Mesozoic of New Zealand: Chapters in the History of the Circum - Pacific Mobile Belt. Quarterley Journal Geological Society of London, (125): 125-170.

Folk, R. L., Andrews, P. B. and Lewis, D. W., 1970. Detrital sedimentary rock classification and nomenclature for use in New Zealand. New Zealand Journal of Geology and Geophysics, (13): 937-968.

Gill, K. R. and Johnston, M. R., 1970. The geology and nickel - copper sulphide mineralisation in the Graham Valley, North - west Nelson. New Zealand Journal of Geology and Geophysics, (13): 477-494.

Grindley, G. W., 1961. Sheet 13 Golden Bay " Geological map of New Zealand 1:250,000". New Zealand Department of Scientific and Industrial Research, Wellington.

Grindley, G. W.,1971. Sheet S8 Takaka (1st ed.). Geological Map of New Zealand 1:63 360. N.Z. Department of Scientific and Industrial Research, Wellington.

Grindley, G. W.,1978. West Nelson. Chapter II. Late Precambrian - Devonian: The early gesynclinal cycle. In Suggate, Stevens and Te Punga (eds.). The Geology of New Zealand. Volume I. Government Printer, Wellington: 80-99.

Grindley, G. W., 1980. Sheet S13 Cobb, Geological Map of New Zealand 1:63,360. Department of Scientific and Industrial Research, Wellington.

Harrison, T. M. and McDougall, I., 1980. Investigations of an intrusive contact, northwest Nelson, New Zealand. II. Diffusion of radiogenic and excess ^{40}Ar in hornblende revealed by $^{40}Ar/^{39}Ar$ age spectrum analysis.Geochimica et Cosmochimica Acta, (44): 2005-2020.

Haskins, L. A., 1984. Petrogenetic modelling use of rare earth elements. In Henderson, P. (eds.). Rare Earth Element Geochemistry. Elsevier, Amsterdam, Oxford, New York.

Haughton, D. R., Roeder, P. L. and Skinner, B. J., 1974. Solubility of sulphur in mafic magmas. Economic Geology, (69): 451-461.

Henderson, J., 1923. Chrysotile asbestos in the Upper Takaka district. Journal of Science

and Technology, (6): 120-123.

Henderson, J., 1950. Cornish stone and feldspar in New Zealand. New Zealand Journal of Science and Technology, (B31): 25-44.

Henderson, J., Macpherson, E. O. and Grange, L. I., 1959. The geology of the Moteuka subdivision. Bulletin of New Zealand Geological Survey, no. 35.

Hess, P. C., 1989. Origins of Igneous Rocks. Harvard University Press.

Hopson, C. A., Coleman, R. G., Gregory, R. T., Pallister, J. S. and Bailey, E. H., 1981. Geologic section through the Semail ophiolite and associated rocks along a Muscat-Irba transect. Journal of Geophysics Res., (86): 2527-2544.

Howell, D. G., 1980. Mesozoic accretion of exotic terranes along the New Zealand segment of Gondwanaland. Geology, (8): 487-491.

Hughes, C., 1982. Igneous Petrology: Developments in Petrology. Elsevier, Amsterdam, Oxford, New York.

Hunter, H. W.,1977. Geology of the Cobb Intrusives, Takaka Valley, northest Nelson, New Zealand. New Zealand Journal of Geology and Geophysics, 20(3): 469-502.

Irvine, T.N., 1963. Origin of the ultramafic complex at Duke Island, southeastern Alaska. Mineralogical Society of America Special Paper, (1): 36-45.

Irvine, T.N., 1974. Petrology of the Duke Island U;tramafic Complex, Southeastern Alaska. The Geological Society of America, Inc. Memoir 138.

Irvine, T.N., 1975. Crystallization sequences in the Muskox intrusion and othe layered intrusions. II. Origin of chromatite layers and similar deposits of magmatic ores. Geochimica et Cosmochimica Acta, (39): 991-1020.

Irvine, T.N., 1977. Origin of chromatite layers in the Muskox intrusion: a new interpretation Geology, (5): 273-277.

Irvine, T.N., 1979. Rocks whose composition is determined by crystal accumulation and sorting. In Yoder, H. S., Jr. The Evolution of the Igneous Rocks: Fiftieth Anniversary Perspectives. Princeton University Press, Princeton, New Jersey.

Korsch, R. J. and Wellman, H. W., 1988. The Geological Evolution of New Zealand and the New Zealand Region. In Nairn, A. E. M., Stehli, F. G. and Uyeda, S. (eds.). The

Ocean Basins and Margins. Volume 7B: The Pacific Ocean. Plenum Press, New York and London: 411-482.

Laird, M. G., 1972. Sedimentology of the Greenland Group in the Paparoa Range, West Coast, South Island. New Zealand Journal of Geology and Geophysics, (15): 372-393.

Landis, C. A., 1980. Little Ben Sandstone, Maitai Group (Permian): Nature and extent of the Hollyford - Eglington region, South Island, New Zealand. New Zealand Journal of Geology and Geophysics, (23): 551-567.

Landis, C. A. and Bishop, D. G., 1972. Plate tectonics and regional stratigraphic - metamorphic relations in the southern part of the New Zealand geosyncline. Geological Society of America, Bulletin, (83): 2267-2284.

Landis, C. A. and Coombs, D. S., 1967. Metamorphic belts and orogenesis in southern New Zealand. Tectonophysics, (4): 501-518.

Leake, B. E., 1978. Nomenclature of Amphiboles. The Canadian Mineralogist, (16): 501-525

Loucks, R.R., 1990. Discrimination of ophiloitic from non - ophiolitic ultramafic - mafic allocthons in orogenic belts by the Al/Ti ratio in clinopyroxene. Geology, (18): 346-349.

Mackinnon, T. C., 1983. Origin of Torlesse and related rocks, South Island, New Zealand. Geological Society of America, Bulletin, (94): 967-985.

Malpas, J., 1978. Magma generation in the upper mantle, field evidence from ophiolite suites, and application to the generation of oceanic lithosphere. Philosphical Transactions of the Royal Society of London, (288): 527-546.

Malpas, J., 1979. The dynamothermal aureole of the Bay of Islands ophiolite suite. Canadian Journal of Earth Sciences, (16): 2086-2101.

Malpas, J., Smith, I. E. M. and Williams, D., 1994. In Ishiwatari et. al. (eds). Proceedings of the 29th International Geological Congress. VSP publishers, the Netherlands. Part D: 29-46.

Maxwell, M., 1977. The petrology and sulphide mineralisation of the Riwaka Complex. Company Report, Mines Division file.

McCallum, I. S., Raedeke, L. D. and Mathez, E. A., 1980. Investigations of the Stillwater Complex. I. Stratigraphy and structure of the banded zone. American Journal of Science, (280A): 59-87.

McKay, A., 1879. The Baton River and Wangapeka districts and Mount Arther Range; New Zealand Geological Survey Report Geological Exploration 1878-79, (12): 121-131.

Mutch, A. R., 1964. Sheet S105 Martins Bay (1st edition) Geological map of New Zealand. 1:63,360 Department of Scientific and Industrial Research, Wellington.

Murray, C. G., 1972. Zoned ultramafic complexes of the Alaskan type: feeder pipes of andesitic volcanoes. In Shagam, R. E. and others (eds). Studies in earth and space sciences (Hess Volume). Geological Society of America Memoir 132: 313-335.

Naldrett, A. J. and Cabri, L. J., 1976. Ultramafic and related rocks, their classification and genesis with special reference to the concentration of nickel sulphides and platinum - group elements. Economic Geology, (71): 1131-1158.

Naldrett, A. J. and Duke, J. M., 1980. Platinum metals in magmatic sulphide ores. Science, (208): 1417-1424.

Naldrett, A. J., 1981. Nickel sulphide deposits: classification, composition and genesis. In Skinner, B. J. (ed). Economic Geology, 75th Anniversary Volume: 628-685.

Naldrett, A. J. and Macdonald, A. J., 1980. Tectonic settings of some Ni - Cu sulphide ores: their importance in genesis and exploration. In Strangeway, D. W. (ed). The continental crust and its mineral deposits. Geological Association of Canada, Special Paper 20: 633-657.

Nicolas, A. 1989. Structures of Ophiolites and Dynamics of Oceanic Lithosphere. Kluwer Academic Publishers.

Oliver, G. J. H., 1980. Geology of the granulite and amphibolite facies gneisses of Doubtful Sound, Fiordland, New Zealand. New Zealand Journal of Geology and Geophysics, (23): 27-42.

Pallister, J. S. And Hopson, C. A., 1981. Semail ophiolite plutonic suite: field relations, phase variations, cryptic variation and layering, and a model of a spreading ridge magma chamber. Journal of Geophysics Res., (86): 2593-2644.

Park, J., 1890. On the geology of the Collingwood County, Nelson. New Zealand Geological Survey Report Geological Exploration 1888-89, (20): 186-243.

Pirajno, F., 1980. Primary magmatic segregation deposits in New Zealand, their characteristics and tectonic setting. The Australian Institute of Mining and Metallurgy, New Zealand: 81-93.

Poldervaart, A. and Hess, H. H., 1951. Pyroxenes in the crystallization of basaltic magma. Journal of Geology, (59): 4872-4890.

Raedeke, L. D. and McCallum, I. S., 1985. Investigations in the Stillwater Complex. II. Petrology and petrogenesis of the ultramafic series. Journal of Petrology, (25): 395-420.

Reid, D. L., 1972. Thermal metamorphism and assimilation of schists by a dioritic magma, Ligar Bay, Northwest Nelson. New Zealand Journal of Geology and Geophysics, (15): 632-642.

Ruckmick, J. C. and Noble, J. A., 1959. Origin of the ultramafic complex at Union Bay, southeastern Alaska.Geological Society of America Bulletin, (70): 981-1018.

Shelley, D.,1970. The structure and petrography of the Constant Gneiss near Charleston, southwest Nelson. New Zealand Journal of Geology and Geophysics, (13): 370-391.

Shelley, D.,1972. Structure of the Constant Gneiss near Cape Foulwind, southwest Nelson, and its bearing on the regional tectonics of the West Coast. New Zealand Journal of Geology and Geophysics, (15):33-48.

Shelley, D.,1975. Temperature and metamorphism during cleavage and fold formation of the Greenland Group, north of Greymouth. Journal of the Royal Society of New Zealand 5 (1): 65-75.

SIGMA, 1988. Anonymous. Unpublished company report regarding the Riwaka Complex, New Zealand.

Smale, D. and Nathan, N., 1980. Heavy minerals in basement rocks of the Paparoa Range, Westland. Unpublished New Zealand Geological Survey report, NZGS G36.

Souch, B. E., Podolsky, T. and the geological staff of the International Nickel Company of Canada, 1969. The sulphide ores of Sudbury: Their particular relation to a distinctive inclusion - bearing facies of the nickel eruptive. Economic Geology, Mon. 4: 252-261.

Sporli, K. B., 1978. Mesozoic tectonics, North Island, New Zealand. Geological Society of America, Bulletin (89): 415- 425.

Sporli, K. B., 1987. Development of the New Zealand Microcontinent. In Monger, J. W. H. and Francheteau, J. (eds.). Circum - Pacific Orogenic Belts and Evolution of the Pacific Ocean Basin: Geodynamics Series (18). American Geophysical Union, Washington, D. C.: 115-132.

St. Louis, R. M., Nesbitt, B. E. and Morton, R. D. Geochemistry of Platinum - Group Elements in the Tulameen Ultramafic Complex, Southern British Columbia. Economic Geology, (81): 961-973.

Suggate, R. P., Stevens, G. R., and Te Punga, M. T. (eds.), 1978.The Geology of New Zealand. Government Printer, Wellington.

Taylor, H. P., Jr. and Noble, J. A., 1960. Origin of the ultramafic complexes in southeastern Alaska. International Geological Conference, 21st, Copenhagen, pt. 13: 175-187.

Taylor, H. P., Jr. and Noble, J. A., 1969. Origin of magnetite in the zoned ultramafic complexes of southeastern Alaska. In Wilson, H. D. B. (eds.) Magmatic Ore Deposits. Economic Geology Monogram, (4): 209-230.

Tistl, M., Burgath, K. P., Hohndorf, A., Kreuzer, H., Munoz, R. and Salinas, R., 1994. Origin and emplacement of Tertiary ultramafic complexes in northwest Columbia: Evidence from geochemistry and K -Ar, Sm - Nd and Rb - Sr isotopes. Earth and Planetary Science Letters, (126): 41-59.

Todd, S. G., Keith, D, W., Schissel, D. J., Leroy, L. L., Mann, E. L. and Irvine, T. N., 1982. The J-M patinum-palladium reef of the Stillwater Complex, Montana. I: Stratigraphy and petrology. Economic Geology, (77): 454-480.

Tulloch, A. J., 1979. Plutonic and metamorphic rocks of the Victoria Range segment of the Karamea Batholith, Southwest Nelson, New Zealand (Ph.D. thesis). University of Otago.

Tulloch, A. J., 1983. Granitoid rocks of New Zealand-A brief review. Geological Society of America Memoir, (159):5-20.

Vogt, J. H. L., 1918. Die Sulphide - silikatschenmelzlosungen. Vidensk. Selsk. Skr I. M. N. K1, No. 1.

Wager, L. R. and Brown, G. M., 1968. Layered Igneous Rocks: Edinburgh, Oliver and Boyd.

Walton, M. S., Jr., 1951. The Blashke Islands ultrabasic complex (Ph.D. thesis). New York,

Columbia University.

Willis, I., 1965. Stratigraphy and structure of the Devonian strata at Baton River, New Zealand. New Zealand Journal of Geology and Geophysics, 8 (1): 1-48.

Wood, B. L., 1978. The Otago Schist Megaculmination: Its possible origins and tectonic signifigance in the Ragitata Orogen of New Zealand. Tectonophysics, (47): 339-368.

Wyllie, P. J., 1967. Ultramafic and Related Rocks. John Wiley and Sons Inc.

APPENDIX A
GEOCHEMICAL ANALYSES

The following pages (Tables A1 through A22) contain listings of the geochemical data for samples collected during field work for this study. This includes samples of drill core provided by the New Zealand Department of Scientific and Industrial Research and Sigma Resources. With respect to the data, please note:

1). All oxides are reported in wt.%, trace elements, rare earth elements as ppm and PGE and AU as ppb.

2). Fe_2O_3 is total Fe for whole rock analyses and FeO is total Fe for microprobe data.

3). "na" is not analysed.

4). "-" is not detected.

5). The analytical procedures for the geochemical determinations can be viewed in appendix B.

Table A1 Olivine compositions of the Fractionation Suite.

Sample	JS-91-56	JS-91-56	JS-91-57	JS-91-57	JS-91-58
SiO2	39.77	40.73	40.53	40.43	39.59
MgO	43.73	45.48	44.87	44.67	43.01
FeO	15.13	13.78	14.23	14.20	16.20
MnO	0.44	0.50	0.21	0.20	0.29
CaO	0.05	0.05	0.02	0.02	0.22
Na2O	0.00	0.00	0.00	0.00	0.00
K2O	0.00	0.00	0.00	0.00	0.00
TiO2	0.00	0.00	0.02	0.00	0.00
Cr2O3	0.00	0.00	0.00	0.00	0.01
Al2O3	0.03	0.00	0.01	0.00	0.03
Total	99.16	100.52	99.87	99.51	99.35

Sample	JS-91-59	JS-91-59	JS-91-61	JS-91-61	JS-91-63
SiO2	40.93	40.65	39.95	39.93	39.60
MgO	46.13	45.23	42.50	42.43	43.17
FeO	12.97	13.72	16.45	16.75	16.17
MnO	0.22	0.19	0.25	0.21	0.22
CaO	0.01	0.03	0.05	0.05	0.02
Na2O	0.00	0.00	0.01	0.00	0.00
K2O	0.00	0.00	0.01	0.00	0.00
TiO2	0.00	0.01	0.01	0.01	0.04
Cr2O3	0.00	0.01	0.00	0.00	0.33
Al2O3	0.01	0.01	0.01	0.01	0.02
Total	100.28	99.82	99.22	99.36	99.59

Sample	JS-91-63	JS-91-63	JS-91-66	JS-91-66	JS-91-68
SiO2	40.17	40.13	40.03	39.77	39.36
MgO	43.87	43.70	42.77	41.80	41.94
FeO	15.17	15.47	16.57	17.80	17.89
MnO	0.24	0.25	0.32	0.31	0.32
CaO	0.01	0.02	0.01	0.01	0.00
Na2O	0.00	0.00	0.00	0.00	0.00
K2O	0.00	0.00	0.00	0.00	0.00
TiO2	0.00	0.02	0.01	0.01	0.00
Cr2O3	0.00	0.00	0.00	0.00	0.00
Al2O3	0.00	0.00	0.00	0.00	0.00
Total	99.44	99.62	99.66	99.71	99.50

Table A1 Cont.

Sample	JS-91-68	JS-91-69	JS-91-69	JS-91-71	JS-91-71
SiO2	39.23	39.59	39.43	39.43	39.23
MgO	42.07	44.34	43.27	42.78	42.46
FeO	17.64	15.88	16.82	17.28	17.44
MnO	0.31	0.27	0.31	0.32	0.29
CaO	0.03	0.01	0.01	0.00	0.01
Na2O	0.01	0.00	0.01	0.01	0.00
K2O	0.00	0.00	0.00	0.00	0.00
TiO2	0.00	0.00	0.00	0.00	0.02
Cr2O3	0.00	0.00	0.00	0.00	0.00
Al2O3	0.00	0.00	0.00	0.00	0.00
Total	99.28	100.09	99.84	99.82	99.45

Sample	JS-91-72	JS-91-72	JS-91-72
SiO2	40.08	39.85	40.17
MgO	41.98	40.90	42.28
FeO	18.23	19.38	17.62
MnO	0.30	0.27	0.32
CaO	0.04	0.03	0.03
Na2O	0.01	0.02	0.00
K2O	0.01	0.00	0.00
TiO2	0.00	0.00	0.00
Cr2O3	0.00	0.00	0.00
Al2O3	0.00	0.01	0.01
Total	100.62	100.45	100.44

Table A2 Clinopyroxene compositions of the Fractionation Suite.

Sample	JS-91-54	JS-91-54	JS-91-54	JS-91-55	JS-91-55
SiO2	53.47	52.36	53.25	52.44	52.59
MgO	17.23	16.68	17.35	16.83	16.85
FeO	3.47	3.73	3.75	3.50	3.60
MnO	0.08	0.09	0.10	0.09	0.09
Na2O	0.23	0.28	0.27	0.24	0.27
K2O	0.00	0.00	0.00	0.00	0.00
TiO2	0.37	0.44	0.37	0.46	0.40
Cr2O3	0.67	0.62	0.67	0.74	0.77
Al2O3	1.60	2.00	1.95	2.00	1.87
CaO	23.07	22.93	22.35	22.85	22.83
Total	100.16	99.15	100.04	99.15	99.27

Sample	JS-91-56	JS-91-57	JS-91-57	JS-91-58	JS-91-59
SiO2	53.03	53.33	52.90	52.03	52.93
MgO	15.40	16.60	16.13	16.46	16.30
FeO	5.10	3.47	3.97	4.17	3.83
MnO	0.12	0.09	0.10	0.09	0.10
Na2O	0.16	0.80	0.90	0.28	0.24
K2O	0.00	0.00	0.00	0.00	0.00
TiO2	0.42	0.39	0.58	0.53	0.52
Cr2O3	0.19	0.69	0.49	0.47	0.66
Al2O3	1.67	1.53	2.07	2.20	1.93
CaO	23.57	23.07	22.90	22.87	22.90
Total	99.67	100.01	100.10	99.08	99.41

Sample	JS-91-59	JS-91-59	JS-91-59	JS-91-61	JS-91-61
SiO2	53.27	52.97	53.33	52.43	53.00
MgO	16.40	16.20	16.43	15.70	16.20
FeO	3.57	3.77	3.67	4.63	4.10
MnO	0.09	0.09	0.09	0.12	0.09
Na2O	0.20	0.36	0.35	0.44	0.33
K2O	0.00	0.00	0.00	0.00	0.00
TiO2	0.45	0.52	0.47	0.54	0.50
Cr2O3	0.52	0.63	0.50	0.47	0.38
Al2O3	1.67	1.90	1.63	2.17	1.70
CaO	23.07	22.83	22.87	22.70	22.77
Total	99.22	99.26	99.40	99.14	99.13

Table A2 Cont.

Sample	JS-91-63	JS-91-63	JS-91-66	JS-91-66	JS-91-68
SiO2	52.90	53.77	52.55	52.87	52.82
MgO	16.00	16.53	15.78	16.07	16.49
FeO	4.18	3.37	4.68	4.30	4.20
MnO	0.10	0.08	0.11	0.07	0.10
Na2O	0.42	0.24	0.90	0.83	0.34
K2O	0.00	0.00	0.00	0.00	0.00
TiO2	0.53	0.37	0.53	0.61	0.48
Cr2O3	0.50	0.38	0.33	0.41	0.45
Al2O3	2.13	1.13	2.30	2.03	2.07
CaO	22.78	23.80	22.78	23.00	23.13
Total	99.49	99.68	99.91	100.21	100.08

Sample	JS-91-68	JS-91-69	JS-91-69	JS-91-71	JS-91-71
SiO2	51.48	51.97	53.34	52.43	54.36
MgO	16.10	16.01	16.01	15.36	16.26
FeO	5.07	4.77	3.90	5.10	3.77
MnO	0.11	0.12	0.13	0.14	0.12
Na2O	0.31	0.33	0.16	0.46	0.10
K2O	0.00	0.00	0.00	0.00	0.00
TiO2	0.68	0.58	0.30	0.50	0.06
Cr2O3	0.47	0.41	0.21	0.44	0.12
Al2O3	3.03	2.53	1.60	2.57	0.49
CaO	22.47	23.10	24.97	23.30	25.33
Total	99.72	99.82	100.62	100.29	100.61

Sample	JS-91-80	JS-91-88	JS-91-88	JS-92-96	JS-91-96
SiO2	49.46	51.83	51.73	52.30	51.50
MgO	13.75	13.30	13.33	14.73	14.23
FeO	7.10	7.53	7.80	6.60	7.13
MnO	0.13	0.27	0.25	0.17	0.17
Na2O	0.46	0.46	0.46	0.43	0.46
K2O	0.00	0.01	0.00	0.00	0.01
TiO2	1.21	0.61	0.62	0.62	0.85
Cr2O3	0.05	0.02	0.02	0.20	0.08
Al2O3	4.75	2.83	2.70	2.38	3.30
CaO	23.00	23.53	23.23	22.35	22.23
Total	99.91	100.42	100.13	99.76	99.97

Table A3 Amphibole compositions of the Fractionation Suite.

Sample	JS-91-56	JS-91-63	JS-91-72	JS-91-72	JS-91-80
Cl	N/A	0.19	0.08	0.11	0.08
SiO2	43.57	43.45	42.83	42.87	40.97
CaO	11.50	12.10	12.13	12.13	12.57
Al2O3	11.27	11.00	11.95	12.00	13.57
Cr2O3	0.18	0.75	0.21	0.26	0.06
TiO2	2.16	2.55	2.75	2.51	3.75
K2O	1.98	1.30	1.23	1.27	1.50
MnO	0.10	0.08	0.09	0.09	0.09
FeO	9.57	6.75	9.20	9.03	10.80
MgO	15.43	16.60	13.53	13.57	11.73
Na2O	2.37	2.65	2.21	2.11	1.85
Total	98.11	97.43	96.15	95.97	96.94

Sample	JS-91-80	JS-91-80	JS-91-80	JS-91-88	JS-91-88
Cl	0.08	N/A	N/A	0.09	0.08
SiO2	42.00	40.37	51.77	41.83	41.13
CaO	12.40	12.00	17.47	12.40	12.30
Al2O3	13.63	12.90	4.97	12.40	12.93
Cr2O3	0.09	0.05	0.03	0.06	0.02
TiO2	3.16	3.83	0.46	3.27	2.93
K2O	0.22	2.05	0.04	1.13	1.18
MnO	0.11	0.09	0.12	0.21	0.21
FeO	11.05	10.30	7.57	13.27	13.53
MgO	11.70	13.60	16.43	10.60	10.27
Na2O	2.21	1.91	0.42	2.05	2.03
Total	96.62	97.11	99.22	97.36	96.65

Sample	JS-91-88	JS-91-88	JS-91-96	JS-91-96
Cl	0.07	0.06	0.06	0.04
SiO2	41.83	41.67	40.73	40.37
CaO	12.40	12.40	12.60	12.37
Al2O3	12.37	12.20	13.27	13.33
Cr2O3	0.03	0.04	0.08	0.07
TiO2	2.98	3.17	3.80	3.88
K2O	1.11	1.13	1.41	1.41
MnO	0.21	0.20	0.12	0.12
FeO	13.10	12.77	10.60	10.27
MgO	10.73	10.80	11.63	11.73
Na2O	2.07	1.95	1.91	2.14
Total	96.85	96.44	96.19	95.77

Table A4 Olivine compositions of the Cumulus Gabbro.

Sample	JS-91-187	JS-91-189	JS-91-192	JS-91-192	JS-91-197
SiO2	39.30	39.23	38.71	39.23	38.22
MgO	42.84	42.46	39.76	41.90	38.38
FeO	17.35	17.48	21.36	18.55	22.10
MnO	0.33	0.35	0.00	0.36	0.35
CaO	0.00	0.01	0.00	0.01	0.03
Na2O	0.00	0.00	0.02	0.00	0.00
K2O	0.00	0.00	0.00	0.00	0.01
TiO2	0.00	0.00	0.00	0.01	0.00
Cr2O3	0.00	0.00	0.00	0.00	0.00
Al2O3	0.00	0.00	0.01	0.01	0.00
Total	99.82	99.52	99.87	100.09	99.09

Sample	JS-91-199
SiO2	38.29
MgO	38.11
FeO	22.61
MnO	0.36
CaO	0.01
Na2O	0.00
K2O	0.00
TiO2	0.00
Cr2O3	0.00
Al2O3	0.00
Total	99.37

Table A5 Clinopyroxene compositions of the Cumulus Gabbro.

Sample	JS-91-187	JS-91-187	JS-91-192	JS-91-192	JS-91-199
SiO2	51.05	50.89	51.87	51.18	51.57
MgO	15.65	15.97	17.23	16.33	16.88
FeO	5.97	6.00	6.30	5.67	6.27
MnO	0.18	0.14	0.15	0.13	0.15
Na2O	0.28	0.28	0.28	0.31	0.28
K2O	0.00	0.00	0.01	0.00	0.02
TiO2	0.62	0.61	0.52	0.58	0.56
Cr2O3	0.32	0.76	0.19	0.13	0.24
Al2O3	3.53	3.93	3.47	4.17	3.37
CaO	21.80	21.10	20.03	20.80	19.97
Total	99.40	99.68	100.06	99.29	99.31

Sample	JS-91-199	JS-91-203	JS-91-203	JS-91-203	JS-91-207
SiO2	50.17	53.07	51.38	51.48	52.49
MgO	15.10	16.33	14.67	14.67	18.37
FeO	5.33	7.47	6.33	6.40	9.77
MnO	0.17	0.20	0.18	0.20	0.27
Na2O	0.39	0.42	0.69	0.71	0.45
K2O	0.06	0.02	0.00	0.00	0.00
TiO2	0.78	0.46	0.73	0.74	0.42
Cr2O3	0.29	0.10	0.28	0.28	0.20
Al2O3	5.00	3.07	3.60	3.60	2.80
CaO	21.70	18.93	22.90	22.80	15.44
Total	98.98	100.06	100.76	100.87	100.20

Sample	JS-91-207	JS-91-207	JS-91-207	JS-91-207	RCNZ-104
SiO2	51.25	54.27	51.15	51.15	51.28
MgO	14.90	24.97	14.33	14.10	15.83
FeO	7.63	17.47	6.97	6.97	7.10
MnO	0.21	0.50	0.20	0.22	0.18
Na2O	0.83	0.02	0.56	0.53	0.29
K2O	0.01	0.00	0.00	0.01	0.00
TiO2	0.62	0.18	0.61	0.61	0.80
Cr2O3	0.22	0.00	0.29	0.19	0.32
Al2O3	3.70	2.43	3.83	3.63	3.70
CaO	21.10	1.15	22.10	22.53	21.03
Total	100.46	100.92	100.05	99.94	100.53

Table A6 Amphibole compositions of the Cumulus Gabbro.

Sample	JS-91-124	JS-91-124	JS-91-133	JS-91-133
Cl	N/A	N/A	N/A	N/A
SiO2	42.93	42.63	41.70	41.53
CaO	11.63	11.70	12.05	11.87
Al2O3	12.43	12.37	11.65	11.93
Cr2O3	0.17	0.10	0.09	0.08
TiO2	2.94	2.97	3.43	3.52
K2O	1.31	1.23	1.62	1.64
MnO	0.11	0.11	0.10	0.11
FeO	9.10	9.07	10.75	10.90
MgO	15.10	14.87	13.35	13.20
Na2O	1.81	2.08	1.75	1.72
Total	97.54	97.09	96.43	96.48

Sample	JS-91-133	JS-91-137	JS-91-137	JS-91-137
Cl	N/A	0.05	0.06	0.46
SiO2	43.77	39.50	39.60	43.50
CaO	12.13	12.57	12.63	12.13
Al2O3	10.12	14.47	15.00	9.73
Cr2O3	0.14	0.02	0.01	0.01
TiO2	2.72	3.56	3.18	0.36
K2O	1.23	1.59	1.35	0.04
MnO	0.11	0.15	0.16	0.15
FeO	10.90	14.30	13.10	16.67
MgO	13.93	9.27	9.73	9.53
Na2O	1.49	1.62	1.75	1.13
Total	96.60	97.09	96.51	97.12

Sample	JS-91-203	JS-91-203	JS-91-203
Cl	N/A	N/A	N/A
SiO2	49.03	45.40	56.80
CaO	11.33	11.75	12.65
Al2O3	9.35	12.25	2.86
Cr2O3	0.00	0.28	0.10
TiO2	0.12	0.22	0.09
K2O	0.17	0.29	0.04
MnO	0.29	0.26	0.22
FeO	13.77	14.75	7.35
MgO	13.97	12.00	19.20
Na2O	1.42	1.93	0.40
Total	99.36	99.05	99.70

Table A7 Average plagioclase composition of the Cumulus Gabbro.

Sample	JS-91-187	JS-91-189	JS-91-192	JS-91-195	JS-91-199
SiO2	49.73	49.50	50.83	50.63	51.07
CaO	14.97	15.37	14.20	14.77	14.23
Al2O3	32.90	33.17	31.80	32.60	32.13
K2O	0.00	0.00	0.08	0.04	0.03
Na2O	3.07	2.93	3.53	3.30	3.47
FeO	0.03	0.03	0.30	0.27	0.38
MgO	0.00	0.00	0.01	0.01	0.02
Total	100.67	101.00	100.74	101.62	101.31

Table A8 Amphibole compositions of the Late Stage Diorite.

Sample	JS-91-42	JS-91-42
Cl	N/A	N/A
SiO2	53.90	45.97
CaO	12.37	17.04
Al2O3	3.02	23.37
Cr2O3	0.03	0.00
TiO2	0.09	0.02
K2O	0.07	0.04
MnO	0.19	0.07
FeO	10.97	7.07
MgO	16.93	0.00
Na2O	0.41	1.22
Total	97.99	94.75

Table A9 Average plagioclase composition of the Late Stage Diorite.

Sample	JS-91-35	JS-91-40
SiO2	43.97	57.33
CaO	19.03	9.27
Al2O3	27.07	28.27
K2O	0.00	0.00
Na2O	1.77	6.53
FeO	6.80	0.02
MgO	0.03	0.00
Total	98.70	101.47

Table A10 Major element whole rock analyses (wt%) of the Fractionation Suite.

Sample	Na2O	MgO	Al2O3	SiO2	P2O5	K2O	CaO	TiO2	MnO	Fe2O3	LOI	total
JS-91-54	-	26.33	1.95	47.42	0.03	0.03	13.65	0.41	0.13	8.82	3.96	99.03
JS-91-56	-	19.56	3.24	48.87	0.01	0.09	16.56	0.68	0.14	9.36	1.52	98.67
JS-91-61	-	19.52	2.34	50.49	0.02	0.02	18.91	0.51	0.11	6.82	2.05	99.13
JS-91-66	-	32.18	1.24	43.80	0.02	0.03	7.36	0.25	0.21	15.32	3.38	100.32
JS-91-73	0.04	17.58	2.26	52.72	0.02	0.06	20.11	0.50	0.12	5.56	0.85	99.06
JS-91-79	-	19.52	2.37	54.25	0.04	0.09	13.10	0.61	0.13	9.43	1.77	99.62
JS-91-84	0.02	15.53	4.51	50.11	0.04	0.08	20.22	1.03	0.11	7.66	0.78	99.43
JS-91-93	0.82	12.70	7.47	45.33	0.98	0.40	17.11	1.94	0.17	12.29	0.98	99.33
JS-91-97	0.30	18.26	3.86	50.58	0.05	0.13	17.14	0.69	0.13	8.00	1.89	99.48
JS-91-115	0.09	13.77	5.53	48.77	0.04	0.07	21.31	1.27	0.12	8.15	0.53	99.22
JS-91-118	0.08	13.29	5.86	47.82	0.01	0.02	21.20	1.50	0.12	9.92	0.28	99.92
JS-91-122	-	34.54	1.12	42.76	0.03	0.01	5.70	0.23	0.21	15.35	6.70	99.93
JS-91-129	-	18.06	3.60	49.01	0.05	0.02	19.15	0.71	0.14	8.32	1.86	99.19
JS-91-146	0.38	12.24	8.68	47.83	0.11	0.24	15.98	1.77	0.18	12.08	1.78	99.58
JS-91-149	-	24.36	5.54	46.74	0.06	0.12	8.41	1.18	0.19	14.00	4.37	100.48

Table A11 Major element whole rock analyses (wt%) of the Cumulus Gabbro.

Sample	Na2O	MgO	Al2O3	SiO2	P2O5	K2O	CaO	TiO2	MnO	Fe2O3	LOI	total
JS-91-133	0.32	14.12	5.54	49.68	0.15	0.36	19.53	1.03	0.13	8.18	0.68	99.13
JS-91-189	1.04	15.32	10.98	47.94	0.05	0.53	11.86	0.57	0.16	10.71	3.41	99.31
JS-91-187	0.46	17.96	6.83	44.91	0.05	0.30	12.89	0.87	0.28	14.89	1.26	99.66
JS-91-192	0.41	21.13	4.00	45.84	0.06	0.20	13.60	0.73	0.18	13.63	0.69	99.95
JS-91-195	0.33	21.26	3.86	43.85	0.03	0.17	12.62	0.64	0.18	16.84	0.62	99.90
JS-91-198	0.51	15.52	11.12	49.22	0.08	0.31	10.23	0.69	0.19	11.64	0.79	99.70
JS-91-199	0.19	19.18	5.40	47.44	0.05	0.17	13.88	0.56	0.18	12.32	1.89	99.57

Table A12 Major element whole rock analyses (wt%) of the Late Stage Diorite.

Sample	Na2O	MgO	Al2O3	SiO2	P2O5	K2O	CaO	TiO2	MnO	Fe2O3	LOI	total
JS-91-23	1.44	6.11	18.01	38.65	1.40	0.82	12.19	3.07	0.15	17.63	1.47	99.58
JS-91-26	1.07	6.85	16.24	38.39	1.57	0.91	11.72	3.48	0.16	19.31	1.75	99.82
JS-91-29	1.25	5.32	18.40	42.31	1.10	0.56	14.68	1.47	0.14	14.08	1.85	99.39
JS-91-32	1.12	6.05	17.65	37.33	1.28	0.52	12.17	3.42	0.15	19.56	1.43	99.37
JS-91-35	1.07	4.56	19.21	39.03	0.91	0.48	12.20	2.54	0.14	17.43	2.23	97.70
JS-91-37	0.38	5.65	16.62	39.40	1.53	0.36	15.64	2.46	0.16	17.17	2.33	99.49
JS-91-39	0.37	4.97	17.21	40.78	1.19	0.27	16.74	1.98	0.11	15.87	1.85	99.61
JS-91-144	0.79	5.02	19.00	40.89	0.25	0.54	13.85	2.12	0.14	17.05	2.42	99.77

Table A13 Major element whole rock analyses (wt%) of the Separation Point Granite.

Sample	Na2O	MgO	Al2O3	SiO2	P2O5	K2O	CaO	TiO2	MnO	Fe2O3	LOI	total
JS-91-185	3.92	5.07	14.96	63.06	0.14	1.35	4.80	0.53	0.06	5.25	2.43	99.24

Table A14 Major element whole rock analyses (wt%) of the Arthur Marble.

Sample	Na2O	MgO	Al2O3	SiO2	P2O5	K2O	CaO	TiO2	MnO	Fe2O3	LOI	total
JS-91-51	0.05	0.55	0.68	4.64	0.02	0.28	64.87	0.10	0.01	0.75	38.14	72.51
JS-91-53	0.08	0.65	0.43	3.54	0.01	0.19	66.85	0.06	0.01	0.56	40.12	72.82

Table A15 Major element whole rock analyses (wt%) of the Onekaka Schist.

Sample	Na2O	MgO	Al2O3	SiO2	P2O5	K2O	CaO	TiO2	MnO	Fe2O3	LOI	total
JS-91-132	6.18	5.69	15.58	54.87	0.33	0.42	4.54	0.88	0.08	6.37	1.92	95.13
JS-91-139	0.57	3.40	16.62	70.34	0.16	3.90	0.58	0.64	0.01	4.43	3.23	101.05

Table A16 Trace and rare - earth element data (ppm) of the Fractionation Suite.

Sample	JS-91-54	JS-91-56	JS-91-61	JS-91-66	JS-91-73
Li	2.51	3.02	2.11	2.67	2.66
Rb	0.98	1.48	0.68	0.68	1.48
Sr	117.97	157.80	139.93	55.91	98.39
Y	4.04	7.62	5.36	2.45	5.01
Zr	11.27	20.18	11.92	6.70	13.50
Nb	0.63	1.53	0.53	0.45	0.93
Mo	0.15	0.15	0.18	0.12	0.15
Cs	0.05	0.22	0.24	0.15	0.31
Ba	11.33	27.06	33.49	11.47	13.77
La	2.21	3.42	2.07	1.44	2.00
Ce	7.27	11.33	7.93	4.38	6.54
Pr	1.23	2.04	1.51	0.72	1.22
Nd	5.90	10.65	8.10	3.74	6.74
Sm	1.58	2.93	2.04	1.02	2.03
Eu	0.47	0.76	0.62	0.29	0.54
Gd	2.99	5.29	4.20	1.78	4.04
Tb	0.21	0.34	0.25	0.11	0.26
Dy	0.93	1.73	1.39	0.59	1.31
Ho	0.19	0.27	0.20	0.10	0.21
Er	0.48	0.77	0.56	0.26	0.56
Tm	0.05	0.10	0.08	0.03	0.07
Yb	0.35	0.70	0.39	0.17	0.46
Lu	0.03	0.08	0.05	0.03	0.06
Hf	0.49	0.83	0.53	0.46	0.59
Ta	0.38	1.03	1.30	0.42	1.05
Tl	0.00	0.06	0.02	0.03	0.03
Pb	0.55	1.23	0.89	0.52	0.69
Bi	0.02	0.02	0.03	0.01	0.07
Th	0.20	0.23	0.07	0.12	0.35
U	0.06	0.07	0.02	0.04	0.09
Nb/Ta	1.65	1.48	0.40	1.09	0.88

Table A16 Cont.

Sample	JS-91-79	JS-91-84	JS-91-93	JS-91-97	JS-91-115
Li	0.33	3.96	5.31	4.46	6.27
Rb	0.32	1.43	3.64	0.98	1.15
Sr	22.98	178.26	547.10	173.20	213.40
Y	11.05	9.81	19.21	9.14	11.79
Zr	11.15	30.19	56.69	30.76	43.63
Nb	0.46	0.95	4.64	2.38	1.22
Mo	0.09	0.09	0.18	0.10	0.17
Cs	0.03	0.10	0.15	0.14	0.14
Ba	7.75	64.68	94.64	34.56	22.44
La	5.97	3.81	13.69	6.23	4.63
Ce	20.59	13.86	44.82	18.03	16.97
Pr	3.26	2.59	7.38	2.79	3.04
Nd	15.88	14.11	37.47	14.12	16.26
Sm	3.51	3.73	8.39	3.62	4.50
Eu	0.81	1.18	2.47	1.07	1.37
Gd	7.26	7.01	15.76	6.87	8.43
Tb	0.43	0.47	0.89	0.42	0.54
Dy	2.52	2.44	4.55	2.12	3.03
Ho	0.45	0.41	0.81	0.36	0.53
Er	1.30	0.99	1.95	0.96	1.31
Tm	0.15	0.12	0.26	0.13	0.16
Yb	0.83	0.64	1.37	0.76	0.91
Lu	0.11	0.09	0.17	0.07	0.12
Hf	0.68	1.41	2.47	1.16	2.24
Ta	0.87	1.32	0.59	0.84	1.46
Tl	0.01	0.03	0.01	0.00	0.01
Pb	0.27	1.08	2.19	2.22	1.00
Bi	0.04	0.05	0.05	0.02	0.04
Th	0.15	0.17	0.43	0.38	0.18
U	0.02	0.05	0.13	0.08	0.05
Nb/Ta	0.53	0.72	7.86	2.83	0.84

Table A16 Cont.

Sample	JS-91-118	JS-91-122	JS-91-129	JS-91-146	JS-91-149
Li	3.30	1.41	3.31	4.86	1.22
Rb	0.45	0.11	0.84	1.63	1.59
Sr	153.87	42.80	109.49	576.56	113.72
Y	11.92	1.96	10.54	23.23	16.24
Zr	55.86	4.70	16.26	33.34	20.98
Nb	0.67	0.28	1.47	5.79	7.06
Mo	0.17	0.07	0.13	0.18	0.10
Cs	0.04	-	0.42	-	0.07
Ba	5.64	3.52	14.42	53.40	59.22
La	4.02	0.88	3.95	12.92	8.49
Ce	16.05	3.00	13.84	39.65	22.75
Pr	3.03	0.55	2.46	6.47	3.49
Nd	16.81	2.93	13.33	31.67	17.15
Sm	4.43	0.83	3.47	7.54	4.60
Eu	1.35	0.22	0.99	1.91	1.08
Gd	8.83	1.37	6.35	14.63	8.77
Tb	0.52	0.08	0.43	0.89	0.60
Dy	2.90	0.47	2.45	5.21	3.60
Ho	0.49	0.08	0.44	0.94	0.66
Er	1.26	0.21	1.07	2.42	1.92
Tm	0.16	0.03	0.14	0.29	0.24
Yb	0.90	0.10	0.79	1.79	1.47
Lu	0.11	0.01	0.11	0.21	0.21
Hf	2.69	0.23	0.78	1.95	0.79
Ta	1.32	0.18	0.87	0.99	0.60
Tl	-	0.00	0.01	0.01	0.00
Pb	0.41	0.49	1.17	2.39	0.94
Bi	0.01	0.02	0.02	0.04	0.08
Th	0.08	0.03	0.16	0.75	1.32
U	0.02	0.01	0.06	0.14	0.52
Nb/Ta	0.51	1.52	1.69	5.85	11.82

Table A17 Trace and rare - earth element data (ppm) of the Cumulus Gabbro.

Sample	JS-91-133	JS-91-185	JS-91-189	JS-91-198	JS-91-199	JS-91-112
Li	5.63	9.29	12.37	5.41	5.54	2.79
Rb	9.09	70.19	19.46	9.43	6.97	2.09
Sr	257.03	658.40	272.08	358.61	159.03	129.52
Y	11.69	9.22	10.49	11.28	10.94	9.13
Zr	40.48	34.18	26.70	26.62	33.25	33.94
Nb	2.93	13.14	2.06	9.22	7.73	1.72
Mo	0.12	3.66	0.67	0.76	0.75	0.18
Cs	0.74	7.31	4.56	0.56	0.64	0.08
Ba	136.76	238.86	133.87	73.64	38.06	20.46
La	7.88	21.88	4.29	5.61	3.56	3.33
Ce	23.01	40.85	10.88	13.83	9.28	11.52
Pr	3.68	4.32	1.64	1.99	1.36	2.01
Nd	17.92	16.17	7.65	9.57	6.99	11.08
Sm	4.39	2.76	2.08	2.52	1.88	3.10
Eu	1.25	0.77	0.71	0.79	0.63	0.89
Gd	7.91	4.72	4.77	5.47	4.55	6.24
Tb	0.53	0.31	0.37	0.36	0.31	0.39
Dy	2.87	1.83	2.20	2.32	2.11	2.26
Ho	0.52	0.36	0.44	0.46	0.40	0.40
Er	1.26	0.96	1.16	1.28	1.21	0.98
Tm	0.17	0.14	0.18	0.19	0.15	0.12
Yb	1.00	0.92	1.03	1.13	1.06	0.69
Lu	0.14	0.14	0.14	0.16	0.14	0.09
Hf	1.94	1.54	0.98	0.99	1.10	1.46
Ta	1.48	1.62	0.26	6.54	4.74	1.04
Tl	0.02	0.26	0.04	0.04	0.07	0.15
Pb	1.55	22.64	8.37	3.01	2.16	0.54
Bi	0.04	0.41	0.64	0.06	0.28	0.02
Th	0.40	13.85	0.71	0.55	0.48	0.21
U	0.09	4.98	0.16	0.11	0.12	0.05
Nb/Ta	1.98	8.10	7.92	1.41	1.63	1.65

Table A17 Cont.

Sample	JS-91-136	JS-91-141	JS-91-141d	JS-91-144	JS-91-187	JS-91-192
Li	2.83	8.91	8.75	15.41	7.13	7.47
Rb	0.84	3.78	3.69	25.09	11.21	7.14
Sr	584.38	2309.01	2247.79	2020.29	182.99	116.18
Y	18.75	13.90	13.59	14.57	12.50	11.70
Zr	75.03	32.50	32.41	7.77	25.79	31.82
Nb	1.45	0.91	0.87	1.96	5.10	4.50
Mo	0.14	0.12	0.09	0.22	0.53	0.50
Cs	0.04	1.43	1.40	0.57	0.60	0.82
Ba	17.79	113.13	114.04	97.92	42.33	40.72
La	12.47	10.25	10.14	8.68	4.05	3.80
Ce	38.52	29.66	29.37	22.80	10.70	10.26
Pr	6.11	4.54	4.48	3.38	1.64	1.59
Nd	30.23	21.78	21.94	16.61	8.39	7.81
Sm	7.42	5.04	4.87	4.07	2.46	2.30
Eu	2.02	1.47	1.45	1.34	0.74	0.72
Gd	12.79	9.67	9.67	8.00	6.00	5.53
Tb	0.81	0.54	0.56	0.52	0.44	0.43
Dy	4.47	2.99	2.98	2.99	2.76	2.56
Ho	0.77	0.51	0.52	0.56	0.55	0.49
Er	1.96	1.28	1.23	1.42	1.60	1.44
Tm	0.28	0.17	0.15	0.20	0.22	0.18
Yb	1.50	0.87	0.79	1.04	1.29	1.10
Lu	0.20	0.12	0.11	0.13	0.18	0.16
Hf	3.49	1.46	1.49	0.52	1.15	1.20
Ta	1.39	0.76	0.76	1.14	3.99	3.05
Tl	0.01	0.03	0.02	0.06	0.09	0.06
Pb	0.87	18.09	19.04	5.16	15.95	3.78
Bi	0.02	0.02	0.01	0.03	1.42	0.34
Th	0.64	0.47	0.43	0.38	0.71	0.57
U	0.11	0.08	0.08	0.07	0.16	0.12
Nb/Ta	1.04	1.20	1.14	1.73	1.28	1.47

Table A17 Cont.

Sample	JS-91-195	JS-91-201	JS-91-203	JS-91-204	JS-91-204d	RCNZ-104
Li	12.49	5.25	13.08	8.93	9.64	9.67
Rb	7.36	2.31	6.85	6.48	6.35	9.66
Sr	108.20	155.49	236.54	138.25	136.41	329.85
Y	11.25	9.63	7.55	13.96	13.84	9.20
Zr	28.15	25.50	17.08	38.47	38.20	18.60
Nb	3.25	2.17	1.29	4.90	4.81	2.42
Mo	0.39	2.04	1.54	0.80	0.68	0.62
Cs	1.46	0.13	0.65	0.24	0.26	0.74
Ba	41.96	32.36	69.09	38.08	37.98	144.11
La	2.90	3.65	2.70	4.66	4.55	6.90
Ce	8.88	9.51	7.33	12.96	12.90	16.67
Pr	1.46	1.46	1.13	1.92	1.98	2.27
Nd	7.69	6.99	5.69	9.54	9.45	9.55
Sm	2.58	1.98	1.56	2.81	2.65	2.11
Eu	0.83	0.61	0.59	0.80	0.88	0.72
Gd	5.90	4.48	3.49	5.97	5.87	4.70
Tb	0.47	0.33	0.25	0.43	0.44	0.31
Dy	2.99	2.09	1.54	2.77	2.73	1.85
Ho	0.56	0.40	0.32	0.54	0.54	0.37
Er	1.51	1.15	0.84	1.56	1.53	1.02
Tm	0.25	0.16	0.12	0.21	0.21	0.15
Yb	1.28	0.93	0.68	1.26	1.17	0.86
Lu	0.18	0.13	0.10	0.19	0.17	0.11
Hf	1.31	0.95	0.69	1.35	1.31	0.80
Ta	4.35	0.64	0.34	2.52	2.41	0.60
Tl	0.14	0.05	0.07	0.04	0.05	0.11
Pb	7.40	4.96	34.86	3.92	3.79	4.24
Bi	1.53	0.67	0.54	0.40	0.36	1.51
Th	0.29	0.60	0.32	0.61	0.59	0.54
U	0.10	0.15	0.06	0.16	0.12	0.12
Nb/Ta	0.75	3.40	3.80	1.94	2.00	4.03

Table A18 Trace and rare - earth element data (ppm) of the Late Stage Diorite.

Sample	JS-91-23	JS-91-26	JS-91-29	JS-91-32
Li	7.42	11.08	11.46	12.36
Rb	17.34	21.88	15.09	24.04
Sr	2025.05	1391.16	1681.33	1537.89
Y	33.08	40.27	18.73	44.56
Zr	36.06	35.64	9.99	39.44
Nb	10.55	11.22	2.44	12.41
Mo	0.19	0.31	0.20	0.34
Cs	1.15	1.44	1.51	1.61
Ba	266.46	259.74	138.84	289.26
La	28.13	29.81	19.92	33.21
Ce	75.84	82.16	52.27	91.50
Pr	11.22	12.13	7.34	13.52
Nd	58.40	58.62	34.14	65.27
Sm	12.64	13.43	7.45	14.97
Eu	3.20	3.39	2.08	3.77
Gd	25.37	26.75	13.32	27.57
Tb	1.54	1.61	0.85	1.79
Dy	8.20	9.04	4.72	10.08
Ho	1.49	1.61	0.84	1.80
Er	3.76	3.96	2.19	4.42
Tm	0.48	0.53	0.28	0.59
Yb	2.54	2.71	1.37	3.02
Lu	0.35	0.39	0.21	0.43
Hf	1.71	1.64	0.62	1.85
Ta	1.80	1.18	1.69	1.32
Tl	0.07	0.08	0.09	0.09
Pb	3.64	3.26	3.38	3.64
Bi	0.06	0.06	0.06	0.07
Th	1.82	2.06	1.19	2.32
U	0.35	0.37	0.22	0.41
Nb/Ta	5.85	9.53	1.44	9.40

Table A18 Cont.

Sample	JS-91-35	JS-91-37	JS-91-39	JS-91-144
Li	12.00	12.54	5.30	15.41
Rb	14.89	12.91	6.77	25.09
Sr	1641.94	1999.03	1155.78	2020.29
Y	14.84	32.35	11.99	14.57
Zr	6.42	21.19	10.01	7.77
Nb	3.35	5.02	2.28	1.96
Mo	0.25	0.26	0.23	0.22
Cs	1.27	0.41	0.62	0.57
Ba	107.81	90.93	76.62	97.92
La	17.51	24.12	15.41	8.68
Ce	42.63	64.28	40.11	22.80
Pr	5.90	9.17	5.70	3.38
Nd	25.85	43.78	26.72	16.61
Sm	5.52	9.47	5.68	4.07
Eu	1.76	2.30	1.46	1.34
Gd	11.39	16.78	9.88	8.00
Tb	0.67	1.09	0.56	0.52
Dy	3.67	5.85	3.28	2.99
Ho	0.65	1.01	0.55	0.56
Er	1.63	2.67	1.46	1.42
Tm	0.25	0.35	0.19	0.20
Yb	1.15	1.82	1.23	1.04
Lu	0.15	0.26	0.13	0.13
Hf	0.44	0.86	0.99	0.52
Ta	1.46	1.17	2.17	1.14
Tl	0.06	0.07	0.04	0.06
Pb	4.22	4.66	1.48	5.16
Bi	0.02	0.05	0.05	0.03
Th	1.19	1.56	1.20	0.38
U	0.25	0.29	0.19	0.07
Nb/Ta	2.30	4.31	1.05	1.73

Table A19 Ni and Cu data (ppm) and Ni/Cu ratios of the Fractionation Suite.

Sample	Ni	Cu	Ni/Cu
JS-91-54	798.87	8.49	94.10
JS-91-56	437.66	14.22	30.78
JS-91-61	481.47	11.70	41.15
JS-91-66	1012.19	11.45	88.40
JS-91-73	346.14	64.41	5.37
JS-91-79	412.75	166.98	2.47
JS-91-84	296.35	293.82	1.01
JS-91-93	171.28	28.77	5.95
JS-91-97	413.74	12.99	31.85
JS-91-112	105.85	311.74	0.34
JS-91-115	177.06	101.08	1.75
JS-91-118	138.60	11.74	11.81
JS-91-122	1129.35	160.63	7.03
JS-91-129	378.42	12.65	29.91
JS-91-146	326.22	234.77	1.39
JS-91-149	880.27	83.68	10.52

Table A20 Ni and Cu data (ppm) and Ni/Cu ratios of the Cumulus Gabbro.

Sample	Ni	Cu	Ni/Cu
JS-91-133	181.21	180.43	1.00
JS-91-185	231.85	139.90	1.66
JS-91-187	1201.18	4574.70	0.26
JS-91-189	564.61	1095.53	0.52
JS-91-192	1424.71	1818.10	0.78
JS-91-195	1961.18	3184.67	0.62
JS-91-198	317.15	183.68	1.73
JS-91-199	815.54	883.74	0.92
JS-91-201	2213.07	4134.42	0.54
JS-91-203	6569.63	1186.89	5.54
JS-91-204	5272.28	4886.43	1.08
JS-91-207	4790.23	10874.10	0.44
JS-91-208	384.14	223.84	1.72
RCNZ-104	9774.52	41863.19	0.23

Table A21 Ni and Cu data (ppm) and Ni/Cu ratios of the Late Stage Diorite.

Sample	Ni	Cu	Ni/Cu
JS-91-23	-	31.27	-
JS-91-26	8.91	48.03	0.19
JS-91-29	35.08	64.19	0.55
JS-91-32	11.49	26.72	0.43
JS-91-35	41.80	44.75	0.93
JS-91-37	82.40	100.99	0.82
JS-91-39	144.23	119.98	1.20
JS-91-136	82.67	174.27	0.47
JS-91-141	51.54	38.36	1.34
JS-91-144	55.23	52.99	1.04

Table A22 Ni, Cu and PGE values and PGE ratios for selected samples of the Fractionation Suite (JS-91-122 and 144) and Cumulus Gabbro. Ni and Cu values in ppm, PGE and Au in ppb.

Sample	JS-91-122	JS-91-149	JS-91-187	JS-91-192
Ni	1129.00	880.00	1201.00	1425.00
Cu	161.00	84.00	4575.00	1818.00
Ru	1.99	0.36	0.36	0.28
Rh	2.14	1.09	0.51	0.64
Pd	1.01	30.26	51.42	28.89
Re	0.00	0.00	0.00	0.00
Os	4.00	0.00	0.00	0.00
Ir	2.00	1.00	0.00	0.00
Pt	5.00	19.00	59.00	28.00
Au	6.00	4.00	140.00	21.00
Pd/Ir	0.44	51.29	122.43	65.66
Pt+Pd/ (Ru+Ir+Os)	0.75	43.19	116.20	61.04

Table A22 Cont.

Sample	JS-91-195	JS-91-203	JS-91-204	RCNZ-104
Ni	1961.00	6570.00	5272.00	9775.00
Cu	3185.00	1187.00	4886.00	41863.00
Ru	0.81	3.98	1.40	2.69
Rh	2.47	13.24	11.79	21.52
Pd	50.63	43.98	97.24	185.67
Re	0.00	0.00	7.00	4.00
Os	1.00	3.00	1.00	3.00
Ir	1.00	8.00	2.00	3.00
Pt	77.00	99.00	25.00	5.00
Au	34.00	3.00	19.00	288.00
Pd/Ir	61.00	5.86	61.16	56.09
Pt+Pd/ (Ru+Ir+Os)	59.77	9.66	29.28	21.97

Table A23 CIPW normative analyses for the rocks of the Fractionation Suite.

Sample	JS-91-54	JS-91-56	JS-91-61	JS-91-66	JS-91-73	JS-91-79	JS-91-84	JS-91-93	JS-91-97
Quartz	0	0	0	0	1.13	5.73	0	0	0
Orthoclase	0.18	0.5	0.12	0.15	0.38	0.54	0.48	2.38	0.78
Albite	0	0	0	0	0.33	0	0.14	6.93	2.54
Anorthosite	5.24	8.59	6.33	3.3	5.8	6.2	11.99	15.51	8.8
Nepheline	0	0	0	0	0	0	0	0	0
Diopside	49.1	58.15	68.88	26.21	73.83	46.29	69.58	50.3	59.98
Hypersthene	11.68	15.91	11.88	14.71	13.83	35.01	10.66	1.49	16.5
Olivine	27.5	9.55	7.27	48.18	0	0	0.75	10.78	5.3
Magnetite	3.58	3.8	2.77	6.22	2.26	3.83	3.11	4.99	3.25
Ilmenite	0.78	1.3	0.96	0.47	0.95	1.16	1.96	3.68	1.32
Apatite	0.07	0.03	0.04	0.05	0.05	0.1	0.09	2.31	0.11
Total Mineral wt%	98.14	97.84	98.25	99.3	98.56	98.87	98.76	98.37	98.57

Sample	JS-91-115	JS-91-118	JS-91-122	JS-91-129	JS-91-133	JS-91-144	JS-91-146	JS-91-149
Quartz	0	0	0	0	0	0	0.82	0
Orthoclase	0.43	0.12	0.06	0.09	2.1	3.22	1.44	0.72
Albite	0.8	0.66	0	0	2.71	6.68	3.19	0
Anorthosite	14.45	15.57	3.04	9.79	12.64	46.7	21.26	14.75
Nepheline	0	0.01	0	0	0	0	0	0
Diopside	72.02	71.14	19.85	67.13	65.99	16.89	45.79	21.09
Hypersthene	2.13	0	14.51	7.4	7.05	2.69	17.59	36.29
Olivine	2.88	4.71	54.65	9.21	2.33	10.72	0	18.67
Magnetite	3.31	4.03	6.23	3.38	3.32	6.92	4.9	5.68
Ilmenite	2.42	2.85	0.44	1.35	1.96	4.02	3.35	2.24
Apatite	0.1	0.04	0.07	0.12	0.34	0.59	0.27	0.14
Total Mineral wt%	98.54	99.12	98.84	98.46	98.44	98.43	98.62	99.59

Table A24 CIPW normative analyses for the rocks of the Cumulus Gabbro.

Sample	JS-91-185	JS-91-189	JS-91-198	JS-91-199
Quartz	16.5	0	0.52	0
Orthoclase	8	3.12	1.8	1.02
Albite	33.13	8.8	4.31	1.64
Anorthosite	19.24	23.74	27.16	13.36
Nepheline	0	0	0	0
Diopside	2.93	27.71	18.41	43.9
Hypersthene	15.48	16.63	40.25	18.07
Olivine	0	12.84	0	14.33
Magnetite	2.13	4.35	4.73	5
Ilmenite	1.01	1.08	1.31	1.07
Apatite	0.34	0.11	0.18	0.12
Total Mineral wt%	98.77	98.38	98.66	98.5

Table A25 CIPW normative analyses for the rocks of the Late Stage Diorite.

Sample	JS-91-23	JS-91-26	JS-91-29	JS-91-32	JS-91-35	JS-91-37	JS-91-39
Orthoclase	4.87	5.37	3.29	3.09	2.87	2.15	1.61
Albite	9.64	9.02	10.56	9.26	9.06	3.18	3.13
Anorthosite	40.23	36.85	42.95	41.6	46.18	42.59	44 51
Nepheline	1.39	0	0	0.13	0	0	0
Diopside	9.09	9.05	18.7	8.61	7	20.61	25.46
Hypersthene	0	4.27	1.71	0	7.51	8.4	7.26
Olivine	16.73	15.67	10.02	17.77	9.7	6.01	3.43
Magnetite	7.16	7.84	5.72	7.94	7.08	6.97	6.44
Ilmenite	5.82	6.6	2.78	6.5	4.82	4.67	3.76
Apatite	3.32	3.72	2.6	3.02	2.15	3.63	2.82
Total Mineral wt%	98.26	98.38	98.34	97.91	96.36	98.21	98.42

APPENDIX B
ANALYTICAL METHODS

B.1 Sample Preparation

Individual rock samples, hand samples only, were split or cut into 250 gram samples making sure to remove and discard any weathered surfaces that could result in erroneous data. Each 250g sample was then crushed in a steel jaw crusher to a particle size of $1cm^3$ and transferred to a tungsten - carbide bowl - puck assembly and powdered to approximately -100 mesh. Between samples the jaw crusher was cleaned with a wire brush to remove any solid residue, followed by a cleaning with a pressurized air gun, and finally wiped clean with methanol. The bowl - puck assembly was cleaned using high purity quartz sand, which was powdered in a similar manner as the samples and discarded. The bowl - puck assembly was then cleaned with a high pressure air gun and finally wiped clean with methanol.

Drill core samples, because of their smaller size (20-40g total) were crushed using a ball - mill assembly to approximately -100 mesh. The ball - mill assembly was cleaned in a similar fashion to the bowl - puck assembly.

B.2 Electron Microprobe Analyses

Standard polished carbon coated thin sections were utilised for electron microprobe analyses (EMPA). EPMA were performed using the CAMECA SX-50 at the Department of Earth Sciences, Memorial University of Newfoundland, equipped with a Link EXL EDS

detector and three CAMECA WDS spectrometers utilizing PET, LIF and TAP spectrometer crystals. Analyses were performed on olivine, clinopyroxene and amphibole using an accelerating voltage of 15K electron volts and a beam current of 20nAmps. Plagioclase analyses were done using an accelerating voltage of 15K electron volts and a beam current of 10nAmps. All analyses were done using a beam diameter of 1μ. Elements in excess of 5 wt% were analysed using the EDS spectrometer, all elements <5 wt% were analysed using one of the WDS spectrometers.

Three analyses were performed on each mineral and averaged to give the reported mineral compositions.

B.3 X - Ray Florescence (XRF) Trace Element Analyses

Trace element analyses were carried out on pressed whole rock powder pellets by XRF using a Fisons/ARL 8420 automatic XRF spectrometer with a rhodium tube, located in the Department of Earth Sciences, Memorial University of Newfoundland. Pressed pellets were made by combining 10g of whole rock powder with 1.5g of Union Carbide phenolic resin (TR - 16933) binder. The mixture was then homogenized using ball bearings that were placed in the sample vial and then put on a roller for a period of not less than 4 minutes. The homogenized powder was pressed at 30 tons/inch^2 for approximately 10 seconds and then baked at 150 ^{0}C for ten minutes. Data reduction was performed on a Hewlett-Packard 9845B mini-computer. Trace elements analysed include: Ni, Cu, Zn, Ga, As, Rb, Sr, Y, Zr, Nb, Ba,

Ce, Pb, Th and U. Precision and accuracy of standards DTS - 1, BHVO - 1, SY - 2, SY - 3 and PACS - 1 can be viewed in Table B.1.

B.4 X - Ray Florescence (XRF) Major Element Analyses

Major - element compositions on the majority of samples were determined using fused beads made of 1.5 g of rock powder, 6 g of lithium metaborate and 1.5 g of lithium tetraborate. Detection limits for pressed pellets are 0.7 - 41 ppm with precision ranging form 0.2% to 3.1%. LOI's were determined by weighing powders before and after drying at 1050 °C. Fused beads have detection limits of 0.006% (K_2O and TiO_2) to 0.079% (Al_2O_3) with precision ranging from 0.2% to 3.2%. Precision and accuracy of standards JB - 1A - G, MRG - 1 - G, SY - 2 - G, SY - 3 - G and BIR - 1 - G can be viewed in Table B.2.

B.5 Inductively Coupled Plasma - Mass Spectrometry (ICP - MS) Techniques

ICP - MS was used to determine abundances of the trace and rare earth elements Li, Rb, Sr, Y, Zr, Nb, Mo, Cs, Ba, La, Ce, Pr, Nd, Sm, Eu, Gd, Tb, Dy, Ho, Er, Tm, Yb, Lu, Hf, Ta, Tl, Pb, Bi, Th and U. The procedure was performed at the Department of Earth Sciences, Memorial University of Newfoundland using a SCIEX ELAN ICP - MS. The method used for ICP - MS analyses employs a Na_2O_2 sinter to increase effectiveness of dissolving resistant phases such as zircons, sulphides and other insoluble phases. Preliminary XRF analyses were

Table B1 Precision and accuracy for XRF trace element analyses. Published values are from Govindaraju (1989).

	DTS-1			BHVO-1			SY-2		
	Mean (ppm) (N=4)	Pub. (ppm)	S. D.	Mean (ppm) (N=4)	Pub. (ppm)	S. D.	Mean (ppm) (N=4)	Pub. (ppm)	S. D.
Ni	2360	2360	8	123	121	2	9	10	1
Cu	5	7	2	137	136	2	0	5	1
Zn	40	46	0	101	105	1	233	248	1
Ga	-	1	1	22	21	1	29	29	1
As	-	0	-	-	0	-	19	17	7
Rb	0	0.1	0.3	8.8	11	0.1	220	217	0.4
Sr	0.3	0.3	0.5	398.1	403	0.8	271	271	0.7
Y	0.1	0	0.2	24.3	27.6	0.2	118	128	0.3
Zr	0.2	4	0.1	181.6	179	0.8	296	280	0.4
Nb	0.2	2.2	0.3	20.9	19	0.5	33.3	29	0.2
Ba	6	2	5	139	139	6	450	460	14
Ce	-	0	-	14	39	16	165	175	18
Pb	6	12	1	2	3	1	86	85	1
Th	1	0	1	1	1	1	347	379	2
U	-	0	-	0	0	1	290	284	1

	SY-3			PACS-1		
	Mean (ppm) (N=4)	Pub. (ppm)	S. D.	Mean (ppm) (N=4)	Pub. (ppm)	S. D.
Ni	6	11	1	49	44	1
Cu	-	17	-	385	452	3
Zn	227	244	1	665	824	3
Ga	28	27	1	16	0	1
As	12	19	3	211	211	6
Rb	210.1	206	0.1	46.8	0	0.3
Sr	308.2	302	0.9	270.6	277	0.6
Y	620.7	718	0.4	15.3	0	0.2
Zr	365.3	320	1	132.7	0	0.7
Nb	253	148	0.5	9.5	0	0.1
Ba	437	450	14	646	0	23
Ce	2230	2230	32	54	0	15
Pb	147	133	2	349	404	0
Th	957	1003	2	-	0	-
U	768	650	2	-	0	-

Table B2 Precision and accuracy for XRF major element analyses. Published values are from Govindaraju (1989).

	JB-1A-G			MRG-1-G			SY-2-G		
	Mean (wt%) (N=4)	Pub. (wt%)	S. D. (%)	Mean (wt%) (N=4)	Pub. (wt%)	S. D. (%)	Mean (wt%) (N=4)	Pub. (wt%)	S. D. (%)
Na2O	2.77	2.77	0.07	0.42	0.75	0.04	4.36	4.36	0.04
MgO	7.87	7.85	0.03	13.76	13.76	0.02	2.66	2.72	0.01
Al2O3	14.6	14.69	0.03	8.5	8.59	0.04	12.17	12.17	0.06
SiO2	52.85	52.81	0.17	39.75	39.71	0.16	60.71	60.71	0.13
P2O5	0.26	0.26	0.01	0.07	0.08	0	0.43	0.43	0.01
S	1446 ppm	9 ppm	25	917 ppm	620 ppm	10	976 ppm	162 ppm	16
Cl	38214 ppm	172 ppm	1013	32402 ppm	173 ppm	912	31301 ppm	142 ppm	1200
K2O	1.42	1.44	0.01	0.18	0.18	0.01	4.49	4.49	0.01
CaO	9.41	9.34	0.05	14.94	14.94	0.01	8.01	8.05	0.03
Sc	31 ppm	29 ppm	8	56 ppm	56 ppm	7	10 ppm	7 ppm	6
TiO2	1.29	1.32	0.01	3.83	3.83	0.03	0.14	0.14	0.01
V	196 ppm	223 ppm	5	534 ppm	534 ppm	8	44 ppm	51 ppm	5
Cr	384 ppm	420 ppm	6	437 ppm	437 ppm	2	6 ppm	10 ppm	1
MnO	0.15	0.15	0	0.17	0.17	0	0.32	0.32	0
Fe2O3	9.22	9.21	0.02	18.21	18.21	0.04	6.48	6.38	0.03

	SY-3-G			BIR-1-G		
	Mean (wt%) (N=4)	Pub. (wt%)	S. D. (%)	Mean (wt%) (N=4)	Pub. (wt%)	S. D. (%)
Na2O	4.27	4.17	0.05	1.58	1.74	0.08
MgO	2.64	2.7	0.01	9.67	9.62	0.04
Al2O3	11.61	11.89	0.04	15.52	15.26	0.01
SiO2	59.75	60.32	0.18	47.89	47.49	0.06
P2O5	0.51	0.55	0.01	0.03	0.05	0
S	510 ppm	516 ppm	6	620 ppm	0 ppm	16
Cl	23900 ppm	152 ppm	872	20303 ppm	26 ppm	352
K2O	4.18	4.28	0.04	0.03	0.03	0
CaO	8.15	8.36	0.03	13.15	13.16	0.04
Sc	6 ppm	7 ppm	9	45 ppm	44 ppm	8
TiO2	0.13	0.15	0.01	0.95	0.95	0.01
V	17 ppm	51 ppm	5	309 ppm	311 ppm	7
Cr	2 ppm	11 ppm	5	362 ppm	380 ppm	2
MnO	0.33	0.32	0	0.17	0.17	0
Fe2O3	6.58	6.57	0.01	11.47	11.19	0.02

performed on ICP - MS samples to determine the concentration of sulphur. Samples with more than 3% sulphur react with the Ni crucibles and were therefore placed in a high - temperature oven for a period of 12 hours where temperature was increased in increments to 1000 ^{0}C over a period of four hours. This temperature was maintained for a period of four hours and then gradually decreased for four more hours. This firing sufficiently oxidized the sulphur as not to pose a problem for the Ni crucibles.

After the samples cooled, 0.2g of sample was accurately weighed into a 30ml Ni crucible and 0.8g of Na_2O_2 added to the crucible. Both the peroxide and the sample were well stirred and a thin layer of peroxide was sprinkled on the surface of the mixture. The crucibles were then placed in a muffle furnace at 480 ^{0}C and sintered for 90 minutes. The crucibles were removed from the oven, covered, cooled and 10ml of water was added to each crucible drop - wise until reaction ceased.

The mixture was then added to a 50ml Teflon centrifuge tube. A final volume of 30ml was made up in each tube using distilled water and then centrifuged for 15 minutes. The liquid was then poured off and the residue was rinsed with 25ml of distilled water and centrifuged. A final centrifuge was then completed using another 25ml of distilled water and following which the liquid was discarded.

To the residue was added 2.5ml of 8N HNO_3 and 1ml of oxalic acid. The crucible was washed with 0.2N HNO_3 and this was also added to the tube. The solutions were then transferred to a clean Teflon tube and made up to 50g with distilled water. A final dilution was then carried out on the samples before running on the ICP - MS. A 2g aliquot of sample

was accurately weighed into a Teflon test tube and added to it was 8g aliquot of 0.2N HNO_3 such that the final sample concentration was approximately 0.2N.

In addition to the samples analysed, a blank, two sample duplicates and three accepted standards including; MRG - 1 (gabbro, Canadian Certified Reference Materials Project standard) and DNC - 1 (diabase, United States Geological Survey standard) were also analysed to determine precision and accuracy (Table B.3).

B.6 Platinum Group Element Analyses (ICP - MS)

The platinum group elements (PGE) were analysed at the Department of Earth Sciences, Memorial University of Newfoundland using a SCIEX ELAN ICP - MS. Samples were prepared by fusing a mixture of 15g of rock powder, 9.6g of Ni carbonyl, 6g S, 18.0g Na_2CO_3, 36g $Na_2B_4)_7$ and 15g SiO_2 in a clay crucible at 1000 ^{0}C for 1.25 hours to produce a NiS button. The button was dissolved in HCl and the PGE were collected by Te precipitation (Jackson et al., 1990). Blanks were prepared in the same way as the samples , except an additional 15g of SiO_2 powder was used instead of rock powder. Accuracy and precision of PGE analyses vary widely, but are good for Pd and Ir (Table B.4).

Table B3 Precision and accuracy for ICP-MS trace element analyses. Published values are from Govindaraju (1989).

	MRG-1			DNC-1		
	Mean (ppm)	Pub. (ppm)	S. D. (%)	Mean (ppm)	Pub. (ppm)	S. D. (%)
Li	3.77	4.2	0.215	4.88	5.1	0.11
Rb	7.76	8.5	0.37	3.87	4.5	0.315
Sr	279	266	6.5	144	145	0.5
Y	11.6	14	1.2	15.5	18	1.25
Zr	94.8	108	6.6	35.7	41	2.65
Nb	23	19.2	1.9	1.73	3	0.635
Mo	1.26	0.87	0.195	0.22	0.7	0.24
Cs	0.59	0.57	0.01	0.2	0.34	0.07
Ba	47.7	61	6.65	101	114	6.5
La	9.12	9.8	0.34	3.68	3.8	0.06
Ce	26.4	26	0.2	8.27	10.6	1.165
Pr	3.82	3.4	0.21	1.08	1.3	0.11
Nd	18.6	19.2	0.3	4.9	4.9	0
Sm	4.51	4.5	0.005	1.42	1.38	0.02
Eu	1.46	1.39	0.035	0.59	0.59	0
Gd	4.02	4	0.01	2.23	2	0.115
Tb	0.55	0.51	0.02	0.37	0.41	0.02
Dy	2.99	2.9	0.045	2.68	2.7	0.01
Ho	0.5	0.49	0.005	0.62	0.62	0
Er	1.19	1.12	0.035	1.91	2	0.045
Tm	0.15	0.11	0.02	0.29	0.1	0.095
Yb	0.81	0.6	0.105	1.94	2	0.03
Lu	0.11	0.12	0.005	0.3	0.32	0.01
Hf	3.75	3.76	0.005	1	1	0
Ta	0.88	0.8	0.04	0.11	0.098	0.006
Tl	0.05	0.055	0.0025	0.03	0.026	0.002
Pb	5.08	10	2.46	6.27	6.3	0.015
Bi	0.14	0.00013	0.069935	0.02	0.02	0
Th	0.82	0.93	0.055	0.27	0.2	0.035
U	0.25	0.24	0.005	0.06	0.1	0.02

Table B.4: Precision and accuracy of PGE analyses.

PTC-1	Accepted	MUN	Mean	Min	Max	SD	COV	LOD
MUN;n=5	ppb	ppb	ppb	ppb	ppb	ppb	%	ppb
Ru	650	440	418	346	503	67	16.0	0.08
Rh	620	609	605	582	626	16	2.7	0.02
Pd	1700	11405	11402	10392	11813	577	5.1	0.13
Re		67	72	55	90	15	20.4	0.04
Os	240	192	139	54	218	66	47.3	0.31
Ir	170	164	170	153	184	11	6.7	0.01
Pt	3000	2699	2609	2165	3250	416	15.9	0.05
Pd/Ir	75	70	67					

Accepted values from McAdam et al. (1973); MUN are accepted values from Memorial University.

APPENDIX C
DRILL CORE SAMPLES

The following pages (Tables C1 through C5) contain sample numbers, locations, drill hole numbers, intervals and geological maps for samples collected from diamond drill holes in the field area. Hand sample locations are indicated on Figure MA - 1.

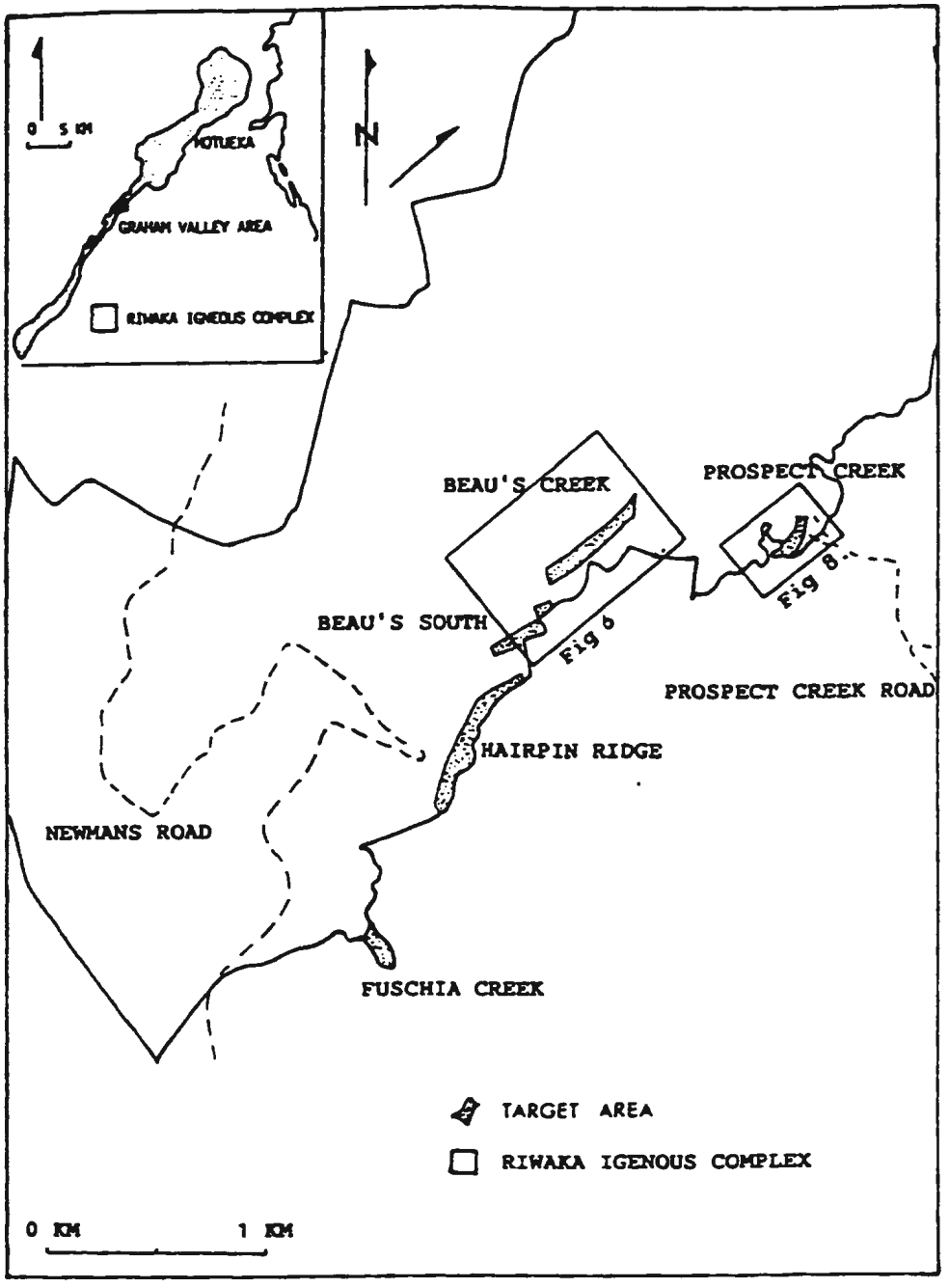

Figure C1 Graham Valley diamond drill hole targets (after, Cowden et al., 1988).

Table C1 Drill core sample locations.

Sample #	Location	Drill Hole #	Interval (feet)
JS-91-185	Beau's Creek	GV-5	77.5
JS-91-187	Prospect Creek	GV-1	75
JS-91-189	Prospect Creek	GV-1	65.5
JS-91-192	Beau's Creek	GV-4	162
JS-91-195	Beau's Creek	GV-4	172.5
JS-91-197	Beau's Creek	GV-4	184
JS-91-198	Beau's Creek	GV-5	78.5
JS-91-199	Beau's Creek	GV-4	166
JS-91-201	Beau's Creek	GV-5	93.5
JS-91-203	Beau's Creek	GV-5	88
JS-91-204	Beau's Creek	GV-5	82
JS-91-207	Beau's Creek	GV-5	85.5
JS-91-208	Beau's Creek	GV-4	182

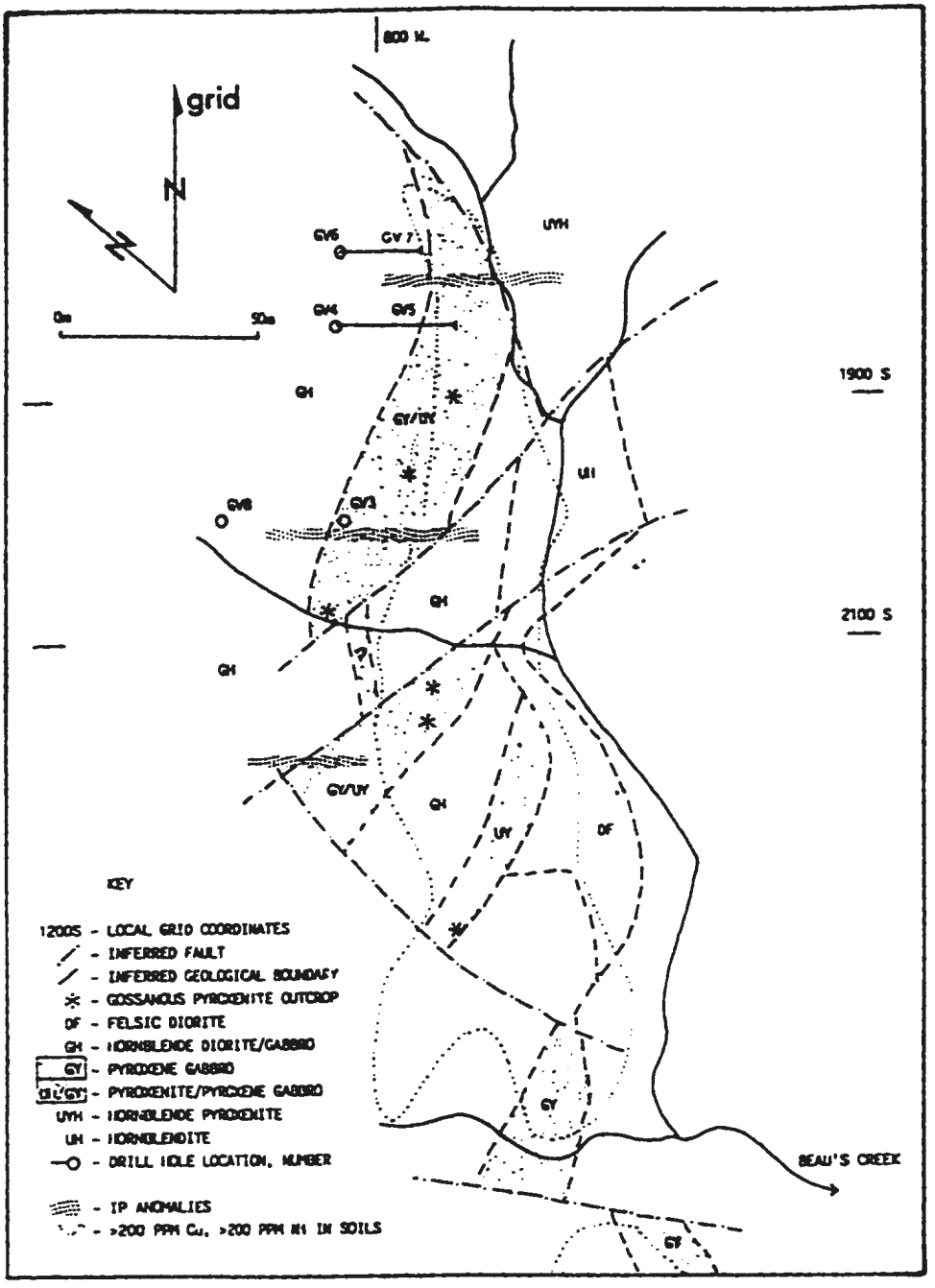

Figure C2 Geological map of the Beau's Creek area and diamond drill hole locations (after, Cowden et al., 1988).

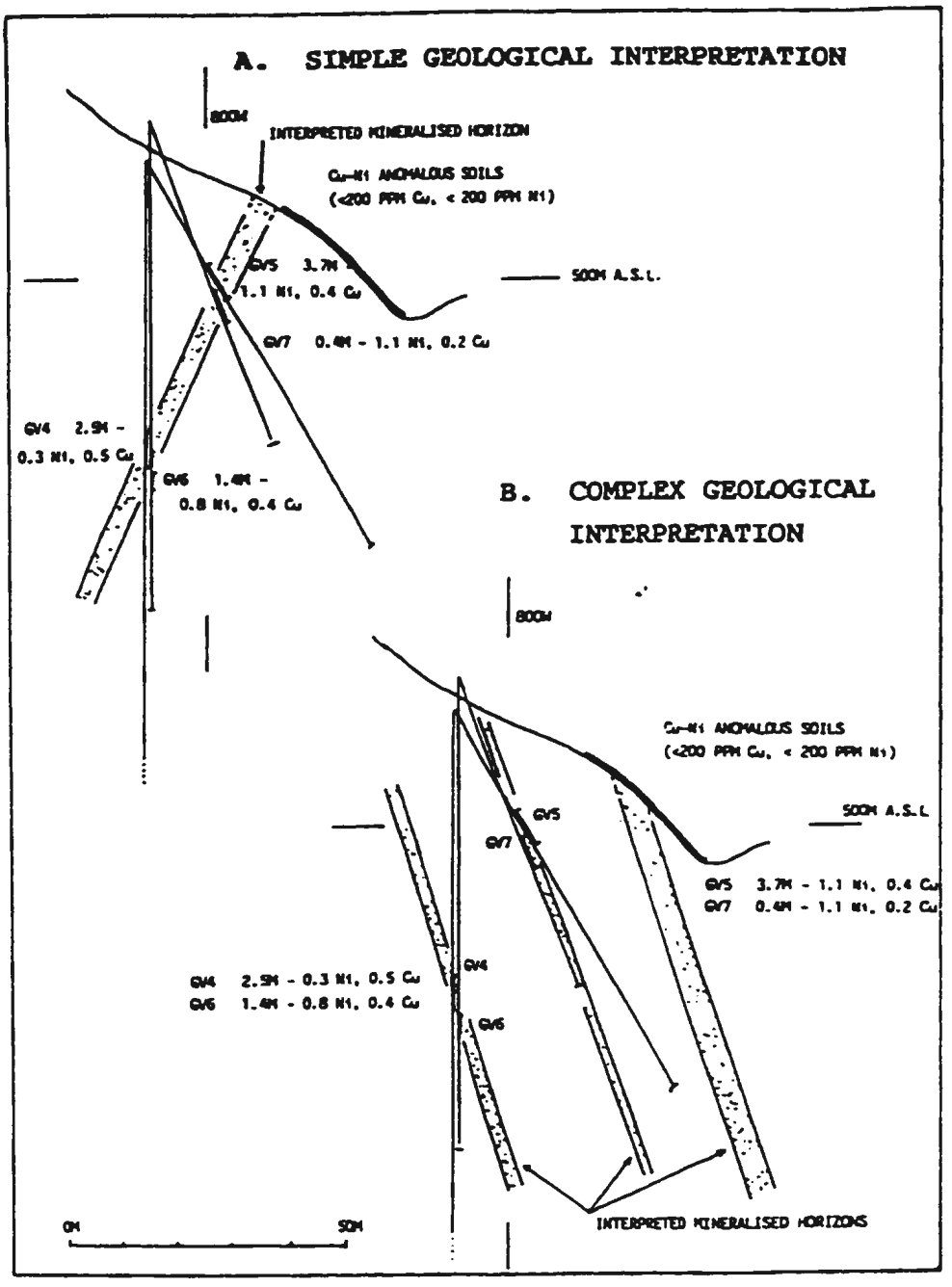

Figure C3 Geological cross sections of the Beau's Creek mineralized zone (after, Cowden et al., 1988).

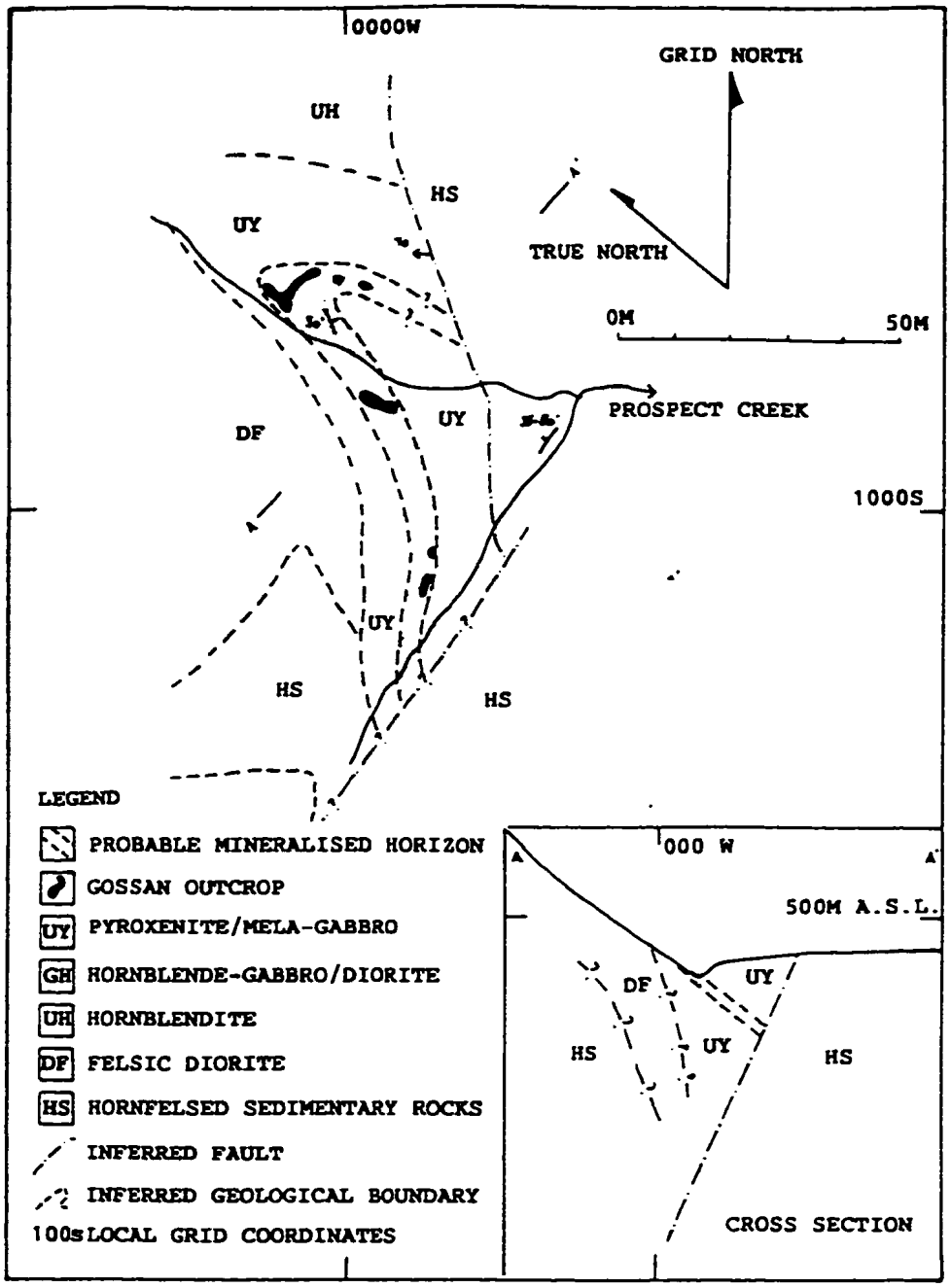

Figure C4 Geological map and cross section of the Prospect Creek area (after, Cowden et al., 1988).

References Cited in Appendices

Cowden, A., Bawden, P. and Inger, M., 1988. Assessment of the nickel - copper - platinum group element mineralisation of the Riwaka Complex, exploration licence 33 - 335 volume 1. Sigma Resources N. L. Unpublished report.

Govindaraju, K., 1989. 1989 compilation of working values and sample descriptions for 272 geostandards. Geostandards Newsletter Special Issue (13).

Jackson, S. E., Fryer, B. J., Gosse, W., Healy, D. C., Longerich, H. P. and Strong, D. F., 1990. Determinations of the precious metals in geological materials by inductively coupled plasma - mass spectrometry (ICP - MS) with nickel sulphide fire - assay collection and tellurium coprecipitation. Chemical Geology (83): 119 - 132.

McAdam, R.C., Sutarno and Moloughney, P. E., 1973. Nobel - metals - bearing sulphide concentrate PTC: its characterization and preparation for use as standard reference material. Department of Energy, Mines and Resources, Ottawa Mines Branch, Technical Bulletin TB 176, 26p.

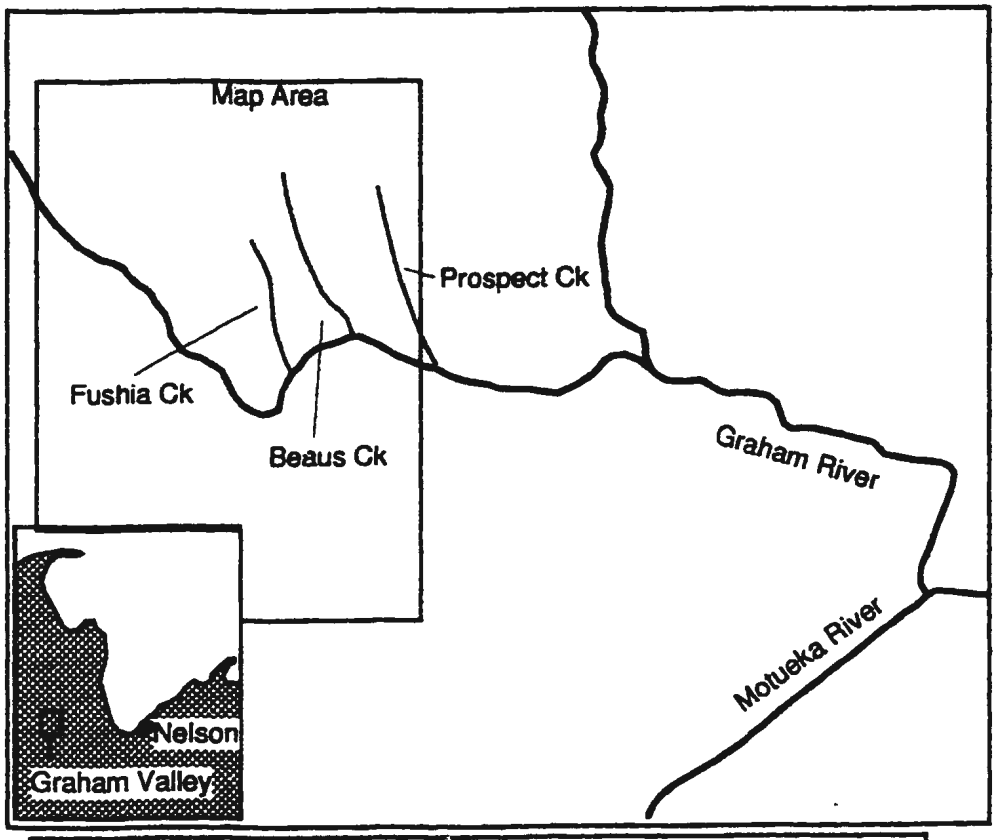

QUATERNARY

Qs — Undifferentiated sediments

LOWER CRETACEOUS

Spg — Separation Point Batholith
Hornblende - biotite granodiorite/granite.

Riwaka Complex

D — Late Stage Diorite
Microdiorite, dolerite, granodiorite, hornblende diorite and porphyritic diorite.

G — Cumulus Gabbro
olivine gabbro, minor hypersthene gabbro.

U — Fractionation Suite
Clinopyroxene - bearing dunite to hornblende clinopyroxenites.

MIDDLE TO UPPER SILURIAN

Aq — Hailes Quartzite
Grey to black quartzite, sandy shale, slate and quartzose sandstone.

UPPER ORDOVICIAN

Aw — Wangapeka Formation
Graphitic argillite to silicious argillite with quartz greywacke and thin quartzite bands toward the top.

LOWER TO UPPER ORDOVICIAN

Am — Arthur Marble
Very pure, cream to, pale grey calcite marble and silicious, graphitic dark grey marble.

Ah — Hornfels and biotite schist

Aw

Qs